Physically Modeling High-Redshift Ultraluminous Infrared Galaxies

Citation

Permanent link

Terms of Use

Share Your Story

Dissertation Advisor: Professor Lars Hernquist   Christopher Charles Hayward

Physically Modeling High-Redshift
Ultraluminous Infrared Galaxies

Abstract

We have used a combination of hydrodynamical simulations, dust radiative transfer, and an empirically based analytical model for galaxy number densities and merger rates in order to physically model the bright high-redshift submillimeter-selected galaxy (SMG) population. We report the results of three projects: In the first we study the dependence of a galaxy's observed-frame submillimeter (submm) flux on its physical properties. One of our principal conclusions is that the submm flux scales significantly more weakly with star formation rate for starbursts than for quiescently star-forming galaxies. Consequently, we argue that the SMG population is not exclusively merger-induced starbursts but rather a mix of merger-induced starbursts, early-stage mergers where two quiescently star-forming disk galaxies are blended into one submm source ("galaxy-pair SMGs"), and isolated disk galaxies. In the second work we present testable predictions of this model by demonstrating how quiescently star-forming and starburst SMGs can be distinguished from integrated data alone. Starbursts tend to have higher luminosity, effective dust temperature, global star formation efficiency ($L_{\mathrm{IR}}/M_{\mathrm{gas}}$), and infrared excess ($L_{\mathrm{IR}}/L_{\mathrm{FUV}}$) and tend to lie significantly above the star formation rate-stellar mass relation defined by quiescently star-forming galaxies. These diagnostics can be used to observationally determine the relative contribution of quiescently star-forming and starburst galaxies

to the SMG population. In the final work we present the SMG number density, cumulative number counts, and redshift distribution predicted by our model. We show that, contrary to previous claims, the observed SMG number counts do not provide evidence for a top-heavy initial mass function. We also show that starbursts and galaxy-pair SMGs both contribute significantly to the bright SMG counts, whereas isolated disks contribute significantly only at the faint end.

Contents

Acknowledgments

First of all, I thank my thesis advisor, Lars. I have really enjoyed working with you these past five years. The level of independence you allowed me has caused me to learn to come up with interesting research topics on my own and to forge my own way ahead on projects (with the help of collaborators, of course). The skills I learned because of this independence will serve me well as a postdoc and beyond. Furthermore, I really appreciate the copious conference travel and collaboration trips you financed. Finally, thank you for advertising my work when you talk with researchers from other institutions and for recommending me strongly enough to convince Volker to hire me! I look forward to many more years of fruitful collaboration with you.

I would like to thank my close collaborators (who are all also great friends). Patrik, my second advisor, thank you for teaching me so much about radiative transfer and coding. Thank you also for setting high standards, challenging me to dig deeper, consistently providing constructive, detailed criticism, and teaching scientific integrity by example. Desika, thanks for being my SMG partner in crime and travel companion (we've had a couple nice "honeymoons" already and hopefully have more coming) and for always being willing to shred up some fresh powder (and for going to great lengths to enable this; I look forward to our next Aspen and/or Obergurgl conferences!) Dusan, thank you for our many discussions of science topics and wine (both types of discussions often took place with wine in hand, of course), and for your skepticism (though perhaps you enjoy playing devil's advocate a bit too much at times!) TJ, thank you for your deep insight about and technical assistance

with GADGET and for generally being a chill, awesome friend.

Thanks to the members of my research exam and thesis advisory committees (Daniel Eisenstein, Giovanni Fazio, Doug Finkbeiner, and Bob Kirshner) for your time, guidance, and scientific and career advice. Thank you to my external thesis committee member, Volker Springel, for coming all the way from Germany for my defense and for delaying the start of my career as a Starbucks barista for at least three years by offering me a postdoc position. I look forward to working with you at HITS. Thanks also to the professors I taught for (Josh Grindlay, Rosanne di Stefano, Bob Kirshner, and Ramesh Narayan); I really enjoyed working with all of you.

I thank my officemate Diego; it has been great sharing an office with you during the past five years. Perhaps we both would have been more productive had we not gotten along so well, but I think the many great discussions we have had, about astrophysics but also more varied topics (since we are self-proclaimed "Renaissance men"), and the fun times were well worth the decreased productivity.

I would like to thank my *many* close friends from the Astronomy Department and other parts of the CfA that I have not yet mentioned, especially Gurtina, Brandon, Phil, Josh, Laura, Claude, Matt, Greg, Paul, Jack (who foolishly bet me $100 I would not graduate — from anything; thankfully I've proved him wrong), Bobby J., Dylan "LH", Nick, both Sarah's, and Cesar. I also thank my many friends from the larger astronomy community, especially my "role model" Nick Scoville, who make conferences very enjoyable experiences rather than a chore.

Jean, Peg, Donna, Nina, Uma, Greg, and the other administrators at CfA deserve much thanks for keeping the place running (and especially for processing my

expense reports!) Jean and Peg were also a great source of friendly conversation, moral support, and general pleasantness.

I would also like to thank NSF, NASA, the Keck Foundation, and the public for directly and indirectly supporting my research. I am fortunate to live and work in a country that strongly supports basic scientific research, and I hope that this continues to be the case.

My academic path did not start at Harvard, of course, and I owe much to the many excellent teachers, professors, and mentors I had in the past. In particular, thanks to my undergrad thesis advisor Joel Bregman, my research mentor Jimmy Irwin, and my professors and advisors at the University of Michigan, especially Mario Matteo, David Gerdes, Jean Krisch, Elleanor Crown, Larry Sklar, Kevin Amidon, and Pat Pranke. I also thank the many excellent teachers I had in high school, especially Ron Arscheene for introducing me to the amazing world of physics and inspiring me to pursue a career as an astrophysicist, which I had not previously understood to be a possibility. I thank my math teachers Ken Dupris, the late Bob Johnson, and Tom Van Houten (who was spot on when he said we should not bother celebrating our high school graduation because that would pale in comparison to when we earn PhDs). I also thank the late Konrad Dzwonkiewicz for teaching me not only the methods of but also the logic behind computer programming, thereby giving me a solid basis that has enabled me to program adequately (though perhaps this is arguable) without any formal classes beyond high school. Thanks also to my debate coaches, Tom Pfannes and Tom Lietz, for teaching me how to coherently and logically support my claims; this has been infinitely helpful for my research career and otherwise. Thanks, finally, to elementary school teachers Scott Burnham and

Vic LeMerise for inspiring me to study space.

Thanks to my non-CfA friends for their support during my time in graduate school and otherwise. In particular, I thank my good friends Jeff and Gavin for providing useful diversion and discussion of topics completely unrelated to astrophysics. Thanks also to Bob Pettibone for fireside chats about alternative cosmological theories and many other topics. I also thank Frank and the rest of the crew of Socrates Newtowne Grille (clearly the best place to have a thesis defense dinner!) and the good people at the Tam for supplying inexpensive liquid relief from the mental strain of too much astrophysics (and, in the case of the former, the best pizza per unit dollar in town).

My most emphatic thanks belongs to those to whom I have dedicated this dissertation. The first dedication is to my parents, Chuck and Judi. I thank them for strongly supporting my academic pursuits, regardless of whether I studied astrophysics or Buddhism, throughout my life. I would not be where I am today had they not stressed the importance of education, encouraged me to follow my dreams, and provided ample financial support and educational opportunities.

The second dedication is to my wife and closest collaborator, Tara. She has been a constant source of support during graduate school—especially the stressful periods—and has tolerated the late nights and frequent travel; I deeply thank her for this. I also strongly appreciate her willingness to move every few years, even if it means across the Atlantic (twice, so far), and her enthusiasm about experiencing new places and cultures both by living in them and traveling to them. I look forward to more adventures with her in Heidelberg and beyond.

For my wife, Tara,

for being my companion

on the road traveled by an academic,

and

For my parents, Chuck and Judi,

for encouraging and supporting

my academic pursuits.

Chapter 1

Introduction

Galaxy mergers have been studied using simulations for many decades, initially including only gravity (e.g., Holmberg 1941; Toomre & Toomre 1972; Toomre 1974) but later also incorporating hydrodynamics (e.g., Hernquist 1989; Barnes & Hernquist 1996). State-of-the-art simulations show good agreement with diverse observational constraints (e.g., Hopkins 2008, and references therein), but, to date, most work has either compared quantities which are known in the N-body/SPH simulations but must be inferred from observations (e.g., mass) or relied on crude methods to calculate spectral energy distributions (SEDs) and images of simulated galaxies that accounted for dust attenuation using an empirically derived attenuation law and did not treat infrared (IR) emission. This is understandable, as including radiative transfer makes an already difficult problem significantly more difficult and is often computationally prohibitive. However, since most information in astronomy is in the form of light, it is vital that theoretical models be able to predict the photometric and spectroscopic properties of simulated galaxies in order to provide

the most direct comparison with observations possible.

Most efforts to perform dust radiative transfer on galactic scales have been limited to semi-analytic models incorporating many simplifying assumptions (e.g., Witt et al. 1992; Gordon et al. 1997; Silva et al. 1998; Bianchi 2008). A notable early exception is that of Bekki & Shioya (2000), who performed dust radiative transfer on sticky particle simulations of galaxy mergers. Note, however, that their calculations rely on various significant simplifications: they use an assumed reddening law rather than directly calculating the attenuation at different wavelengths, they do not include scattering, they assume that the dust in each gas particle emits as a single modified blackbody rather than calculating the emission from each dust species, and they do not include dust self-absorption.

In the past few years multiple authors have written codes that perform full 3-D radiative transfer on galaxy merger simulations (Jonsson 2006; Jonsson et al. 2010; Li et al. 2008; Chakrabarti & Whitney 2009). These codes significantly improve upon earlier work in numerous ways: they treat arbitrary 3-D geometries (some with adaptive grids); they include dust absorption, scattering, and re-emission, calculated using a full dust model for a range of wavelengths; and they properly treat dust self-absorption. Furthermore, they are specifically designed to use outputs from hydrodynamic simulations to specify the radiative transfer problem (namely, the input SEDs from stars and AGN and the 3-D distribution of sources and dust). Thus by using one of these codes it is now possible to self-consistently calculate UV-mm SEDs of simulated galaxies so that simulations of galaxy formation can be directly confronted by observations without recourse to intermediary methods designed to infer physical properties from observables.

While the focus of my first-author papers and this dissertation is the submillimeter-selected galaxy (SMG) population, I have worked with a variety of collaborators to apply the combination of GADGET-2 hydrodynamic simulations and SUNRISE dust radiative transfer to various other galaxy populations. In Narayanan et al. (2010a) we presented an early model for SMGs, which I have refined and expanded on in later work. We used simulations of major mergers of gas-rich $z \sim 2-3$ galaxies to show that the observed range of submillimeter (submm) fluxes and typical SED of SMGs are consistent with what SUNRISE predicts for merger-driven starburst galaxies. In Narayanan et al. (2010b) we showed that the same simulated galaxies would often be classified as dust-obscured galaxies (DOGs), a population of 24 μm-selected $z \sim 2$ galaxies that has recently garnered much interest, and we used the simulations to further our understanding of the DOG population and how it is connected to SMGs.

The above papers focused on rapidly star-forming dusty galaxies. However, we have also used SUNRISE to analyze merger remnants in order to study the population of compact, quiescent galaxies at $z \sim 2$. In Wuyts et al. (2010) we showed that mergers of gas-rich disks scaled to $z \sim 3$ produce compact remnants with sizes similar to those observed. An especially interesting result of the SUNRISE analysis is that the simulated merger remnants have negative mass-to-light ratio gradients because of a combination of stellar age, stellar metallicity, and extinction gradients; consequently the mass may be even *more compact* than the light.

Though the above studies focused on high-redshift galaxies we have not ignored the local universe. In Younger et al. (2009a) we modeled local ultra-luminous infrared galaxies (ULIRGs) in order to study how the mid-IR colors of ULIRGs depend on

the strength of the AGN contribution. In Snyder et al. (2011) we used a suite of local galaxy merger simulations to determine when the mergers would be classified as post-starburst (aka E+A or K+A) galaxies. Perhaps the most interesting result from that work is that the typical timescale for which a merger is classified as a post-starburst galaxy is only $\sim 0.1 - 0.3$ Gyr, which is significantly shorter than the canonically assumed timescale of 1 Gyr (the lifetime of A stars), primarily because the star formation histories of mergers are not simply instantaneous bursts. As a result, the previously claimed tension between the observed abundance of post-starburst galaxies and merger rates is no more. Finally, in Bush et al. (2010) we turned our attention to disk galaxies in order to understand the observed extended UV (XUV) disks. We showed that Type I XUV disks—where the XUV emission occurs in regular spiral patterns—occur naturally when extended gas disks are included in the simulations, but we could not reproduce Type II XUV disks.

In this dissertation I describe three projects that focus on submillimeter-selected galaxies. Chapter 2 describes the modifications I made to the model we originally presented in Narayanan et al. (2010a), analyzes how the observed submm flux depends on physical properties of the simulated galaxies, and presents some interesting implications for the SMG population. Chapter 3 elaborates our proposal that SMGs are a mix of quiescently star-forming and starburst galaxies and presents observational diagnostics to distinguish quiescent and starburst star formation modes from integrated data alone. Chapter 4 presents the submm number counts predicted by our model and demonstrates that matching the observed counts does not require use of a top-heavy initial mass function. Chapter 5 summarizes the conclusions of these studies and discusses future research.

Chapter 2

What Does a Submillimeter

Galaxy Selection Actually Select?

The Dependence of Submillimeter

Flux Density on Star Formation

Rate and Dust Mass

Christopher C. Hayward, Dušan Kereš, Patrik Jonsson, Desika Narayanan, T. J. Cox, & Lars Hernquist, 2011, arXiv:1101.0002, to be published in *The Astrophysical Journal*

Abstract

We perform 3-D dust radiative transfer (RT) calculations on hydrodynamic simulations of isolated and merging disk galaxies in order to quantitatively study the dependence of observed-frame submillimeter (submm) flux density on galaxy properties. We find that submm flux density and star formation rate (SFR) are related in dramatically different ways for quiescently star-forming galaxies and starbursts. Because the stars formed in the merger-induced starburst do not dominate the bolometric luminosity and the rapid drop in dust mass and more compact geometry cause a sharp increase in dust temperature during the burst, starbursts are very inefficient at boosting submm flux density (e.g., a $\gtrsim 16\times$ boost in SFR yields a $\lesssim 2\times$ boost in submm flux density). Moreover, the ratio of submm flux density to SFR differs significantly between the two modes; thus one cannot assume that the galaxies with highest submm flux density are necessarily those with the highest bolometric luminosity or SFR. These results have important consequences for the bright submm-selected galaxy (SMG) population. Among them are: 1. The SMG population is heterogeneous. In addition to merger-driven starbursts, there is a subpopulation of galaxy pairs, where two disks undergoing a major merger but not yet strongly interacting are blended into one submm source because of the large ($\gtrsim$ 15", or $\sim$ 130 kpc at $z = 2$) beam of single-dish submm telescopes. 2. SMGs must be very massive ($M_\star \gtrsim 6 \times 10^{10} M_\odot$). 3. The infall phase makes the SMG duty cycle a factor of a few greater than what is expected for a merger-driven starburst. Finally, we provide fitting functions for SCUBA and AzTEC (sub)mm flux densities as a function of SFR and dust mass and bolometric luminosity and dust mass; these

should be useful for calculating (sub)mm flux density in semi-analytic models and cosmological simulations when performing full RT is computationally not feasible.

2.1   Introduction

Submillimeter-selected galaxies (SMGs; Smail et al. 1997; Barger et al. 1998; Hughes et al. 1998; Eales et al. 1999; see Blain et al. 2002 for a review) are extremely luminous (bolometric luminosity $L_{\mathrm{bol}} \sim 10^{12} - 10^{13} L_{\odot}$; e.g., Kovács et al. 2006), high-redshift (Chapman et al. 2005) galaxies powered primarily by star formation rather than active galactic nuclei (AGN; Alexander et al. 2005a,b, 2008; Valiante et al. 2007; Menéndez-Delmestre et al. 2007, 2009; Pope et al. 2008; Younger et al. 2008, 2009b). Because of their high dust content, SMGs emit almost all of their luminosity in the IR. As the name suggests, a galaxy is defined as an SMG if it is detected in the submm (historically, 850 μm flux density $S_{850} \gtrsim 3 - 5$ mJy; the nature of the population is sensitive to the adopted flux density cut, so we define an SMG as a source with $S_{850} > 3$ mJy), which requires $L_{\mathrm{IR}} \gtrsim 10^{12} L_{\odot}$ (Kovács et al. 2006; Coppin et al. 2008), so SMGs are typically ultra-luminous infrared galaxies (ULIRGs). Locally, ULIRGs are almost exclusively merging galaxies (Sanders & Mirabel 1996; Lonsdale et al. 2006), so one might expect that at least some SMGs are also merging galaxies. Indeed, many observations support a merger origin for SMGs (e.g., Ivison et al. 2002, 2007, 2010; Chapman et al. 2003; Neri et al. 2003; Smail et al. 2004; Swinbank et al. 2004; Greve et al. 2005; Tacconi et al. 2006, 2008; Bouché et al. 2007; Biggs & Ivison 2008; Capak et al. 2008; Younger et al. 2008, 2010; Iono et al. 2009; Engel et al. 2010). Furthermore, in Narayanan et al. (2010a,

hereafter N10) we combined hydrodynamic simulations and dust RT calculations to show that major mergers can reproduce the full range of submm flux densities and typical UV-mm spectral energy distribution (SED) of SMGs (cf. Chakrabarti et al. 2008; Chakrabarti & Whitney 2009). Semi-analytic models also predict that the SMG population is dominated by merger-induced starbursts rather than quiescent star formation (Baugh et al. 2005; Fontanot et al. 2007; Swinbank et al. 2008; Lo Faro et al. 2009; Fontanot & Monaco 2010; González et al. 2011; but cf. Granato et al. 2004).

However, because of the much greater rate of gas supply onto galaxies at high redshift (e.g., Kereš et al. 2005; Dekel et al. 2009), gas fractions (Erb et al. 2006; Tacconi et al. 2006, 2010; Daddi et al. 2010) and SFRs (Daddi et al. 2007; Noeske et al. 2007a,b) of galaxies at fixed galaxy mass increase rapidly with redshift. Thus, at $z \sim 2 - 3$ even a "normal" star-forming galaxy can reach ULIRG luminosities (e.g., Hopkins et al. 2008c, 2010a; Daddi et al. 2005, 2007; Dannerbauer et al. 2009). Furthermore, roughly estimating submm counts using estimates of high-redshift major merger rates and the short duty cycle of merger-induced starbursts suggests that there may not be enough major mergers to account for the SMG population (Davé et al. 2010). This motivates the view that, instead, typical SMGs may be massive, gas-rich disks quiescently forming stars and fueled by continuous gas supply from mergers and smooth accretion (Carilli et al. 2010, but cf. Daddi et al. 2009b).

The mode of star formation responsible for the majority of the SMG population is still a matter of debate, as it is difficult to discriminate between the two scenarios given the currently available data. A better understanding of the submm galaxy selection can clarify the nature of the SMG population.

Since SMGs have redshifts $z \sim 1 - 4$ (Dannerbauer et al. 2002; Chapman et al. 2005; Younger et al. 2007, 2008; Capak et al. 2008; Greve et al. 2008; Schinnerer et al. 2008; Daddi et al. 2009a,b; Knudsen et al. 2010), the observed submm flux density traces rest-frame $\sim 150 - 400$ μm, longward of the peak of the IR SED. Thus the observed submm flux density is sensitive to both the total IR luminosity and the "dust temperature"[1] of the SED, which depend on the luminosity from stars and AGN absorbed by the dust, the mass and composition of the dust, and the spatial distribution of stars, AGN, and dust. Galaxies do not have identical SED shapes, so the dependence on dust temperature implies that galaxies with the highest submm flux density are not necessarily those with the highest bolometric luminosity. Furthermore, because star formation histories are more complicated than an instantaneous burst, the luminosity and instantaneous SFR are not necessarily linearly proportional. Thus the relationship between submm flux density and SFR is potentially more complicated than the relationship between submm flux density and bolometric luminosity. We therefore cannot say a priori that the galaxies with the highest submm flux densities are the most rapidly star-forming or most luminous bolometrically. Indeed, it has already been observationally demonstrated that submm selection does not select all the brightest galaxies in a given volume, as there are galaxies with luminosities and redshifts comparable to those of SMGs that are undetected in the submm because of their relatively hot SEDs (Chapman et al.

[1]As is convention, we will use the term "dust temperature" to denote the temperature derived from a single-temperature modified blackbody fit to the SED. This is simply a parameterization of the SED shape rather than a physical temperature. In our simulations dust grains have a continuum of temperatures, depending on both grain size and the local radiation field heating the dust.

2004; Chapman et al. 2010; Casey et al. 2009; Casey et al. 2011; Hwang et al. 2010; Magdis et al. 2010; Magnelli et al. 2010). A submm galaxy selection is clearly biased toward galaxies with cold SEDs; however, the details of the selection bias are yet to be understood.

Despite the basic physical reasons that one does not expect a simple relation between submm flux density and SFR, a linear relation between submm flux and SFR has been used explicitly (and, even more frequently, implicitly) to infer SFR from observed submm flux densities (e.g., Chapman et al. 2000; Peacock et al. 2000; Blain et al. 2002; Scott et al. 2002; Webb et al. 2003; van Kampen et al. 2005; Tacconi et al. 2008; Wang et al. 2011), typically because the data sets do not have enough photometric data points to precisely constrain the IR SED shape (*Herschel* data are already helping greatly in this regard; e.g., Chapman et al. 2010; Dannerbauer et al. 2010; Magnelli et al. 2010). Furthermore, some theoretical studies (Davé et al. 2010) have assumed that SMGs are the most rapidly star-forming galaxies in order to identify SMGs in cosmological simulations without performing RT. If SFR and submm flux density are not simply related this approach is problematic.

It is clear that a better understanding of the relationship between submm flux density and SFR and, more generally, what galaxy properties a submm galaxy selection selects for, is needed. In other work we have combined hydrodynamic simulations and dust RT to show that major mergers of massive, gas-rich disk galaxies can reproduce the 850 μm flux densities (N10), CO properties (Narayanan et al. 2009), number densities (Hayward et al. 2011, Chapter 4), and intersection with the dust-obscured galaxy (DOG) population (Narayanan et al. 2010b) of SMGs. Motivated by the success of our simulations in reproducing a variety of SMG

properties, we use them here to quantify how submm flux density depends on SFR, L_{bol}, dust content, and geometry. The aim of this study is to clarify for what galaxy properties a submm selection criterion selects and to provide a discriminant among the different modes of star formation that could power SMGs.

2.2 Methods

We combine high-resolution GADGET-2 (Springel et al. 2001; Springel 2005) 3-D N-body/smoothed-particle hydrodynamics (SPH) simulations with the SUNRISE (Jonsson 2006; Jonsson et al. 2010) polychromatic Monte Carlo dust RT code in order to predict the submm flux densities of high-redshift isolated and merging disk galaxies. The simulations presented here, part of the larger suite presented in Chapter 4, are described in N10, so here we will only summarize and describe differences from that work. This combination of GADGET-2 and SUNRISE has been successfully shown to reproduce the SEDs/colors of local SINGS (Kennicutt et al. 2003; Dale et al. 2007) galaxies (Jonsson et al. 2010); local ULIRGs (Younger et al. 2009a); massive, quiescent, compact $z \sim 2$ galaxies (Wuyts et al. 2009, 2010); 24 μm-selected galaxies (Narayanan et al. 2010b); K+A/post-starburst galaxies (Snyder et al. 2011); and XUV disks (Bush et al. 2010), among other populations. The success of our approach at modeling diverse galaxy populations—both local and high-redshift—lends credibility to its application to modeling SMGs.

2.2.1   Hydrodynamic Simulations

GADGET-2[2] (Springel et al. 2001; Springel 2005) is a TreeSPH (Hernquist & Katz 1989) code that computes gravitational interactions via a hierarchical tree method (Barnes & Hut 1986) and gas dynamics via SPH (Lucy 1977; Gingold & Monaghan 1977). It conserves both energy and entropy (Springel & Hernquist 2002). The simulations include radiative heating and cooling as in Katz et al. (1996). Star formation is modeled via the volume-density dependent Kennicutt-Schmidt (KS) law (Kennicutt 1998a; Schmidt 1959), $\rho_{\mathrm{SFR}} \propto \rho_{\mathrm{gas}}^{1.5}$, with a minimum density threshold; this index is consistent with observations of $z \sim 2$ disks (Krumholz & Thompson 2007; Narayanan et al. 2008a, 2011a). The density threshold used is $n \sim 0.1$ cm^{-3}, much less than that of the dense molecular gas from which stars form ($n \sim 10^2 - 10^3$ cm^{-3}). For this reason, and because we do not track the formation of molecular gas, the KS law employed should be considered simply an empirically- and physically-motivated prescription to encapsulate physics we do not resolve. The SF prescription has been calibrated to reproduce the global K-S law (see Section 3 of Springel & Hernquist 2003). Recently, some authors (e.g., Hopkins et al. 2011) have presented simulations that resolve the density threshold for molecular gas formation; we plan to compare such simulations to our current simulations in future work.

The structure of the interstellar medium (ISM) is modeled via a two-phase sub-resolution model in which cold, dense clouds are embedded in a diffuse, hot medium (Springel & Hernquist 2003). This medium is pressurized by supernova

---

[2]A public version of GADGET-2 is available at `http://www.mpa-garching.mpg.de/~volker/gadget/index.html`.

feedback, which heats the diffuse ISM and evaporates the cold clouds (Cox et al. 2006b). Metal enrichment is calculated by assuming each gas particle behaves as a closed box. Black hole particles accrete via Eddington-limited Bondi-Hoyle accretion and deposit 5 per cent of their emitted luminosity—calculated from the accretion rate assuming 10 per cent radiative efficiency, $L_{\rm bol} = 0.1\dot{M}c^2$—to the surrounding ISM as thermal energy (Springel et al. 2005; Matteo et al. 2005). We refer the reader to the references given above for the full details of the GADGET-2 code and the sub-resolution models employed.

We focus on two simulations, one isolated disk and one major merger. We embed exponential disks with baryonic mass $4 \times 10^{11} M_\odot$ in $9 \times 10^{12} M_\odot$ dark matter halos described by a Hernquist (1990) density profile. The disks are initially 60 per cent gas and are scaled to $z \sim 3$ as described in Robertson et al. (2006a,b). The gravitational softening lengths are $200h^{-1}$ pc for the dark matter particles and $100h^{-1}$ pc for the star, gas, and black hole particles. We use 6×10^4 dark matter, 4×10^4 stellar, 4×10^4 gas, and 1 black hole particle per disk galaxy. For the major merger, we initialize two such disks on parabolic orbits with initial separation $R_{\rm init} = 5R_{\rm vir}/8$ and pericentric distance twice the disk scale length (Robertson et al. 2006b). The orbit we focus on is the 'e' orbit of Cox et al. (2006a). We have checked that the differences between quiescent star formation and starbursts are insensitive to orbit as long as a strong starburst is induced (some orbits do not induce strong starbursts, but those are irrelevant for the purpose of studying the differences between starbursts and quiescent star formation), and the larger suite of simulations used to derive the fitting functions includes a variety of orbits.

2.2.2 Radiative Transfer

Every 10 Myr we save snapshots of the GADGET-2 simulations and use the 3-D Monte Carlo dust RT code SUNRISE[3] (Jonsson 2006; Jonsson et al. 2010) in post-processing to calculate the SEDs of the simulated galaxies. While we will summarize the key features of SUNRISE here, we encourage the reader to see Jonsson (2006) and Jonsson et al. (2010) for full details. Except where noted, we use the fiducial parameters given in Jonsson et al. (2010). SUNRISE calculates the emission from the stars and AGN in the GADGET-2 simulations and the attenuation and re-emission from dust. STARBURST99 (Leitherer et al. 1999) SEDs are assigned to all star particles according to their ages and metallicities. Star particles present at the start of the GADGET-2 simulation are assigned ages assuming that their stellar mass was formed at a constant rate equal to the SFR of the initial snapshot and gas and stellar metallicities via a closed-box model, $Z = -y \ln f_g$, where f_g is the initial gas fraction and $y = 0.02$. Black hole particles are assigned the luminosity-dependent templates of Hopkins et al. (2007) by assuming that the bolometric luminosity of a black hole particle is $L_{\mathrm{bol}} = 0.1 \dot{M} c^2$, where $\dot{M}$ is the black hole accretion rate from the GADGET-2 simulations.

To calculate the dust density, and thus optical depth along a given line-of-sight, SUNRISE projects the GADGET-2 gas-phase metal density onto a 3-D adaptive mesh refinement grid using the SPH smoothing kernel. We have assumed 40 per cent of the metals are in dust (Dwek 1998; James et al. 2002). We use a maximum refinement level of 10, resulting in a minimum cell size of $55h^{-1}$ pc. By performing runs with

---

[3]SUNRISE is publicly available at `http://code.google.com/p/sunrise/`.

higher levels of refinement we have checked that the observed-frame submm flux density is converged to within 10 per cent. We use the Milky Way R=3.1 dust model of Weingartner & Draine (2001) as updated by Draine & Li (2007). Dust models with different FIR opacity will lead to different relationships between submm flux density and dust mass, but we show how to rescale for different values of the opacity in Equation 2.13.

Once the dust density grid is constructed and the input sources are assigned SEDs, SUNRISE performs Monte Carlo RT by randomly emitting photon packets from the source particles and randomly drawing interaction optical depths from the appropriate probability distribution. We use 10^7 photon packets total for each stage of the RT, having confirmed that this results in Monte Carlo noise of less than a few percent. The photon packets are scattered and absorbed by dust as they traverse the ISM. For each grid cell, the temperature of each dust species is calculated assuming the dust is in thermal equilibrium, and the dust re-emits the absorbed energy as a modified blackbody.

A SUNRISE feature key to this work is its treatment of dust self-absorption. In high-density regions, the dust can be opaque to its own emission, so the contribution of the dust emission to dust heating must be computed in addition to the contribution from stars and AGN. SUNRISE computes the equilibrium dust temperatures self-consistently by iteratively performing the transfer of the dust emission and the temperature calculation using a reference field technique similar to that of Juvela (2005). (The details of the SUNRISE implementation are in Jonsson et al. 2010 and Jonsson & Primack 2010.) This algorithm ensures accurate dust temperatures, and thus submm flux densities, even for the highly optically thick

central starbursts.

The results of the SUNRISE calculation are spatially resolved, multi-wavelength (we use only 120 wavelengths here because of memory constraints) SEDs observed from 7 cameras distributed isotropically in solid angle, though in this paper we only utilize the integrated flux densities in the SCUBA (Holland et al. 1999) and AzTEC (Wilson et al. 2008) bands. For the purpose of calculating observed flux densities we assume the simulated galaxies are at redshift $z = 2$.

Differences from Narayanan et al.

The primary difference between our simulations and those of N10 and Narayanan et al. (2010b) is the treatment of the ISM on sub-resolution scales. In order to model the effects of HII and photodissociation regions (PDRs), SUNRISE assigns star particles with ages less than 10 Myr SEDs from the HII region template library of Groves et al. (2008). The time-averaged fraction of solid angle obscured by the PDR, f_{PDR}, strongly affects the resulting attenuation and IR emission (for a detailed discussion see Groves et al. 2008). Narayanan et al. assumed $f_{\mathrm{PDR}} = 1$ (so that the young stars are completely obscured by PDRs for 10 Myr) in order to match the observed range of 850 μm flux densities. Furthermore, they neglected the dust associated with the cold phase of the Springel & Hernquist (2003) ISM model, typically $\gtrsim 30$ per cent of the total gas mass and $\gtrsim 90$ per cent of the gas mass in the central regions for snapshots classified as SMGs.

Motivated by concerns over applicability of the Groves et al. (2008) models to the extreme ISM densities and pressures encountered in our simulations, we set

$f_{\mathrm{PDR}} = 0$, eliminating all significant dust obscuration from the sub-resolution PDR model. Instead, we use the total gas density in the SPH simulations (i.e., both the diffuse and cold phases) to calculate the dust density. Since the dust mass implicit in the Groves et al. (2008) PDRs is not tied to the total dust mass of the simulated galaxy, it is possible that one can have more dust mass in the sub-resolution PDRs than is available in the galaxy. It is also possible that the sum of the dust mass in the PDRs is less than the total available in the cold phase of the sub-resolution ISM. Our treatment ensures that neither scenario can occur.

Our assumed ISM structure (cold phase volume filling factor of unity) is similar to what is observed for the dense cores of local ULIRGs (Scoville et al. 1991; Downes & Solomon 1998; Sakamoto et al. 1999, 2008; Papadopoulos et al. 2010). Furthermore, it leads to effective far-IR optical depths (inferred from modified blackbody fitting using $L_\nu \propto (1 - e^{-\tau_\nu}) B_\nu(T_d)$; see below for details) consistent with what is observed for local ULIRGs and SMGs, $\tau = 1$ at rest-frame $\lambda \sim 200 \mu$m for the simulations versus at rest-frame $\lambda \sim 200 - 270$ μm for local ULIRGs (Lisenfeld et al. 2000; Papadopoulos et al. 2010; Rangwala et al. 2011) and SMGs (Lupu et al. 2010; Conley et al. 2011) (but cf. Kovács et al. 2010). However, it is still important to note that the sub-resolution ISM structure is the key uncertainty in these calculations (Younger et al. 2009a). While unresolved clumpy dust can significantly affect the resulting SED (Witt & Gordon 1996; Városi & Dwek 1999), a more detailed treatment is beyond the scope of this work. The trends presented in this work should be qualitatively insensitive to the sub-resolution ISM assumption because, as explained below, the dominant drivers of the differences between the quiescent star formation and starburst cases are the contribution from stars formed

pre-burst to the luminosity at the time of the burst and the rapid gas consumption during the burst, both of which do not depend on the treatment of sub-resolution clumpy dust.

2.3 Results

Figure 2.1 shows the time evolution of the observed SCUBA 850 μm flux density (mJy), SFR ($M_\odot$ yr^{-1}; calculated by dividing the mass of stars formed in the last 10 Myr of the simulation by 10 Myr), bolometric luminosity L_{bol} ($L_\odot$), initial fraction of baryonic mass that is gas f_g, dust mass M_d ($M_\odot$), and dust temperature[4] T_d (K) for the isolated disk galaxy (*left*) and merger (*right*), where all quantities except f_g have been normalized by dividing by their maximum values, given in the legend. When calculating the observed flux density we have assumed the simulated galaxy is at $z = 2$. The disk is somewhat unstable initially; after the disk settles, L_{bol}, SFR, and S_{850} decrease steadily with time. Over the 2 Gyr of the simulation the gas fraction decreases from 60 per cent to 20 per cent. As the gas is consumed, the SFR,

---

[4]We have calculated T_d by fitting the modified blackbody $L_\nu \propto (1 - \exp[-(\nu/\nu_0)^\beta])B_\nu(T_d)$ to the rest-frame 20 - 1000 μm SED, allowing all parameters to vary. Here ν_0 is the frequency at which the effective optical depth $\tau_\nu = 1$. We have assumed the opacity has a power-law dependence on ν in the IR, $\kappa_\nu \propto \nu^\beta$. Note we have not used the optically thin form $L_\nu \propto \nu^\beta B_\nu(T_d)$, as is almost always done, because we find that the first form, which does not assume optical thinness, provides a significantly better fit to our SEDs. This is because our simulated SMGs can be optically thick out to rest-frame $\gtrsim 100$ μm, which is supported by recent *Herschel* observations from Lupu et al. (2010) and Conley et al. (2011), who found $\tau \sim 1$ at rest-frame $\lambda \sim 200$ μm. Our fitting procedure gives systematically higher T_d (by as much as 20 K) than when the optically thin form is used, so comparisons of our dust temperatures to other results should take this into account.
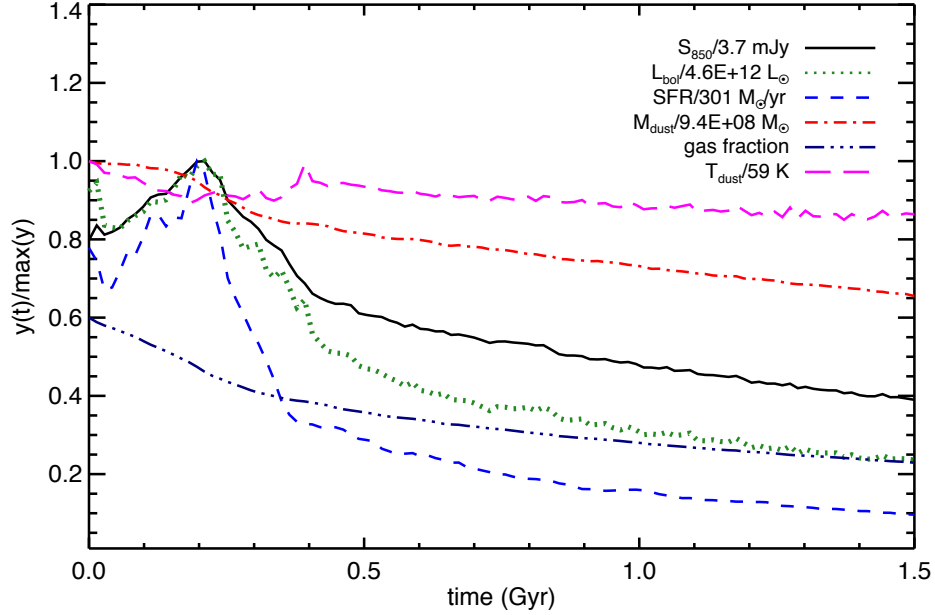
Figure 2.1.—: The isolated disk simulation's observed-frame integrated SCUBA 850 μm flux density (mJy, assuming $z = 2$; solid black) measured from one of the seven viewing angles, bolometric luminosity ($L_\odot$; dotted green), SFR ($M_\odot$ yr^{-1}; dashed blue), dust mass M_d ($M_\odot$; dash dot red), gas fraction f_g (dash dot dot dot navy), and dust temperature (derived from SED fitting) T_d (K; long dashed magenta) versus time (Gyr). Except for f_g, the quantities have been normalized by dividing by their maximum values, given in the legend. Once the disk reaches equilibrium, S_{850}, $L_{\rm bol}$, SFR, and f_g concomitantly decrease exponentially with time as the gas is converted into stars. M_d also decreases, but by less than a factor of 2, because the decreasing f_g is offset by the increasing metallicity of the gas. T_d decreases from ~ 60 K to ~ 50 K.

and thus L_{bol}, both decrease, by factors of ~ 10 and ~ 5, respectively. S_{850} decreases by $\sim 2.5\times$. M_d also decreases as a result of the decrease in gas mass, but only by ~ 40 per cent because the decrease in gas mass is partially mitigated by metal enrichment of the gas from star formation, as the metallicity doubles over the course of the simulation. While it may seem counter-intuitive that M_d decreases with time, for a simple closed-box model assuming dust traces metals and constant yield it can be shown (Edmunds & Eales 1998) that for $f_g \lesssim 0.6$ the dust mass increases at most by ~ 0.1 dex, and it decreases monotonically with f_g for $f_g \lesssim 0.4$. Furthermore, the preferential consumption of metal-enriched gas that occurs in our models should result in a lower dust mass than the simple closed-box case of Edmunds & Eales (1998), which assumes perfect mixing.

The behavior of the merger (Figure 2.2) is qualitatively different from that of the isolated disk. Initially, SFR, L_{bol}, and S_{850} are roughly equal to the sum of the isolated values for the two progenitor disks, because the disks are too gas-rich at first passage ($t \sim 0.1$ Gyr) for tidal torques to cause a strong starburst, as a significant stellar bar is required for the gas to efficiently loose angular momentum (Hopkins et al. 2009b). However, at final coalescence of the two disks (~ 0.7 Gyr) tidal torques induce a strong starburst, causing the SFR to increase by a factor of $\gtrsim 16$. The peak of the burst is very narrow and significant luminosity from previously formed stars remains, so the bolometric luminosity increases by a much smaller amount ($\sim 7\times$) than the SFR. Moreover, as the gas is rapidly consumed in the starburst, M_d plummets by a factor of 3. Along with the more compact geometry, the decreased dust mass causes the SED to become hotter, with T_d increasing from ~ 50 K to ~ 65 K. The increase in dust temperature during the starburst is qualitatively consistent

with observations, as local ULIRGs (i.e., merger-induced starbursts) tend to have hotter dust temperatures (~ 42 K) than less luminous (quiescent) galaxies (~ 35 K) (Clements et al. 2010). The increased T_d partially offsets the increase in S_{850} caused by the increased luminosity. The combination of the significant pre-burst contribution to L_{bol}, the small mass of stars formed in the burst, and the increased T_d cause S_{850} to increase by $\lesssim 2\times$ even though the SFR increases by $\gtrsim 16\times$ in the burst.

Figure 2.2.—: Same as Figure 2.1, but for the major merger simulation. All quantities are totals for the two-disk system. Compared to the isolated disk the time evolution is more complex: Initially S_{850}, SFR, $L_{\rm bol}$, and M_d are roughly just the sums of the values for the isolated progenitor disks. At first passage ($t \sim 0.1$ Gyr), the SFR is not elevated much beyond the baseline rate because the disks are very gas-rich and thus lack the massive stellar bar needed to efficiently remove angular momentum from the gas (Hopkins et al. 2009b). As the two disks coalesce ($t \sim 0.7$ Gyr), tidal torques cause a burst of star formation, resulting in the sharp increase in the SFR ($\gtrsim 16\times$), $L_{\rm bol}$ ($\sim 7\times$), and S_{850} ($\lesssim 2\times$) at ~ 0.7 Gyr. The increase in $L_{\rm bol}$ is much less than that boost in SFR because the luminosity of the stars formed during the burst is only ~ 6x the luminosity from stars already formed pre-burst. T_d increases sharply from ~ 50 K to ~ 65 K because of the strong increase in $L_{\rm bol}$, concurrent decrease in M_d, and more compact geometry. This mitigates the increase in S_{850} that occurs from increased $L_{\rm bol}$. The second, minor peak in $L_{\rm bol}$, which occurs ~ 40 Myr after the peak SFR, corresponds to the peak AGN luminosity. Pre-coalescence, f_g decreases at a rate similar to the isolated disk case. At coalescence the gas is rapidly consumed in the central starburst. M_d decreases by a factor of 4.5, with the bulk of the decrease occurring at coalescence.
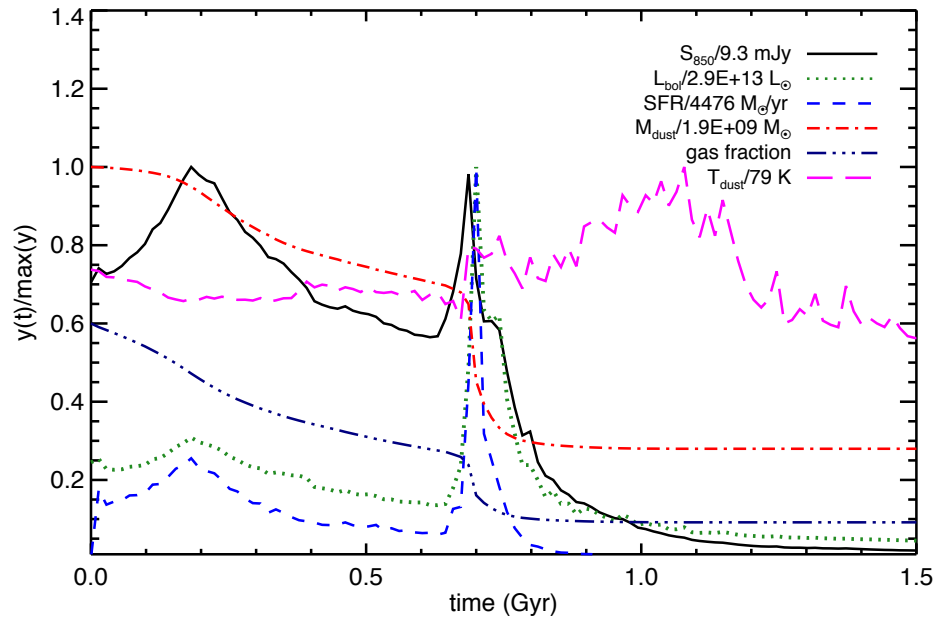
Figure 2.2 (Continued).

2.3.1 The Relationship Between Submm Flux Density and SFR

Figures 2.3 and 2.4 show the observed SCUBA 850 μm flux density in mJy versus SFR in units of $M_\odot$ yr^{-1} for the isolated disk and major merger, respectively, viewed from all of the 7 cameras. The submm flux density of the isolated disk is tightly correlated with SFR, increasing monotonically as SFR$^{0.4}$ (see best-fit curve). This correlation occurs because once the disk settles, L_{bol} and SFR both decrease exponentially with time. The dust mass also decreases, but by less than a factor of 2 over the 2 Gyr of the simulation (see Figure 2.1). Both the decreased luminosity and the decreased dust mass cause the submm flux density to decrease.

The case for the major merger (Figure 2.4) is again qualitatively different. Pre-coalescence, the relationships are essentially the same as for the isolated disks. This is because S_{850}, SFR, L_{bol}, and M_d at this stage are essentially just the sum of the two disks' isolated values, and multiplying all quantities by the same factor (2 for the major merger here) does not change the power-law index. The normalization of the relation is ~ 1.5 greater for the merging disks than for the isolated disk. The reason is as follows: An isolated disk of SFR s has $S_{850} = As^{0.4}$, where A is the normalization of the SFR-S_{850} relation for the isolated disk. For a non-interacting system of two identical disks to have total SFR equal to that of the single isolated disk, the two disks must each have SFR $= 0.5s$. Thus the total submm flux density of the system is the submm flux density of a single disk of SFR $0.5s$, which we calculate using the isolated relation, multiplied by 2. This is $S_{850} = 2A(0.5s)^{0.4} = 1.5As^{0.4}$. Therefore the normalization of the SFR-S_{850} relation for the sum of two identical
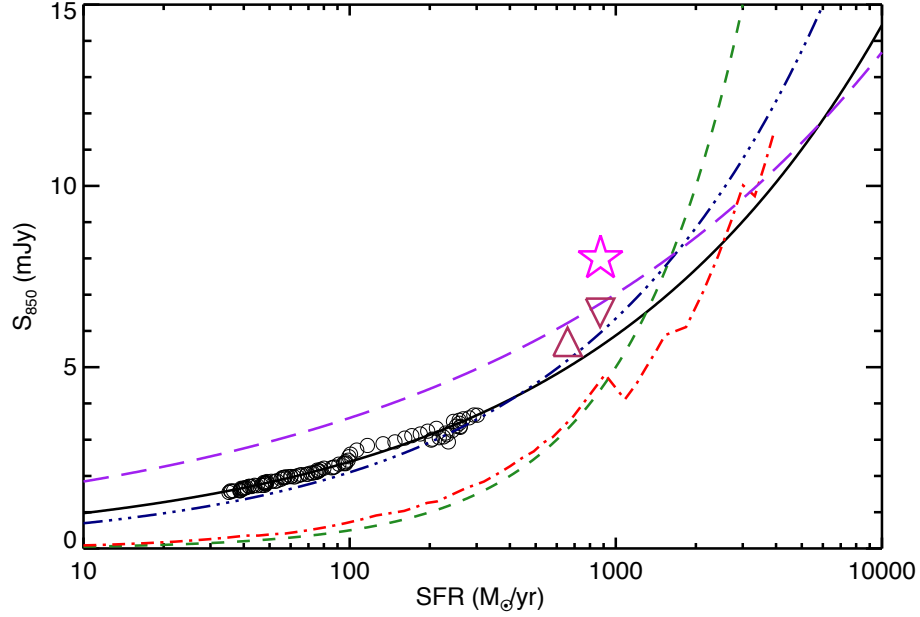
Figure 2.3.—: Integrated SCUBA 850 μm flux density (mJy) versus SFR ($M_\odot$ yr^{-1}) for the isolated disk viewed from all of the 7 different cameras. The best-fit power law (solid line), linear relation $S_{850} = 0.5$ mJy (SFR/100 $M_\odot$ yr^{-1}) (green dashed line; normalization from Neri et al. 2003 and Equation 2.15), the relation for the Chary & Elbaz (2001) templates (red dash dot), the Magnelli et al. (2010) relations for their entire sample (navy dash dot dot dot) and excluding the lensed SMGs (purple long-dashed), the value for the Pope et al. (2008) composite SED (magenta star), and the median (maroon upward-pointing triangle) and mean (maroon downward-pointing triangle) from Michałowski et al. (2010a) are also shown. The submm flux density is tightly correlated with both SFR and $L_{\rm bol}$, increasing essentially monotonically as SFR$^{0.4}$.
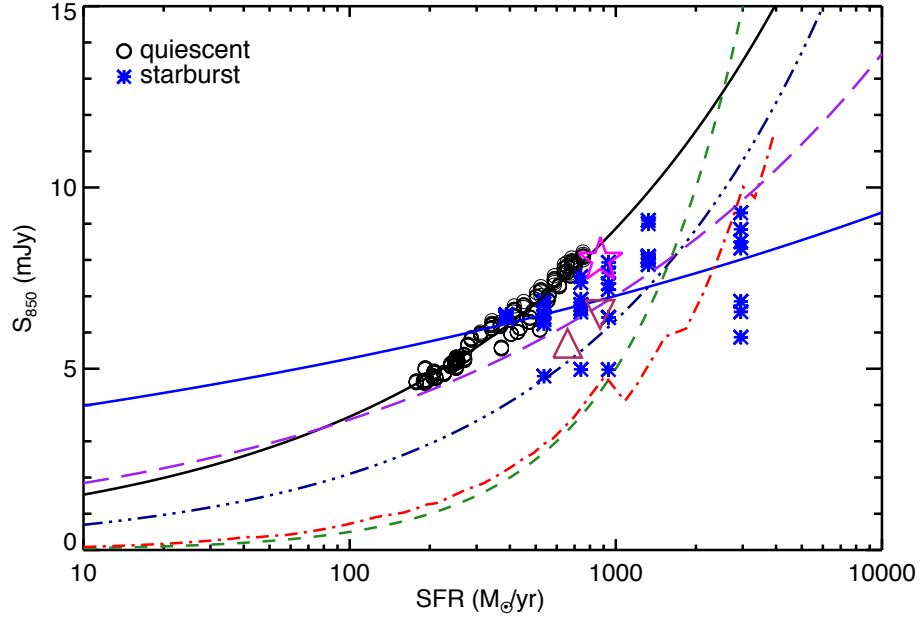
Figure 2.4.—: Same as Figure 2.3, but for the major merger. Pre-coalescence (black open circles) the power-law index is the same as for the isolated disks because the SFR, L_{bol}, dust mass, and submm flux density are essentially two times the isolated disk values (see Figure 2.2), so only the normalization changes. During the coalescence-induced starburst (blue asterisks), the relationship is significantly shallower, with submm flux density scaling as $\text{SFR}^{0.1}$. This is due to two effects: 1. The stars formed before the peak of the starburst contribute significantly to L_{bol} at the starburst peak, so $L_{\text{bol}} \not\propto \text{SFR}$. 2. The rapid gas consumption during the burst causes M_d to plummet, and the decrease in dust mass and more compact geometry cause T_d to increase sharply, mitigating the increase of S_{850} caused by the increased L_{bol}.

disks is 1.5 times that of the individual disk relation. This fact has important implications for the SMG population, which we discuss in Section 2.4.2.

On the other hand, the merger-induced burst is significantly less effective at boosting the submm flux density. For a given SFR, the submm flux density is significantly less than for the isolated and pre-coalescence (quiescent star formation) cases. This is because of two reasons: 1. The sharp decrease in dust mass and more compact geometry cause an increase in dust temperature, mitigating the increase in S_{850} caused by increased $L_{\rm bol}$. 2. The significant luminosity contributed by stars formed before the starburst causes $L_{\rm bol}$ to increase sub-linearly with SFR.[5] During the burst, $L_{\rm bol} \approx L_{\rm pre-peak} + \alpha\,{\rm SFR}$, where α is the luminosity per unit SFR for an instantaneous burst. Thus $L_{\rm bol}$ is not proportional to SFR when $L_{\rm pre-peak}$ is non-negligible compared to the luminosity of newly-formed stars, which is the case here because a relatively small fraction of the stellar mass is formed in the sharp, short-duration burst. For the burst, the submm flux density scales as ${\rm SFR}^{0.1}$ (see best-fit curve), significantly more weakly than for quiescent star formation, and the ratio of submm flux density to SFR is significantly lower. Hence, bursts of star formation are significantly less effective at boosting submm flux density than one might naively expect.

It is interesting to note that, during the starburst, the observed submm flux density can vary significantly with viewing angle (e.g., for the snapshot with peak SFR, S_{850} varies in the range $\sim 6 - 9$ mJy depending on the camera). We have

---

[5]In principle the AGN can also cause such an effect, but for snapshots classified as SMGs the typical AGN contribution to the IR luminosity is $\lesssim 10$ per cent, so the AGN is sub-dominant.

confirmed that this variation is due to dust self-absorption: the central regions of the starburst can be so obscured that even the IR emission is significantly anisotropic. As a result, the dust temperature, and thus submm flux density, depends on the line-of-sight. Though we will not explore this possibility further in this work, we note that differences in viewing angle may be enough to account for the spread of dust temperatures observed for high-z ULIRGs. In other words, from one viewing angle a simulated galaxy may be identified as an SMG whereas from another viewing angle the same galaxy could be identified as a hot-dust-dominated ULIRG undetected in the submm.

Figures 2.3 and 2.4 also show the linear relation $S_{850} = 0.5$ mJy $(\mathrm{SFR}/100\ M_\odot\ \mathrm{yr}^{-1})$ (green dashed lines; obtained using the $S_{850} - L_{\mathrm{IR}}$ relation from Neri et al. 2003 and Equation 2.15), the relation for the Chary & Elbaz (2001) templates (red dash dot), the Magnelli et al. (2010) relations for their entire sample (navy dash dot dot dot) and excluding the lensed SMGs (purple long-dashed), the value for the Pope et al. (2008) composite SED (magenta star), and the median (maroon upward-pointing triangle) and mean (maroon downward-pointing triangle) from Michałowski et al. (2010a). The Chary & Elbaz (2001) and Pope et al. (2008) values were obtained by redshifting the templates to $z = 2$ and converting L_{IR} of each template to SFR using Equation (2.15). We used Equation (2.15) to convert the Magnelli et al. (2010) relations from L_{IR} to SFR.

The typical values from Pope et al. (2008) and Michałowski et al. (2010a) are consistent with the data from our major merger simulation. As explained above, the relations we find are much shallower than linear, so the Neri et al. (2003) relation differs significantly from our relations for both the quiescent and starburst modes.

The Chary & Elbaz (2001) templates are also very discrepant because high-redshift ULIRG SEDs are often better fit by local templates appropriate for less luminous, colder galaxies (e.g., Pope et al. 2006; Dannerbauer et al. 2010; Rex et al. 2010). The Magnelli et al. (2010) relations agree better with our simulations: for the full sample, $S_{850} \propto \mathrm{SFR}^{0.48}$. This is a slightly steeper relation than what we find for quiescent disks and significantly steeper than that for starbursts. When the six lensed SMGs are removed from their sample, Magnelli et al. find $S_{850} \propto \mathrm{SFR}^{0.29}$. The power-law index of this relation is less than that for our quiescent disks but greater than that for our starbursts. The lensed SMGs tend to be intrinsically fainter and thus less likely to be strong starbursts than the non-lensed population, so it is reasonable that inclusion of the lensed SMGs leads to a steeper relation. While it is interesting that the Magnelli et al. relation for the unlensed SMGS is crudely consistent with what we expect for a mixed population, one should not over-interpret this comparison. As we will discuss below, S_{850} cannot be determined solely from SFR because the dust mass plays a significant role also. However, a robust conclusion that should be drawn from Figure 2.4 is that, in the simulations, the starburst mode is less efficient at boosting submm flux than the quiescent mode.

2.3.2 Dependence of (Sub)mm Flux Density on SFR, L_{bol}, and M_d

For a given SFR, galaxies of different masses tend to also have different dust masses; thus the normalization of the S_{850}-SFR relation varies for different mass simulations though the scalings are similar. As a result, one cannot calculate the submm flux

density given only the SFR, but it is possible to parameterize the submm flux density as a function of SFR and dust mass. Since much of the discrepancy in the S_{850}-SFR relations for quiescent star formation and starbursts is caused by the rapid decrease in dust mass during the starburst, we expect that including dust mass in our parameterization will eliminate much of the difference between quiescent and starburst star formation modes. We have analyzed the full set of simulations from our SMG number counts work (Chapter 4), which includes a range of progenitor disk baryonic masses ($\sim 3.5 \times 10^{10} - 4 \times 10^{11} M_\odot$) and mass ratios ($\sim 0.1 - 1$), fitting the (sub)mm flux density as a power law in both SFR and dust mass. Both the quiescent and starburst phases are included. Perhaps surprisingly, the following relations (for simulated galaxies placed at redshift $z = 2$) hold to within ~ 0.1 dex for all but a few outliers over the range 0.5 mJy $\lesssim S_{850} \lesssim 15$ mJy:

$$
\begin{aligned}
S_{850} &= 0.65 \text{ mJy} \left(\frac{\text{SFR}}{100 \ M_\odot \ \text{yr}^{-1}} \right)^{0.42} \left(\frac{M_d}{10^8 M_\odot} \right)^{0.58} \\
S_{1.1} &= 0.30 \text{ mJy} \left(\frac{\text{SFR}}{100 \ M_\odot \ \text{yr}^{-1}} \right)^{0.36} \left(\frac{M_d}{10^8 M_\odot} \right)^{0.61},
\end{aligned}
\tag{2.1}
$$

where S_{850} and $S_{1.1}$ are the fluxes in the SCUBA 850 μm and AzTEC 1.1 mm bands, respectively.

Note that the SFR exponent in these relations is similar to that for the S_{850}-SFR relation for quiescent SF (~ 0.4). As explained in Section 2.3.1, the sharp decrease in dust mass during the starburst is one of the main reasons the S_{850}-SFR relation is much shallower for starbursts than for quiescent SF. Adding M_d as a parameter effectively decouples this effect; in other words, *for fixed dust mass* the S_{850}-SFR relations for the two SF modes are much more similar than when the evolution of the dust mass is taken into account. Remaining differences caused by the contribution

from stars formed pre-burst to the burst luminosity, AGN contribution, geometry, and other factors prevent Equation (2.1) from recovering S_{850} exactly, but the small scatter suggests that these factors are subdominant.

We can also fit the (sub)mm flux density as a function of L_{bol} and M_d:

$$S_{850} = 0.40 \text{ mJy} \left(\frac{L_{\mathrm{bol}}}{10^{12} L_\odot} \right)^{0.52} \left(\frac{M_d}{10^8 M_\odot} \right)^{0.60} \qquad (2.2)$$

$$S_{1.1} = 0.20 \text{ mJy} \left(\frac{L_{\mathrm{bol}}}{10^{12} L_\odot} \right)^{0.46} \left(\frac{M_d}{10^8 M_\odot} \right)^{0.63}.$$

These fitting functions are accurate to within ~ 0.15 dex. Replacing L_{bol} with the bolometric IR luminosity L_{IR} yields a similar result. Figures 2.5 and 2.6 show how well these fitting functions reproduce the (sub)mm flux density of our simulated galaxies. It is discussed in more detail in Section 2.3.2.

Relations for an Optically Thin Modified Blackbody

It is instructive to compare the above relations to those for a single-temperature mass of dust transparent to its own emission, the model which is implicit in the standard method of fitting a modified blackbody to the IR SED. For a mass of dust in thermal equilibrium with temperature T_d we can express the submm flux density as a function of dust bolometric luminosity L_d and dust mass M_d or SFR and M_d. Assuming $z = 2$ and far-IR spectral index $\beta = 2$, the relations are (see the Appendix for a derivation)

$$S_{850} = 1.4 \text{ mJy} \left(\frac{\text{SFR}}{100 \ M_\odot \ \text{yr}^{-1}} \right)^{1/6} \left(\frac{M_d}{10^8 M_\odot} \right)^{5/6} \qquad (2.3)$$

and

$$S_{850} = 1.4 \text{ mJy} \left(\frac{L_d}{10^{12} L_\odot} \right)^{1/6} \left(\frac{M_d}{10^8 M_\odot} \right)^{5/6}. \qquad (2.4)$$
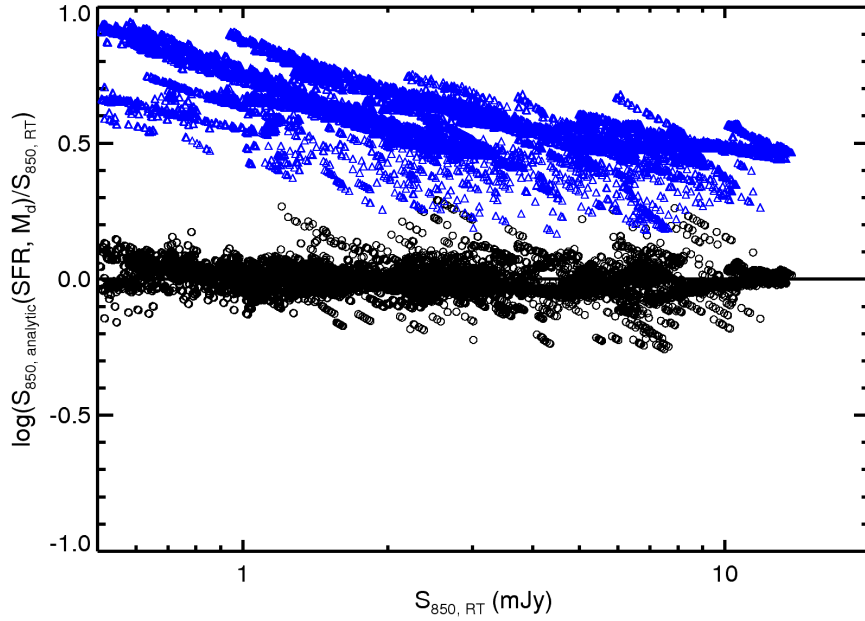
Figure 2.5.—: Logarithm of the ratio of the submm flux density calculated using one of the analytic forms ($S_{850,\text{analytic}}$) to the submm flux density calculated through the full RT ($S_{850,\text{RT}}$) versus $S_{850,\text{RT}}$ for all time snapshots of our simulated galaxies. Black circles show the ratio when $S_{850,\text{analytic}}$ is calculated from the SFR and M_d of our simulated galaxies using Equation (2.1). Blue triangles show the ratio when the optically thin modified blackbody model (Equation 2.3) is used. The line $S_{850,\text{analytic}} = S_{850,\text{RT}}$ is shown to guide the eye.
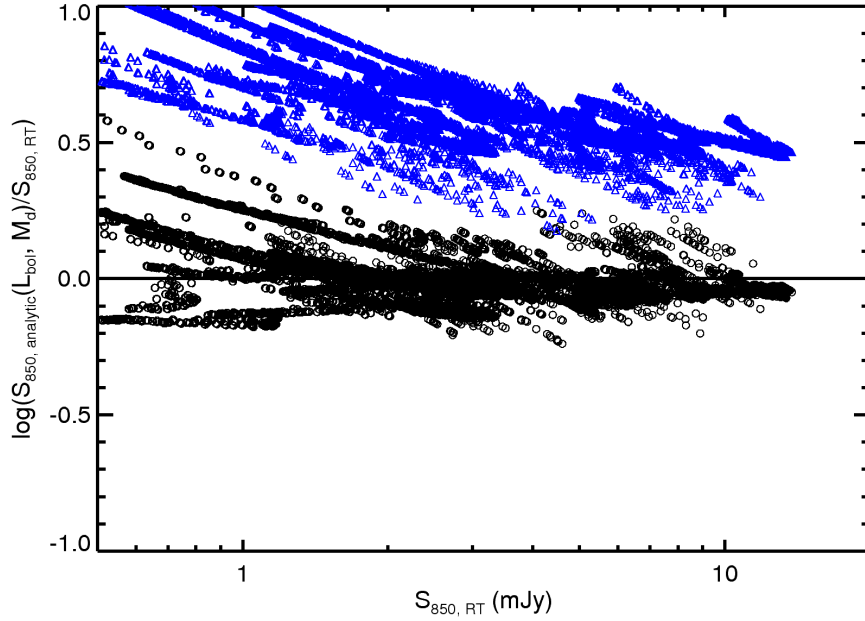
Figure 2.6.—: Same as Figure 2.5, except now the black circles show the values when Equation (2.2) is used to calculate the submm flux density from L_{bol} and M_d of the simulation snapshots, and the blue triangles show the values when Equation (2.4) is used, assuming $L_{\mathrm{bol}} \approx L_d$. In both cases the simple optically thin modified blackbody model overpredicts the submm flux density by $\gtrsim 0.3$ dex for the simulated SMGs, and the overprediction is worse for lower S_{850}.

These should be compared to Equations (2.1) and (2.2), respectively, by assuming $L_{\rm bol} \approx L_d$ (i.e., the luminosity emitted by stars and AGN is completely absorbed by dust), which is a reasonable approximation for snapshots classified as SMGs ($S_{850} > 3$ mJy). The submm flux depends only weakly on redshift for the redshift range of interest ($1 \lesssim z \lesssim 5$), scaling as $(1 + z)^{\beta-1} D_A^{-2}$, where D_A is the angular diameter distance at redshift z (see Equation 2.13).

**Comparison of the Relations to the Full Radiative Transfer**

Figures 2.5 and 2.6 show the logarithm of the ratio of the submm flux density calculated using the above equations ($S_{850,\rm analytic}$) to the submm flux density calculated through the RT ($S_{850,\rm RT}$) versus $S_{850,RT}$. Figure 2.5 shows the results when Equations (2.1, black circles) and (2.3, blue triangles) are used to calculate S_{850} from SFR and M_d. Figure 2.6 shows the results when $L_{\rm bol}$ and M_d are used instead, with the black circles corresponding to Equation (2.2) and the blue triangles Equation (2.4). The fitting functions derived from the simulations are able to reproduce S_{850} from SFR ($L_{\rm bol}$) and M_d to within ~ 0.1 (0.15) dex. The simple modified blackbody model tends to overpredict the submm flux density by $\gtrsim 0.3$ dex; the typical over-prediction is ~ 0.5 dex (a factor of 3). (Note that the corresponding uncertainties in SFR, $L_{\rm bol}$, and M_d for fixed observed submm flux density would be less because the submm flux density scales with these quantities sublinearly.) Furthermore, the error in the prediction correlates with SFR ($L_{\rm bol}$) and dust mass because of the differences in the power-law indices for the fitting functions and the modified blackbody relations.

The optically thin modified blackbody model fails for multiple reasons. From SED fitting we find that the simulated galaxies can have effective optical depth $\tau > 1$ out to rest-frame ~ 200 μm. For fixed dust temperature, the optically thin assumption will result in an overestimate of the luminosity density at wavelengths for which $\tau \gtrsim 1$ because $(1 - \exp[-(\nu/\nu_0)^{\beta}]) < (\nu/\nu_0)^{\beta}$ for all $\nu > 0$. Thus Equation (2.7) will overestimate L_d for fixed T_d and M_d. If L_d and M_d are fixed, the dust temperature will be *underestimated* when optical thinness is assumed, and, therefore, the submm flux density will be overestimated. Also, $L_d \approx L_{\rm bol}$ is less accurate an approximation for the faintest sources than for the brightest because $L_d/L_{\rm bol}$ increases with $L_{\rm bol}$ (Jonsson et al. 2006). If $L_d < L_{\rm bol}$, the assumption that $L_d \approx L_{\rm bol}$ will overestimate L_d and thus overestimate the submm flux density; this may explain why the overprediction is worse for lower S_{850}. Finally, we have seen above that the assumption $L_{\rm bol} \propto$ SFR is invalid during the burst.

2.4 Discussion

We have demonstrated that the submm flux density of a galaxy scales differently with SFR for quiescent star formation and starbursts. The ratio of sub-mm flux density to SFR is significantly less for merger-induced bursts than for quiescent star formation. This is because of the rapid decrease in dust mass and more compact geometry during the starburst, which causes the SED to become hotter, and the significant contribution from stars formed pre-burst to the luminosity during the burst, which makes the luminosity increase by a much smaller factor than the SFR. As a result, merger-induced starbursts are less efficient at boosting submm flux

density than one might naively expect.

Our results have a number of important implications; we discuss these now.

2.4.1 Predicting (Sub)mm Flux Densities from Models

One implication of this study is that, at a fixed redshift, the galaxies with highest submm flux density are not necessarily those with the highest bolometric luminosities or SFRs. Thus theoretical models, be they simulations or semi-analytic, must explicitly calculate the submm flux density of their simulated galaxies in order to select which are SMGs as opposed to simply selecting the most rapidly star-forming or most luminous objects. However, the computational expense required to self-consistently calculate the submm flux density limits this approach to idealized, non-cosmological simulations (as done here), individual galaxies excised from cosmological zoom-in simulations, or semi-analytic models in which various simplifying assumptions must be made. As an alternative to performing RT, cosmological simulations and semi-analytic models can use the relations among (sub)mm flux density, SFR or bolometric luminosity, and dust mass presented herein (Equations 2.1 and 2.2) to assign (sub)mm flux density to simulated galaxies. Additionally, observers can use the relations to estimate the instantaneous SFR given (sub)mm flux density and dust mass (obtained from fitting the IR SED using the full modified blackbody as we have done or by measuring the gas mass and assuming a dust-to-gas ratio; ignoring uncertainties on (sub)mm flux density, a dust mass accurate to a factor of 2 gives SFR accurate to a factor of 3).

2.4.2 Heterogeneity of the SMG Population

These results also imply that the SMG population is heterogeneous. We have seen that it is possible for a quiescently star-forming disk to have submm flux density equal to that of a merger with much higher SFR (Figure 2.4). Furthermore, since the scaling of submm flux density with SFR is sublinear, adding two equal disks (and thus doubling the dust mass and SFR of the system) increases the submm flux density more than simply boosting the SFR by a factor of 2; Equation (2.1) shows that SFR would have to be boosted by $5\times$ to achieve a $2\times$ boost in submm flux density if dust mass is kept constant. When the sharp increase in dust temperature during the starburst and the narrowness of the burst are accounted for the effect becomes even stronger: in Figure 2.1 we see that a $\gtrsim 16\times$ increase in SFR gives a $\lesssim 2\times$ increase in submm flux density.

The single-dish submm telescopes used for wide-field surveys of SMGs have beam sizes $\gtrsim 15''(\gtrsim 130$ kpc at $z = 2)$. Thus, during a merger the two progenitor galaxies will spend a considerable amount of time within the area of the beam. From the above arguments, we see that this is a very efficient way to create an SMG, but this contribution has been relatively unappreciated. We argue that the SMG population attributable to mergers is bimodal: some are merger-induced starbursts and some are two (or more) infalling disks (normal galaxies that are not yet interacting strongly) blended into one submm source ("galaxy-pair SMGs").[6] Note

---

[6]Wang et al. (2011) recently presented high-resolution submm continuum images of two SMGs which were previously identified as single sources but are resolved as 2 or 3 distinct submm sources in their images. The sources are at significantly different redshifts and thus physically unrelated. Our galaxy-pair SMGs are also two

also that not only major mergers but also favorably oriented minor mergers (see, e.g., Cox et al. 2008; Hopkins et al. 2009b) can contribute to the SMG population.

Furthermore, the most massive, rarest "isolated disks", and even small groups, may also contribute; we expect this contribution to be subdominant because SMGs are on the exponential tail of the mass function, but we defer a precise determination of their contribution to future work. Though both the merger-induced starburst and galaxy-pair populations are mergers, only in the former is the star formation merger-driven (and only partially, as the baseline star formation that would occur in the disks even if they were not interacting is significant). Given that the physically meaningful property of local ULIRGs is not that their IR luminosities are $\geq 10^{12} L_\odot$ but that they are powered by merger-driven star formation and AGN, only the merger-driven starburst category of SMGs should be considered physically analogous to local ULIRGs.

The observational signatures and physical implications of this bimodality will be discussed in future work. Here we simply note that the galaxy-pair contribution is supported observationally by the frequency of multiple radio (Ivison et al. 2002, 2007; Chapman et al. 2005; Younger et al. 2009c), 24 μm (Pope et al. 2006), and 350 μm (Kovács et al. 2010) counterparts to SMGs; by CO interferometry showing that a large fraction of SMGs are resolved binaries (Tacconi et al. 2006, 2008; Bothwell

sources blended into one, but they are distinct from the type of SMGs Wang et al. observed because they are merging and thus physically connected. Both types of blended sources are potentially important SMG subpopulations that complicate our understanding of SMGs, and it is crucial to understand the relative contributions of merger-induced starbursts, galaxy pairs/infall-stage mergers, quiescently star-forming disks, and physically unrelated, blended sources.

et al. 2010; Engel et al. 2010); and by the SMGs that have morphologies that do not resemble merger remnants (e.g., Bothwell et al. 2010; Carilli et al. 2010; Ricciardelli et al. 2010; Targett et al. 2011).[7]

2.4.3 SMG Masses

The masses of SMGs are hotly debated, with different authors finding masses discrepant by $\sim 6\times$ for the same SMGs (Michałowski et al. 2010a,b; Hainline et al. 2010). Accurate masses are important in order to test potential evolutionary relationships among SMGs and other galaxy classes (e.g., Brodwin et al. 2008; Bussmann et al. 2009a,b; Narayanan et al. 2010b; Rothberg & Fischer 2010) and to check that number densities of SMGs are consistent with observed stellar mass functions. Stellar mass determinations from SED fitting are limited by uncertainties in stellar evolution tracks, the initial mass function, star formation histories, dust attenuation, and AGN contamination. Since our models use star formation histories, attenuation (from the geometry of stars, AGN, and dust), and AGN components that originate directly from the hydrodynamic simulations instead of the standard assumptions—e.g., instantaneous burst or exponential star formation histories, the Calzetti attenuation law (Calzetti et al. 1994, 2000; Calzetti 1997)—we can provide constraints on SMG stellar masses that are complementary to those derived from SED fitting.

Given the inefficiency of bursts at boosting submm flux density that we

---

[7]Note, however, that the Bothwell et al. (2010) and Carilli et al. (2010) objects that resemble disk galaxies may in fact be the molecular disks that re-form rapidly after a gas-rich merger (Narayanan et al. 2008b; Robertson & Bullock 2008).

have demonstrated above, SMGs must be very massive, because smaller galaxies undergoing even very strong bursts cannot make SMGs. Our models require $M_\star \gtrsim 6 \times 10^{10} M_\odot$ to reach $S_{850} \gtrsim 3$ mJy, and typical masses are higher. The area of the $S_{850} - M_\star$ plot spanned by our models agrees well with the observationally derived values of Michałowski et al. (2010a). About half of the Hainline et al. (2010) values lie in the area spanned by our models, whereas the other half have lower masses. However, the single-component star formation histories assumed by Hainline et al. may cause the stellar masses to be underestimated by $\sim 2\times$, which would resolve much of the discrepancy. A detailed comparison of the mass estimates will be presented in Michałowski et al. (2011).

2.4.4 SMG Duty Cycles

Understanding the duty cycle of SMGs is important for predicting submm counts from models, quantifying the contribution of SMGs to stellar mass buildup, and interpreting star formation efficiencies of SMGs. Since the submm flux density depends on luminosity heating the dust, dust mass, and geometry, the submm duty cycle depends on the same factors. As we have seen, the starburst induced at merger coalescence causes a sharp peak in SFR, L_{bol}, and submm flux density. However, the duty cycle is limited because of the sharp cutoff in SFR, and thus drop in L_{bol}, after the burst and the significant drop in dust mass that occurs as highly enriched gas is consumed in the burst.

Since the submm flux density depends more strongly on dust mass than either SFR or L_{bol} (see Equations 2.1 and 2.2), it is more efficient if one can keep more

dust around at the expense of lower SFR. The quiescent star formation mode does exactly this. As a result, the galaxy-pair phase (discussed in Section 2.4.2) adds significantly to the submm duty cycle. Figure 2.1 shows that the galaxy-pair phase has a longer submm duty cycle than the burst, though the lack of smooth accretion in our simulations—and thus need for starting with very high initial gas fractions—complicates a precise determination of the relative flux densities and duty cycles of the galaxy-pair and starburst phases. Regardless, it is clear that the galaxy-pair phase increases the SMG duty cycle significantly, alleviating some of the tension between the submm counts estimated from high-redshift major merger rates and short (~ 100 Myr) starburst duty cycles by Davé et al. (2010) and the observed submm counts. Inclusion of both SMG populations is crucial to match the observed SMG number counts without resorting to a top-heavy initial mass function (see Chapter 4).

2.4.5 Implications for IR SED Fitting

One reason the single-temperature, optically thin modified blackbody fails is that the effective optical depth of our simulated SMGs can be greater than 1 out to rest-frame ~ 200 μm. This is consistent with the effective optical depths derived by Lupu et al. (2010) and Conley et al. (2011) when they fit a general modified blackbody (i.e., not assuming optical thinness) to the IR SEDs of their SMGs. By assuming optical thinness and only fitting longward of the FIR peak, one overestimates the luminosity density at wavelengths for which $\tau \gtrsim 1$ (see Section 2.3.2).[8] Consequently, the

[8]This may explain why Pope et al. (2006) found that the submm flux density tends to overpredict L_{IR}, and the overprediction is worse for SMGs at low redshift where

assumption of optical thinness yields a colder dust temperature (by as much as ~ 20 K) than if optical thinness is assumed.

In the pre-*Herschel* era, often flux densities in only a few FIR bands and at 1.4 GHz were available for large samples of SMGs. As a result of the limited number of data points, models more complex than the optically thin modified blackbody (e.g., the full modified blackbody used here or models assuming a distribution of temperatures) could not provide a better description of the IR SEDs (e.g., Kovács et al. 2006). Recently, some authors have used models incorporating a distribution of temperatures (e.g., Kovács et al. 2010; Michałowski et al. 2010a), finding that such models better described the IR SEDs (Kovács et al. 2010). Now that *Herschel* PACS (Dannerbauer et al. 2010; Magnelli et al. 2010) and SPIRE (Chapman et al. 2010) have provided data over the entire FIR SED for large samples of SMGs it is possible to perform more sophisticated fitting for many SMGs. Given the physical inferences that are drawn from effective dust temperatures obtained via FIR SED fitting, it is important to have as robust a method as possible and to take full advantage of the available data. We will present such a method in future work.

2.4.6   Limitations of Our Model

At this point we find it instructive to define the limitations of this work so that the results can be placed in an appropriate context and future experiments can be designed for maximal impact. One of the primary limitations, both for the RT and the hydrodynamics, is the treatment of the sub-resolution ISM, especially—because

the SED is sampled further from the IR peak.

we focus upon the submm flux—the structure, distribution, and composition of the dust which dominates emission at submm wavelengths. In fact, the differences between the model employed in this work and that we used in N10 were motivated by a desire for a simpler treatment of the sub-resolution ISM (see Section 2.2.2). In N10, stars with age ≤ 10 Myr dominated the submm flux, so the submm flux was closely tied to the SFR (see Fig. 1 of N10). Our simplified assumptions (no sub-resolution PDR model, uniform ISM density on scales below the SPH smoothing length) result in submm flux that is tied more directly to the bolometric luminosity than the instantaneous SFR because stars with age > 10 Myr contribute significantly to the bolometric luminosity and, because they are still deeply embedded in dust, the submm flux.

While our model has the advantages of simplicity and strict physical consistency (because the obscuration originates purely from the hydrodynamic simulations rather than from sub-resolution PDRs), we still must make an assumption about the sub-resolution structure of the ISM. By assuming uniform density on scales below the smoothing length we only include clumpiness that arises from the hydrodynamic simulations, so this assumption may be considered conservative. The assumption is also simplistic, of course, because the real ISM has significant structure on scales $\lesssim 100$ pc. However, proper treatment of RT through a clumpy medium is a significant area of research in and of itself (e.g., Hobson & Padman 1993; Witt & Gordon 1996; Városi & Dwek 1999) and thus beyond the scope of this work. A study of the effects of sub-resolution dust clumpiness on galaxy SEDs and efforts to devise a better treatment of sub-resolution dust clumpiness in SUNRISE are underway.

We also caution that modifications to the simple star formation prescription

and ISM treatment in the hydrodynamical simulations themselves could change the amplitude and duration of starbursts (Cox et al. 2006b; Springel et al. 2005). However, while changing the SF prescription or ISM treatment could change the relative contribution of quiescent and starburst star formation modes to the star formation history of a given merger, this alone should not change the differences between quiescent star formation and starbursts which lead to the significantly different relationships between SFR and submm flux. Changing the SF or ISM prescription could substantially alter the spatial distribution of dust and stars and thereby modify the detailed relations between SFR/L_{bol}, M_d, and S_{850}. However, because geometry is relatively unimportant in setting the relations, this uncertainty should have a relatively limited influence on our results. Furthermore, changing the feedback implementation can alter the evolution of the IR SEDs (Chakrabarti et al. 2007). Ongoing and future studies, with much higher resolution and more advanced tracking of the clumpy ISM (e.g., Hopkins et al. 2011), will improve the predictive power of our models.

Furthermore, we stress that the simulations presented here are not cosmological. We adopt this approach because it enables us to achieve the high resolution necessary to perform RT in order to accurately calculate the submm flux density; to survey the parameter space of progenitor masses, mass ratios, and orbits; and to avoid uncertainties in modeling realistic galaxy populations in a cosmological environment. The primary drawback of this approach for our present purposes is the lack of gas accretion, which cosmological hydrodynamic simulations show is a significant driver of star formation for the high-redshift, massive galaxies with which we are concerned (Kereš et al. 2005, 2009; Dekel et al. 2009). Gas accretion can

continually replenish the gas in the galaxy, maintaining relatively high gas fractions and relatively constant star formation histories (e.g., Davé et al. 2010).

Inclusion of cosmological gas accretion would alter the time evolution presented in Figures 2.1, but it would not significantly alter the differences between the quiescent and merger-induced burst modes of star formation. This is because mergers would still superimpose a strong burst of star formation and sharp decrease in gas mass over the baseline evolution. Furthermore, unless smooth accretion significantly affects the geometry of stars and dust in the simulated galaxies, it will not have a significant effect on the relationship between submm flux, L_{bol}, and dust mass (the relationship between submm flux, SFR, and dust mass may be more affected because the relation between SFR and L_{bol} may be changed significantly). Thus inclusion of cosmological gas accretion should not qualitatively alter our results.

2.4.7 Connections to Previous Work

In previous work, we developed a model relating the evolution of galaxies, starbursts, and quasars (Hopkins et al. 2006a,b, 2008a, 2009d; Somerville et al. 2008). A principal conclusion from these analyses is that while starbursts driven by gas-rich mergers can account for many instances of unusual activity in galaxies, they provide only a minor contribution to the star formation history of the Universe (Hopkins et al. 2006c). Indeed, Hopkins et al. (2010a) emphasize that much of the star formation during galaxy interactions occurs in the 'quiescent' mode and should not be counted as part of a merger-induced starburst. This is supported by the

decomposition of the light profiles of nearby ongoing mergers (Hopkins et al. 2008b) and local cusp (Hopkins et al. 2009a) and core (Hopkins et al. 2009c) ellipticals. All of these objects exhibit evidence of "excess" central light (Rothberg & Joseph 2004; Kormendy et al. 2009), indicative of relic starbursts (Mihos & Hernquist 1994, 1996) caused by merger-driven inflows of gas (Barnes & Hernquist 1991, 1996). The integrated mass in these components agrees well with estimates of the cosmic history of merger-induced starbursts (Hopkins & Hernquist 2010).

The results presented herein extend these conclusions to high-redshift phenomena. Critically, we find that "quiescent" star formation during galaxy interactions, i.e., star formation which occurs during the infall/pair stage, is a key element in understanding the brightest submm sources, especially their number counts and duty cycles, and connecting them to other high-redshift populations including quasars (Hopkins et al. 2008a; Narayanan et al. 2008b) and compact spheroidal galaxies (Wuyts et al. 2009, 2010). Just as nearby LIRGs represent a heterogeneous collection of merging and isolated systems, it is natural to suggest that the population of high-redshift SMGs is heterogeneous, as we have argued here.

2.5 Conclusions

We have combined high-resolution 3-D hydrodynamic simulations of high-redshift isolated and merging disk galaxies and 3-D Monte Carlo dust RT calculations to study the SMG selection, focusing on the relationships among submm flux density, SFR, bolometric luminosity, and dust mass. Our main conclusions are the following:

1. The relationship between SFR and submm flux density differs significantly for quiescent and starburst star formation modes. Starbursts produce significantly less submm flux density for a given SFR, and the scaling between submm flux density and SFR is significantly weaker for bursts than for quiescent star formation. Bursts are a very inefficient way to boost submm flux density (e.g., a starburst that increases SFR by $\gtrsim 16\times$ increases submm flux density by $\lesssim 2\times$). Another consequence is that the galaxies with highest submm flux density are not necessarily those with highest SFR or bolometric or infrared luminosity.

2. The (sub)mm flux density of our simulations can be parameterized as a power law in SFR and dust mass (L_{bol} and dust mass) to within $\sim 0.1(0.15)$ dex. The scaling derived from the commonly used optically thin modified blackbody model systematically overpredicts the submm flux density by $\gtrsim 2\times$ because numerous assumptions of the model (optical thinness in the FIR, $L_{\mathrm{IR}} \propto$ SFR, $L_{\mathrm{bol}} \approx L_{\mathrm{IR}}$) do not hold. The fitting functions we provide (Equations 2.1 and 2.2) should be useful for calculating the flux density in semi-analytical models and cosmological simulations when full RT cannot be performed and for interpreting observations.

3. Mergers create SMGs through another mechanism besides the strong starburst induced at coalescence—they cause the two infalling disks to be observed as one submm source because both disks will be within the large (~ 15", or 130 kpc at $z = 2$) beam of the single-dish submm telescopes used to identify SMGs during much of the infall stage. For major mergers, this effect boosts the submm flux density by $2\times$. To achieve the same boost in submm flux

density one would have to boost the SFR of a quiescent disk by $\sim 6\times$ or induce a starburst that boosts the SFR by $\gtrsim 16\times$. This implies that the SMG population is heterogeneous: it is composed of both late-stage major mergers and two (or more) infalling disks observed as a single submm source ("galaxy-pair SMGs"). The largest quiescently star-forming galaxies may also contribute. Thus, unlike local ULIRGs, SMGs are a mix of quiescent and starburst sources.

4. SMGs must be very massive: to reach $S_{850} \gtrsim 3$ mJy, stellar mass of at least $6 \times 10^{10} M_{\odot}$ is required, and typical values are higher.

5. The submm duty cycles of our simulated galaxies are a factor of a few longer than what one would expect if all SMGs were merger-driven bursts because the relatively gentle decline in SFR, L_{bol}, and dust mass during the galaxy-pair phase results in a longer duty cycle for the galaxy-pair phase than for the starburst. The duty cycle of the latter is limited because the peak in luminosity is narrow and the dust temperature increases sharply during the burst.

6. Fitting the SEDs of SMGs with an optically thin modified blackbody tends to yield significantly lower dust temperatures than when the full opacity term is used because the effective optical depths can be ~ 1 out to rest-frame $\sim 200~\mu$m, both for our simulated SMGs and observed SMGs. Therefore, one should be cautious when interpreting effective dust temperatures derived via fitting an optically thin modified blackbody to the FIR SED, especially when comparing SMGs to galaxies for which optical thinness in the IR may be a reasonable approximation.

Future work will include predictions of (sub)mm number counts from our model, an investigation of the observational signatures and physical implications of the proposed SMG bimodality, and an improved method for fitting IR SEDs of galaxies.

2.6 Appendix: Derivation of the Relations Given in Section 2.3.2

Here we derive the relations for submm flux density as a function of dust bolometric luminosity L_d and dust mass M_d (Equation 2.4) and SFR and M_d (Equation 2.3) for an optically thin modified blackbody. One can model galaxy SEDs with more complex models (e.g., Dale et al. 2001; Dale & Helou 2002; Chakrabarti & McKee 2005, 2008; Kovács et al. 2010), but for the sake of simplicity and because the optically thin modified blackbody is commonly used for SED fitting we only consider an optically thin modified blackbody here. Consider a mass M_d of dust with temperature T_d. Assuming the dust is optically thin at rest-frame frequency ν_r, the luminosity density emitted by the dust at that frequency is

$$L_{\nu_r} = 4\pi \kappa_{\nu_r} M_d B_{\nu_r}(T_d), \tag{2.5}$$

where κ_{ν_r} is the dust opacity (m^2 kg^{-1}) at rest-frame frequency ν_r and $B_{\nu_r}(T_d)$ is the Planck function. We assume a power-law opacity in the IR,

$$\kappa_{\nu_r} = \kappa_0 \left(\frac{\nu_r}{\nu_0} \right)^{\beta}, \tag{2.6}$$

where κ_0 is the opacity at frequency ν_0. Integrating Equation (2.5) over ν gives the total dust luminosity,

$$L_d = \Gamma(4+\beta)\zeta(4+\beta)\frac{8\pi h}{c^2}\left(\frac{kT_d}{h}\right)^4 M_d\kappa_0\left(\frac{kT_d}{h\nu_0}\right)^\beta,\tag{2.7}$$

where Γ and ζ are Riemann functions, h is the Planck constant, c is the speed of light, and k is the Boltzmann constant.

Solving for the effective dust temperature yields

$$T_d = \frac{h}{k}\left[\frac{L_d c^2 \nu_0^\beta}{\Gamma(4+\beta)\zeta(4+\beta)8\pi\kappa_0 h M_d}\right]^{1/(4+\beta)}.\tag{2.8}$$

If we place the mass of dust at redshift z, the flux density at observed-frame frequency ν_o is

$$S_{\nu_o}(T_d) = (1+z)\frac{L_{\nu_r}}{4\pi D_L^2}\tag{2.9}$$

$$= (1+z)\frac{4\pi\kappa_{\nu_r}M_d B_{\nu_r}(T_d)}{4\pi D_L^2}\tag{2.10}$$

$$= (1+z)^{\beta-3}\frac{\kappa_0 M_d}{D_A^2}\left(\frac{\nu_o}{\nu_0}\right)^\beta B_{\nu_o(1+z)}(T_d),\tag{2.11}$$

where we have related angular diameter distance D_A and luminosity distance D_L using $D_L = (1+z)^2 D_A$. In the Rayleigh-Jeans limit, $B_\nu(T) = 2k\nu^2 T/c^2$, so

$$S_{\nu_o}(T_d) = (1+z)^{\beta-1}\frac{2k\kappa_0}{c^2 D_A^2}\left(\frac{\nu_o}{\nu_0}\right)^\beta \nu_o^2 M_d T_d.\tag{2.12}$$

By substituting T_d from Equation (2.8) into Equation (2.12) we find

$$S_{\nu_o} = \frac{2h\kappa_0}{c^2 D_A^2}\nu_o^2\left(\frac{\nu_o}{\nu_0}\right)^\beta\left(\frac{\nu_0^\beta c^2}{\Gamma(4+\beta)\zeta(4+\beta)8\pi\kappa_0 h}\right)^{1/(4+\beta)}(1+z)^{\beta-1}L_d^{1/(4+\beta)}M_d^{(3+\beta)/(4+\beta)}.\tag{2.13}$$

For the Weingartner & Draine (2001) $R_V = 3.1$ Milky Way dust model, which we use in our RT calculations, $\beta \approx 2$ and the 850 μm opacity is $\kappa_{850} = 0.050$ m^2

kg^{-1}, consistent with the value James et al. (2002) derived from submm observations
of local galaxies, 0.07 ± 0.02 m^2 kg^{-1}, and with the results of Dunne et al. (2003).
Thus the observed 850 μm flux density is

$$S_{850} = 1.5 \text{ mJy } (1 + z) \left(\frac{D_A}{1 \text{ Gpc}} \right)^{-2} \left(\frac{L_d}{10^{12} L_\odot} \right)^{1/6} \left(\frac{M_d}{10^8 M_\odot} \right)^{5/6}. \qquad (2.14)$$

The Kennicutt (1998b) SFR-L_{IR} calibration converted to a Kroupa (2001)
initial mass function is

$$L_{\text{IR}} \approx L_{\text{bol}} \approx 9 \times 10^9 L_\odot (\text{SFR}/M_\odot \text{ yr}^{-1}). \qquad (2.15)$$

This conversion assumes all starlight is absorbed by dust and the contribution
from AGN and old stars is negligible; as discussed above, these assumptions are all
violated at some level. (If these assumptions were true, the power-law indices in
Equations (2.1) and (2.2) would be identical.) However, since the above calibration
is ubiquitously applied, we will give the relation that results when we use it; the
relation is

$$S_{850} = 1.5 \text{ mJy } (1 + z) \left(\frac{D_A}{1 \text{ Gpc}} \right)^{-2} \left(\frac{\text{SFR}}{100 \ M_\odot \text{ yr}^{-1}} \right)^{1/6} \left(\frac{M_d}{10^8 M_\odot} \right)^{5/6}. \qquad (2.16)$$

Assuming $\Omega_m = 0.27, \Omega_\Lambda = 0.73$, and $h = 0.7$, the angular diameter distance at
$z = 2$ is 1.77 Gpc (Wright 2006). Thus for $z = 2$ we recover Equation (2.4),

$$S_{850} = 1.4 \text{ mJy } \left(\frac{L_d}{10^{12} L_\odot} \right)^{1/6} \left(\frac{M_d}{10^8 M_\odot} \right)^{5/6}. \qquad (2.17)$$

This should be compared to Equation (2.2). In terms of SFR, we get Equation (2.3),

$$S_{850} = 1.4 \text{ mJy } \left(\frac{\text{SFR}}{100 \ M_\odot \text{ yr}^{-1}} \right)^{1/6} \left(\frac{M_d}{10^8 M_\odot} \right)^{5/6}. \qquad (2.18)$$

This should be compared to Equation (2.1).

Even if the underlying power-law index of the dust opacity curve is $\beta = 2$, for a distribution of dust temperatures a single-temperature modified blackbody with $\beta = 1.5$ may better fit the SED (Dunne & Eales 2001; Chakrabarti & McKee 2008). Note also that the fitted dust temperature and β are degenerate, and the fitted values can depend sensitively on both noise in the data and temperature variations along the line-of-sight (Shetty et al. 2009a,b). Since $\beta = 1.5$ is often assumed when fitting SEDs and determining dust masses of SMGs (e.g., Kovács et al. 2006, 2010; Coppin et al. 2008; Chapman et al. 2010), so we will provide the relations for $\beta = 1.5$ also. They are:

$$S_{850} = 1.9 \text{ mJy } (1+z)^{0.5} \left(\frac{D_A}{1 \text{ Gpc}} \right)^{-2} \left(\frac{L_d}{10^{12} L_\odot} \right)^{0.18} \left(\frac{M_d}{10^8 M_\odot} \right)^{0.82}, \qquad (2.19)$$

and

$$S_{850} = 1.9 \text{ mJy } (1+z)^{0.5} \left(\frac{D_A}{1 \text{ Gpc}} \right)^{-2} \left(\frac{\text{SFR}}{100 \ M_\odot \text{ yr}^{-1}} \right)^{0.18} \left(\frac{M_d}{10^8 M_\odot} \right)^{0.82}. \qquad (2.20)$$

For $z = 2$,

$$S_{850} = 1.0 \text{ mJy } \left(\frac{L_d}{10^{12} L_\odot} \right)^{0.18} \left(\frac{M_d}{10^8 M_\odot} \right)^{0.82}, \qquad (2.21)$$

and

$$S_{850} = 1.0 \text{ mJy } \left(\frac{\text{SFR}}{100 \ M_\odot \text{ yr}^{-1}} \right)^{0.18} \left(\frac{M_d}{10^8 M_\odot} \right)^{0.82}. \qquad (2.22)$$

The equations can be rescaled to different values of κ_0 using $S_{\nu_o} \propto \kappa_0^{(3+\beta)/(4+\beta)}$ and to different submm wavelengths using $S_{\nu_o} \propto \nu_o^{2+\beta}$ (see Equation 2.13).

Chapter 3

Observationally Distinguishing Starburst and Quiescent Star Formation Modes: The Bimodal Submillimeter-Selected Galaxy Population as a Case Study

Abstract

Observational evidence supports the existence of two modes of star formation, quiescent and starburst. In Chapter 2 we have suggested that the high-redshift bright submillimeter-selected galaxy (SMG) population is heterogeneous, with major

mergers contributing both at early stages, where quiescently star-forming, infalling disks are blended into one submm source ("galaxy-pair SMGs"), and late stages, where mutual tidal torques drive gas inflows and cause strong starbursts. Thus the SMG population is powered by a mix of both star formation modes. In this work we combine hydrodynamic simulations of major mergers with 3-D dust radiative transfer calculations to determine observational diagnostics that can distinguish between quiescently star-forming galaxies and starbursts via integrated data alone. These diagnostics can be used to test our claim that the SMG population attributable to major mergers is bimodal and to observationally determine what star formation mode dominates a given galaxy population. A robust prediction of our models is that the objects with the highest effective dust temperatures (T_d) and infrared (IR) luminosities should be almost exclusively starbursts; thus *Herschel* data can be effectively used to distinguish star formation modes. Starbursts should also have higher $L_{\mathrm{IR}}/M_{\mathrm{gas}}$ and obscuration than quiescently star-forming galaxies and should lie above the star formation rate-stellar mass (SFR-$M_\star$) relation. Finally, we show that the fitted T_d and power-law index of the dust emissivity in the far-IR, β, can significantly depend on the fitting method used. As a result, these parameters should be interpreted with caution.

3.1 Introduction

3.1.1 The Two Modes of Star Formation

Star formation is one of the fundamental processes driving galaxy formation: it depletes the gas content of galaxies, enriches the interstellar medium (ISM) with metals, and deposits energy and momentum via supernovae, stellar winds, and radiation pressure. Furthermore, the light emitted by stars encodes much information about the current physical properties of a galaxy and the galaxy's formation history. Thus understanding star formation is crucial for understanding galaxy formation and evolution.

An increasing amount of observational evidence supports the notion that there are two modes of star formation, typically referred to as quiescent[1] (that occurring in normal disk galaxies) and starburst (found in unstable disks and merging galaxies at first passage and coalescence, though whether a starburst is induced in the latter depends on factors such as gas content, orbit, and mass ratio of the progenitors; e.g., Cox et al. 2008).[2] For example, starbursts seem to obey a different Kennicutt-Schmidt (KS) relation (Kennicutt 1998a; Schmidt 1959) than quiescently star-forming disk galaxies; the normalization of the KS relation for starbursts is $\sim 4 - 10\times$ greater than that for quiescently star-forming disks (Daddi et al. 2010;

---

[1]Confusingly, the term "quiescent" is also used to refer to galaxies that have little or no star formation; here the term quiescent always means "quiescently star-forming".

[2]Strictly speaking there should not be two *distinct* modes but instead a continuous variation in global star formation efficiency. However, we will use the notion of two modes for conceptual simplicity and to be consistent with other literature.

Genzel et al. 2010). The ratio of IR luminosity to molecular gas mass is larger in starbursts by a similar factor. The relationship between SFR and dust mass also shows a bimodal behavior (da Cunha et al. 2010).

Furthermore, at a given redshift, most star-forming galaxies lie on a tight relation between SFR and $M_\star$ ($M_\star$; Daddi et al. 2007; Noeske et al. 2007a,b; Karim et al. 2011). The relation arises because star formation is supply-limited, so, on average, SFR correlates well with cosmological gas accretion rates, which, in turn are well-correlated with halo mass (Kereš et al. 2005, 2009; Faucher-Giguere et al. 2011). In this picture, starbursts are transient events that cause a galaxy to move significantly above the SFR-$M_\star$ relation for a short ($\sim 50 - 100$ Myr) time. During the burst the gas is rapidly consumed, the SFR declines sharply, and the galaxy returns to the SFR-$M_\star$ relation or is quenched and falls well below it.

There are multiple physical reasons that star formation efficiency can be higher in starbursts than in quiescently star-forming galaxies. They have been discussed by many authors (e.g., Kennicutt 1998a; Krumholz & McKee 2005; Leroy et al. 2008; Genzel et al. 2010), so we will only recapitulate them here. For example, suppose that galaxies convert some fixed fraction $\epsilon_{\rm ff}$ of their gas mass into stars per free-fall time $t_{\rm ff}$. Then the SFR is

$$\dot{\rho}_\star = \epsilon_{\rm ff} \frac{\rho_{\rm gas}}{t_{\rm ff}} \propto \epsilon_{\rm ff} \rho_{\rm gas}^{1.5}, \tag{3.1}$$

where $\epsilon_{\rm ff}$ is the fraction of mass converted into stars per free-fall time, and we have used $t_{\rm ff} = (G\rho_{\rm gas})^{-0.5}$. If the scale height is relatively constant then this can be re-cast in terms of surface densities,

$$\dot{\Sigma}_\star = \epsilon_{\rm ff} \frac{\Sigma_{\rm gas}}{t_{\rm ff}} \propto \epsilon_{\rm ff} \Sigma_{\rm gas}^{1.5}. \tag{3.2}$$

In this formulation of the KS law, if one believes there are two modes of star formation then ϵ_{ff} must be greater for starburst galaxies than for quiescently star-forming disks.

An alternative form for the star formation law given by Elmegreen (1997) and Silk (1997) is

$$\dot{\Sigma}_\star = \epsilon_{\mathrm{dyn}} \frac{\Sigma_{\mathrm{gas}}}{t_{\mathrm{dyn}}}. \qquad (3.3)$$

In this scenario a different normalization of the KS law for starbursts and quiescently star-forming disks could arise if ϵ_{dyn} is constant and the relevant dynamical times for starbursts are significantly ($\sim 10\times$) shorter for mergers than for quiescently star-forming disks. The latter holds because star formation in merger-driven starbursts typically occurs on smaller scales and at higher densities than in quiescently star-forming disks.

Two modes of star formation are implicitly included in the Springel & Hernquist (2003, hereafter SH03) sub-resolution ISM model employed in our simulations. The distinction between the two modes is described in detail in Section 4.2 of SH03. We will summarize the details here, but we refer the reader to that work for a more thorough explanation. In the quiescent mode star formation is self-regulated, as the cold, star-forming clouds are evaporated on a timescale significantly less than the timescale needed to convert the cloud entirely to stars. This self-regulation results in a relatively low star formation efficiency. At sufficiently high densities, the time needed to evaporate the clouds becomes longer than the time needed to entirely convert the clouds to stars. Thus the star formation is no longer self-regulated; this is the starburst mode. The strong tidal torques encountered during a galaxy

merger can drive gas to densities high enough to result in a starburst, as can bar instabilities.

Though there are simple physical reasons one might expect different star formation efficiency in starbursts and quiescently star-forming disks and some observational support for such a difference, significant theoretical and observational hurdles must be overcome before the bimodality is accepted as fact. Furthermore, it can be difficult to observationally determine which mode of star formation dominates a given galaxy population; this complicates efforts to understand the underlying physics. This is especially a problem at high-redshift because lessons learned from the local universe may not apply to high-redshift galaxies. For example, at high redshift gas-accretion rates are significantly higher than locally (e.g., Kereš et al. 2005), so gas fractions (Erb et al. 2006; Tacconi et al. 2006, 2010; Daddi et al. 2010) and star formation rates (Daddi et al. 2007; Noeske et al. 2007a,b) of galaxies at fixed galaxy mass increase rapidly with redshift. Consequently, even a typical star-forming galaxy at $z \sim 2$ can reach ULIRG luminosities (e.g., Daddi et al. 2005, 2007; Hopkins et al. 2008c, 2010a; Dannerbauer et al. 2009). It would thus be useful to have simple observational diagnostics that can be used to determine which mode of star formation dominates a given galaxy or galaxy population. This is one of the goals of this paper.

The rest of the paper is organized as follows: In Section 3.1.2 we review the physical reasons for and evidence in favor of the "bimodality" of the SMG population we proposed in Section 2.4.2. We describe our simulation methodology in Section 3.2. Section 3.3 presents multiple observational diagnostics that can be used to distinguish between quiescently star-forming galaxies and starbursts from integrated

data alone, including the luminosity-effective T_d relation, star formation efficiency, obscuration, and the SFR-$M_\star$ relation. In Section 3.4 we discuss some implications of our work, and in Section 3.5 we summarize and conclude.

3.1.2 The Bimodality of the SMG Population

Submillimeter-selected galaxies (SMGs; Smail et al. 1997; Barger et al. 1998; Hughes et al. 1998; Eales et al. 1999; see Blain et al. 2002 for a review) are a class of high-redshift (median $z \sim 2.3$; Chapman et al. 2005) galaxies notable for their extreme luminosities (bolometric luminosity $L_{\rm bol} \sim 10^{12} - 10^{13} L_\odot$; e.g., Kovács et al. 2006), almost all of which is emitted in the IR. Since they seem to be powered by star formation rather than active galactic nuclei (AGN; Alexander et al. 2005a,b, 2008; Valiante et al. 2007; Menéndez-Delmestre et al. 2007, 2009; Pope et al. 2008; Younger et al. 2008, 2009b), they have inferred SFRs of $\sim 10^2 - 10^4 M_\odot$ yr^{-1}, much greater than those of even the most extreme local galaxies.

It has long been known that during major mergers tidal torques drive significant amounts of gas inward, resulting in a strong burst of star formation (Hernquist 1989; Barnes & Hernquist 1991, 1996; Mihos & Hernquist 1996). Locally, ultra-luminous infrared galaxies (ULIRGs, defined by $L_{\rm IR} > 10^{12} L_\odot$) are exclusively late-stage major mergers (e.g., Sanders & Mirabel 1996; Veilleux et al. 2002; Lonsdale et al. 2006, and references therein), so the strong gas inflows induced during the near-coalescence stage of a major merger seem necessary to power the most luminous and rapidly star-forming galaxies.

The identification of ULIRGs with late-stage major mergers in the local universe

has caused many researchers to suspect that SMGs, some of the most IR-luminous galaxies at high redshift, are also late-stage major mergers. There is much observational evidence that supports this picture (e.g., Ivison et al. 2002, 2007, 2010; Chapman et al. 2003; Neri et al. 2003; Smail et al. 2004; Swinbank et al. 2004; Greve et al. 2005; Tacconi et al. 2006, 2008; Bouché et al. 2007; Biggs & Ivison 2008; Capak et al. 2008; Younger et al. 2008, 2010; Iono et al. 2009; Engel et al. 2010; Riechers et al. 2011a,b). Furthermore, by combining hydrodynamic simulations with dust radiative transfer (RT), we have shown that simulated major mergers have observed 850 μm fluxes and typical spectral energy distribution (SEDs; Narayanan et al. 2010a; Chapter 2; but cf. Chakrabarti et al. 2008), stellar masses (Michałowski et al. 2011), and CO properties (Narayanan et al. 2009) consistent with observed SMGs. Semi-analytic models (SAMs) typically also find that merger-induced starbursts (though not necessarily major mergers, as minor-merger-induced starbursts dominate in some models) account for the bulk of the SMG population (Baugh et al. 2005; Fontanot et al. 2007; Swinbank et al. 2008; Lo Faro et al. 2009; Fontanot & Monaco 2010; González et al. 2011; but cf. Granato et al. 2004). However, Davé et al. (2010) have argued that there are not enough major mergers to account for the observed SMG population; they argue that a significant fraction of the population must be massive disks fueled by smooth accretion and minor mergers.

In Section 2.4.2 we have suggested a modification to the canonical picture: we argue that SMGs are not purely late-stage major mergers but rather a heterogeneous population, composed of late-stage major mergers, early-stage major mergers (which we term "galaxy-pair SMGs"), physically unrelated galaxies blended into one submm source (Wang et al. 2011), and, at the fainter end of the population, some isolated

galaxies and minor mergers. The reason that early-stage mergers also contribute is that observed submm flux increases rather weakly with SFR, and the starburst mode is significantly less efficient at boosting submm flux than the quiescent mode. Physically, submm flux scales more weakly in starbursts for two reasons: 1. In high-redshift mergers significant star formation occurs before the starburst is induced. This contamination by old stars causes the bolometric luminosity to increase sublinearly with SFR. For the merger shown in Figure 2.2, the stars formed pre-burst account for $\sim 1/7$ of the bolometric luminosity at the time of the burst. 2. Driven primarily by the strong drop in dust mass during the merger, the effective T_d of the SED increases sharply during the starburst. This effect mitigates the increase in submm flux caused by the increased luminosity. These two effects result in a very weak scaling ($S_{850} \propto \mathrm{SFR}^{0.1}$, compared to $S_{850} \propto \mathrm{SFR}^{0.4}$ for the quiescently star-forming galaxies). For the specific merger shown in 2.2, an increase in SFR of $\sim 16\times$ causes a $\lesssim 2\times$ boost in the submm flux.

Furthermore, the large (~ 15 arcsec, or ~ 130 kpc at $z \sim 2$) beams of the single-dish submm telescopes used to detect SMGs cause the two merger disks to be blended into a single source for much of the pre-coalescence stage of the merger. The combination of the inefficiency of starbursts at boosting submm flux and the blending of the disks during the early stages of a merger causes early-stage mergers to be an efficient way to create SMGs. The brightest SMGs should still be merger-induced starburst, but early-stage mergers must provide a significant contribution to the population.

There is already much evidence that some SMGs are early-stage mergers. For example, Engel et al. (2010) used submm interferometry to show that approximately

half of their SMG sample are well-resolved binary systems. (See also Tacconi et al. 2006, 2008; Bothwell et al. 2010; Riechers et al. 2011a,b.) Two of the 12 SMGs in the Engel et al. sample consist of two well-separated, resolved components (projected separations $\gtrsim$ 20 kpc), and it is possible that they have missed one component of galaxy-pair SMGs with more widely separated components because of the limited field of view. In such widely separated systems the star formation induced by the tidal torques exerted by the disks upon one another is not sufficient to drive a strong starburst, so the disks would form stars at similar rates even if the companion was absent. Thus such systems should be considered physically analogous to normal disk galaxies rather than late-stage mergers because they are forming stars via the quiescent rather than starburst mode. In addition to the evidence from CO interferometry, support for the galaxy-pair contribution is provided by the frequency of multiple radio (e.g., Ivison et al. 2002, 2007; Chapman et al. 2005; Clements et al. 2008; Younger et al. 2009c; Yun et al. 2011) and 24 μm (e.g., Pope et al. 2006; Yun et al. 2011) counterparts to SMGs and SMGs with morphologies that appear more like disks than late-stage mergers (e.g., Bothwell et al. 2010; Carilli et al. 2010; Ricciardelli et al. 2010; Targett et al. 2011). (Note, however, that in gas-rich mergers disks can rapidly re-form, potentially confusing interpretation of these results; Narayanan et al. 2008b; Robertson & Bullock 2008.)

We have shown that physical arguments and observations suggest that the SMG population is a mix of quiescently star-forming galaxies and starbursts. Thus SMGs differ significantly from local ULIRGs, which are exclusively starburst- or AGN-dominated, so one should draw comparisons between the two populations with care. The heterogeneity complicates physical interpretation of the SMG population.

For example, one should not apply a CO-H_2 conversion factor appropriate for starbursts to the quiescently star-forming subpopulation of SMGs. Furthermore, proper treatment of all these subpopulations is key for reproducing the observed SMG number counts (Chapter 4). However, the relative contributions of these various subpopulations is not observationally well-determined yet, and predictions of the relative contributions depend sensitively on uncertain model details. We do not predict the relative contributions in the present work (this will be presented in Chapter 4). Instead, we wish to determine how one can observationally distinguish between starburst-driven (late-stage merger) SMGs and those powered by quiescent star formation even when only integrated data are available. One can then use these diagnostics to observationally constrain the relative contributions of starbursts and quiescently star-forming galaxies to the SMG population, thereby testing the bimodality we claim exists. Furthermore, since most diagnostics presented here rely on FIR photometry, the wealth of data provided by *Herschel* will enable application of these diagnostics to increasingly varied galaxy populations.

3.2 Simulation Methodology

We analyze high-resolution GADGET-2 (Springel et al. 2001; Springel 2005) 3-D N-body/smoothed-particle hydrodynamics (SPH) simulations of isolated and merging disk galaxies with the SUNRISE (Jonsson 2006; Jonsson et al. 2010) polychromatic Monte Carlo dust RT code to calculate synthetic SEDs of the simulated galaxies. We discuss the details of our methodology in Chapter 2, so here we will only briefly summarize the methodology and provide details about the specific simulations

used in this work. The combination of GADGET-2 and SUNRISE has been used to successfully reproduce (with minimal parameter tuning) the SEDs/colors of a variety of galaxy populations, both low- and high-redshift, including: local SINGS (Kennicutt et al. 2003; Dale et al. 2007) galaxies (Jonsson et al. 2010); local ULIRGs (Younger et al. 2009a); extended ultraviolet (XUV) disks (Bush et al. 2010); 24 μm-selected galaxies (Narayanan et al. 2010b); massive, quiescent, compact $z \sim 2$ galaxies (Wuyts et al. 2009, 2010); and K+A/post-starburst galaxies (Snyder et al. 2011), among other populations. These successes support our application of GADGET and SUNRISE to modeling high-redshift ULIRGs.

3.2.1 Hydrodynamic Simulations

GADGET-2(Springel et al. 2001; Springel 2005) is a TreeSPH (Hernquist & Katz 1989) code that computes gravitational interactions via a hierarchical tree method (Barnes & Hut 1986) and gas dynamics via SPH (Lucy 1977; Gingold & Monaghan 1977; Springel 2010). It explicitly conserves both energy and entropy (Springel & Hernquist 2002). Radiative heating and cooling is included following Katz et al. (1996). Star formation is implemented using a volume-density dependent KS law (Kennicutt 1998a), $\rho_{\rm SFR} \propto \rho_{\rm gas}^{1.5}$, with a minimum density threshold. The assumed KS index $N = 1.5$ is consistent with observations of $z \sim 2$ disks (Krumholz & Thompson 2007; Narayanan et al. 2008a, 2011a), suggesting that it is reasonable to use this prescription in our simulations of $z \sim 2$ mergers. The gas is enriched with metals assuming each particle behaves as a closed box, so those gas particles with higher SFRs are more rapidly metal-enriched.

We use the sub-resolution two-phase ISM model of SH03. In this model, cold, dense clouds are embedded in a diffuse, hot medium. Supernova feedback (Cox et al. 2006a), radiative heating and cooling, and star formation control the exchange of energy and mass in the two phases. A simple model for black hole accretion and AGN feedback (Springel et al. 2005; Matteo et al. 2005) is included. Black hole sink particles with initial masses $10^5 M_\odot$ are included in both initial disk galaxies. They accrete via Eddington-limited Bondi-Hoyle accretion (Hoyle & Lyttleton 1939; Bondi & Hoyle 1944). The luminosity of each black hole is calculated from the accretion rate $\dot{M}_{\rm BH}$ assuming the radiative efficiency appropriate for a Shakura & Sunyaev (1973) thin disk, 10 per cent. Thus $L_{\rm bol} = 0.1\dot{M}c^2$. We deposit 5 per cent of the luminosity emitted by the black holes to the surrounding ISM.

The simulations are initialized in the following manner: We embed exponential disks with initial gas fraction 80 per cent in dark matter halos described by a Hernquist (1990) profile. The progenitor disks are scaled to $z \sim 3$ as described in Robertson et al. (2006a,b) so that the mergers occur at $z \sim 2$. We use gravitational softening lengths of $200h^{-1}$ pc for the dark matter particles and $100h^{-1}$ pc for the star, gas, and black hole particles and 6×10^4 dark matter, 4×10^4 stellar, 4×10^4 gas, and 1 black hole particle per disk galaxy. Two identical disks are initialized on parabolic orbits with initial separation $R_{\rm init} = 5R_{\rm vir}/8$ and pericentric distance twice the disk scale length (Robertson et al. 2006b). Since we are interested in the difference between quiescently star-forming disks and starburst galaxies we analyze only the subset of equal mass mergers taken from the simulation suite that we use to predict SMG number counts in Chapter 4. The physical parameters of the major mergers used are summarized in Table 3.1.

Table 3.1.   Merger models

Name	M_{halo} $(h^{-1}M_\odot)$	$M_{\star,\mathrm{init}}$ $(h^{-1}M_\odot)$	$M_{\mathrm{gas,init}}$ $(h^{-1}M_\odot)$	$f_{\mathrm{gas,init}}$	R_{init} $(h^{-1}$ kpc$)$	R_{peri} $(h^{-1}$ kpc$)$	θ_1 (deg)	ϕ_1 (deg)	θ_2 (deg)	ϕ_2 (deg)
b6i	6.2×10^{12}	5.3×10^{10}	2.2×10^{11}	0.8	70	6.7	0	0	71	30
b6j	6.2×10^{12}	5.3×10^{10}	2.2×10^{11}	0.8	70	6.7	-109	90	71	90
b6k	6.2×10^{12}	5.3×10^{10}	2.2×10^{11}	0.8	70	6.7	-109	-30	71	-30
b6l	6.2×10^{12}	5.3×10^{10}	2.2×10^{11}	0.8	70	6.7	-109	30	180	0
b6m	6.2×10^{12}	5.3×10^{10}	2.2×10^{11}	0.8	70	6.7	0	0	71	90
b6n	6.2×10^{12}	5.3×10^{10}	2.2×10^{11}	0.8	70	6.7	-109	-30	71	30
b6o	6.2×10^{12}	5.3×10^{10}	2.2×10^{11}	0.8	70	6.7	-109	30	71	-30
b6p	6.2×10^{12}	5.3×10^{10}	2.2×10^{11}	0.8	70	6.7	-109	90	180	0
b5.5i	3.2×10^{12}	2.7×10^{10}	1.1×10^{11}	0.8	57	5.3	0	0	71	30
b5.5j	3.2×10^{12}	2.7×10^{10}	1.1×10^{11}	0.8	57	5.3	-109	90	71	90
b5.5k	3.2×10^{12}	2.7×10^{10}	1.1×10^{11}	0.8	57	5.3	-109	-30	71	-30
b5.5l	3.2×10^{12}	2.7×10^{10}	1.1×10^{11}	0.8	57	5.3	-109	30	180	0
b5.5m	3.2×10^{12}	2.7×10^{10}	1.1×10^{11}	0.8	57	5.3	0	0	71	90
b5.5n	3.2×10^{12}	2.7×10^{10}	1.1×10^{11}	0.8	57	5.3	-109	-30	71	30
b5.5o	3.2×10^{12}	2.7×10^{10}	1.1×10^{11}	0.8	57	5.3	-109	30	71	-30
b5.5p	3.2×10^{12}	2.7×10^{10}	1.1×10^{11}	0.8	57	5.3	-109	90	180	0
b5i	1.6×10^{12}	1.4×10^{10}	5.6×10^{10}	0.8	44	4.0	0	0	71	30
b5j	1.6×10^{12}	1.4×10^{10}	5.6×10^{10}	0.8	44	4.0	-109	90	71	90
b5k	1.6×10^{12}	1.4×10^{10}	5.6×10^{10}	0.8	44	4.0	-109	-30	71	-30
b5l	1.6×10^{12}	1.4×10^{10}	5.6×10^{10}	0.8	44	4.0	-109	30	180	0
b5m	1.6×10^{12}	1.4×10^{10}	5.6×10^{10}	0.8	44	4.0	0	0	71	90
b5n	1.6×10^{12}	1.4×10^{10}	5.6×10^{10}	0.8	44	4.0	-109	-30	71	30
b5o	1.6×10^{12}	1.4×10^{10}	5.6×10^{10}	0.8	44	4.0	-109	30	71	-30
b5p	1.6×10^{12}	1.4×10^{10}	5.6×10^{10}	0.8	44	4.0	-109	90	180	0

3.2.2 Radiative Transfer

We have used the the 3-D Monte Carlo dust RT code Sunrise (Jonsson 2006; Jonsson et al. 2010) in post-processing to calculate the far-UV-mm SEDs of each simulated merger at 10 Myr intervals. We will briefly describe the Sunrise calculation, but we encourage the reader to see Jonsson et al. (2010) for full details. Sunrise uses the stellar and black hole particles from the Gadget-2 simulations as radiation sources. Each stellar particle is treated as a single-age stellar population and assigned a Starburst99 (Leitherer et al. 1999) SED template appropriate for its age and metallicity. The stars in the initial disks are assigned ages by assuming that the population was formed at a constant rate equal to the SFR of the initial snapshot. We assume the gas and stars present in the initial disks have metallicity $Z = 0.015$, which results in the galaxies being roughly on the $z \sim 2$ mass-metallicity relation during the starburst. The black hole particles are assigned SEDs using the luminosity-dependent templates of Hopkins et al. (2007). These templates are derived from observations of unreddened quasars, so they include the intrinsic AGN emission and hot dust emission from the torus.

Sunrise calculates the dust distribution by projecting the Gadget-2 gas-phase metal density onto a 3-D adaptive mesh refinement grid using the SPH smoothing kernel and assuming a dust-to-metal ratio of 0.4 (Dwek 1998; James et al. 2002). We use a minimum cell size of $55h^{-1}$ pc, which we have determined is sufficient to ensure the SEDs are converged to within $\lesssim 10$ per cent at all wavelengths. We use grain compositions, size distributions, and optical properties from the Milky Way R=3.1 dust model of Weingartner & Draine (2001) as updated by Draine & Li (2007).

To perform the RT we use 10^7 photon packets for each stage, or $\sim 10\times$ the number of grid cells. We have checked that this limits Monte Carlo noise to less than a few percent. SUNRISE randomly emits the photon packets from the sources and randomly draws interaction optical depths using the appropriate probability distributions. At the interaction optical depth the photon packet is scattered or absorbed. This is repeated until the photon packet leaves the grid.

The energy absorbed by the dust is re-radiated in the IR. SUNRISE assumes the dust is in thermal equilibrium, so the physical T_d is calculated by setting the luminosity absorbed by each grain equal to the energy emitted by the grain. The equilibrium temperature of a grain depends on the local radiation field heating the grain and its absorption cross section, so there are in principle $n_{\mathrm{cells}} * n_{\mathrm{grain\ sizes}}$ different values of the physical T_d in a given SUNRISE calculation. This is important to keep in mind when one considers fitting IR SEDs with modified blackbodies, as discussed below.

In high-density environments the ISM can be optically thick in the IR; this is especially common in the central regions of the late-stage mergers modeled here. Consequently, one must account for attenuation of the dust emission (aka dust self-absorption). Furthermore, since the IR emission can also heat the dust, one must iterate the T_d calculation and RT of the dust emission until the T_d values for each grain species and grid cell are converged. SUNRISE uses a reference field technique similar to that of Juvela (2005) to perform this iteration. We encourage the interested reader to see Jonsson et al. (2010) and Jonsson & Primack (2010) for details.

The Sunrise calculation yields spatially resolved, multi-wavelength (for these simulations 120 wavelengths sampling the UV-mm range) SEDs for each galaxy snapshot observed from 7 different viewing angles distributed uniformly in solid angle. The data are analogous to that yielded by integrated field unit spectrographs (IFUs). For this work we spatially integrate to calculate integrated SEDs for the system. When calculating observed flux densities we assume the simulated galaxies are at redshift $z = 2$ unless otherwise noted.

3.3   Observational Diagnostics to Distinguish Between Star Formation Modes

In this section we present multiple observational diagnostics that can distinguish between quiescently star-forming and starburst systems, or, for SMGs, among the early-stage merger, galaxy-pair SMGs and the late-stage, merger-induced starburst SMGs. We present diagnostics that rely only on integrated broadband photometry and CO line intensities (to determine gas mass). Spatially resolved data, such as that provided by (sub)mm interferometers and near-IR integral field unit (IFU) spectrographs, can potentially provide more diagnostic power but come at a much greater observational cost. However, even with, e.g., high-resolution IFU data it can be difficult to distinguish between disk galaxies and mergers (Robertson & Bullock 2008). Furthermore, given the high attenuation of SMGs even near-IR observations do not probe the central starburst regions, and, pre-ALMA, the physical spatial resolution in the IR is still poor for objects at these redshifts. Thus diagnostics

that make use of only integrated data will continue to be crucial for distinguishing between star formation modes and understanding the properties of high-redshift galaxies.

We have identified the starburst phase by defining the baseline SFR as the minimum SFR that occurs between first-passage and coalescence and selecting all snapshots where the SFR is $> 3\times$ that baseline SFR. We have chosen this factor so that the star formation induced by the merger dominates that which would occur in the disks even if they were not merging. Increasing (decreasing) the threshold would result in less (more) sources identified as bursts and amplify (diminish) the differences between modes that we describe below. The snapshots that meet this criterion are labeled "starburst" and plotted as blue triangles. Since the mutual gravitational torques are sub-dominant at first passage relative to internal instabilities, the galaxies are primarily quiescently star-forming prior to the starburst induced at coalescence. We thus label all snapshots before the starburst phase "quiescent" and plot them with black circles.

Since our focus is the bright SMG population we have only plotted snapshots for which observed-frame $S_{850} > 5$ mJy. Note, however, that there is typically no reason these diagnostics will not work for other galaxy populations unless we specifically indicate otherwise. We have also neglected all snapshots with greater than 40 per cent gas fraction in order to remain consistent with observational constraints (Tacconi et al. 2006, 2008). Such high initial gas fractions are required, however, to maintain sufficient gas until the time of coalescence, as our simulations do not include any additional gas supply beyond what the galaxies start with. We have checked that the results are qualitatively the same when we use an initial gas

fraction of 60 per cent and include all snapshots. All quantities plotted are totals for the entire system because we wish to present observational diagnostics based on integrated data alone. Finally, note that we plot data from idealized simulations without applying any weighting to account for cosmological abundances. Thus the exact distribution of data in the various diagnostic plots we present is not necessarily representative of the SMG population. What is meaningful, however, is when quiescently star-forming disk and starburst galaxies occupy distinct regimes in a diagnostic plot; this is a clear prediction for how the star formation modes should differ and how one can observationally disentangle the classes in order to determine their relative contributions to a given galaxy population.

3.3.1 Luminosity-Effective T_d Relation

Far-IR (FIR) galaxy SEDs are often described in terms of an effective T_d obtained via fitting a simple modified blackbody to the FIR SED (Hildebrand 1983). The equation for a single-temperature (single-T) modified blackbody is

$$S_\nu = S_0(1 - e^{-(\nu/\nu_0)^\beta})B_\nu(T_d), \tag{3.4}$$

where S_ν is the flux density at rest-frame frequency ν, S_0 is the normalization, ν_0 is the frequency at which the effective optical depth $\tau = 1$, β is the effective slope of the emissivity in the FIR, T_d is the effective dust temperature, and $B_\nu(T_d)$ is the Planck function. Typically it is assumed that optical depths in the FIR are small, so $(1 - \exp[-(\nu/\nu_0)^\beta]) \approx (\nu/\nu_0)^\beta$. Thus

$$S_\nu = S_0'\nu^\beta B_\nu(T_d), \tag{3.5}$$

where $S_0' = S_0/\nu_0^\beta$. We shall refer to the form given in Equation (3.5) as the single-T optically thin (OT) modified blackbody. We refer the reader to Section 2.6 for more details about the modified blackbody forms. The parameters determined using this fitting method should not be interpreted too literally. For example, β and T_d are degenerate (e.g., Sajina et al. 2006), and the β one derives from the fitting depends strongly on both noise in the data and temperature variations along the line-of-sight (Shetty et al. 2009a,b). The fit β is thus not necessarily equal to the intrinsic power-law (PL) index of the dust emissivity in the FIR. Furthermore, adding a significant component of very cold dust can mimic the effect of high effective optical depth, so τ and the temperature distribution are also degenerate (Papadopoulos et al. 2010). Thus one should use caution when attempting to infer physical conditions from the parameters derived by modified blackbody fitting; we demonstrate this in Section 3.3.1.

In order to compare to observations in a meaningful way and provide testable predictions from our models, we fit modified blackbodies to the FIR SEDs of our simulated galaxies. In keeping with the vast majority of the literature we have used Equation (3.5) to derive T_d from the simulated photometry. In Figure 3.1 we show the distribution of our simulations on the $T_d - L_{\mathrm{IR}}$ plot when we derive T_d by fitting Equation (3.5) to the simulated *Herschel* SPIRE (Griffin et al. 2010) 250, 350, and 500 μm, SCUBA (Holland et al. 1999) 850 μm, and AzTEC (Wilson et al. 2008) 1.1 mm photometry. In Figure 3.2 we have also used the simulated *Herschel* PACS (Poglitsch et al. 2010) 100 and 160 μm photometry in the fit. We have excluded the PACS 70 μm point because for the assumed $z = 2$ this is rest-frame 23 μm, a regime of the spectrum dominated by stochastically heated grains. If we include this
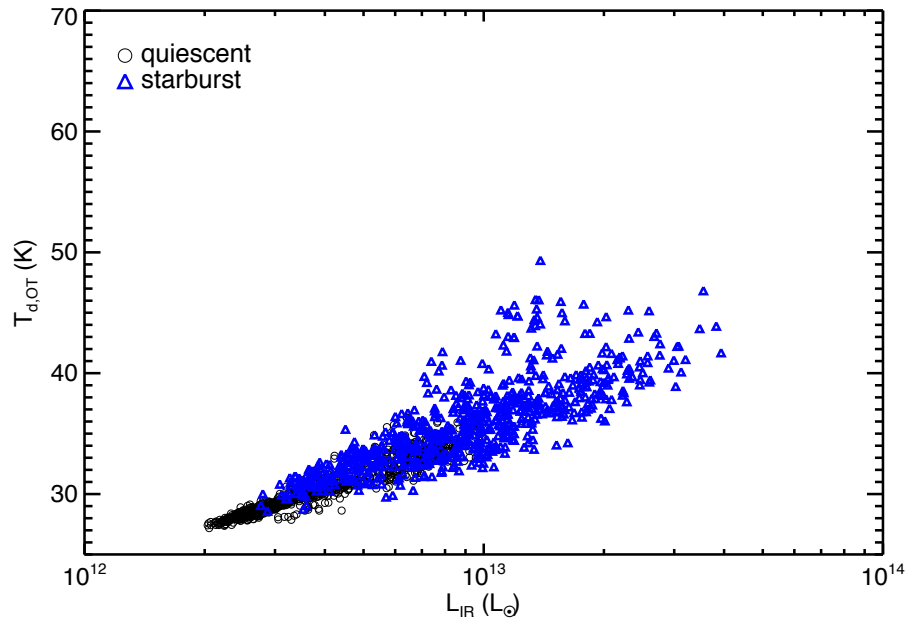
Figure 3.1.—: Effective T_d derived from fitting the single-T OT modified blackbody (Equation 3.5) to the simulated SPIRE, SCUBA, and AzTEC photometry versus total infrared luminosity L_{IR}. Effective T_d correlates strongly with luminosity, and the sources in the high-T_d, high-L_{IR} region of the plot are almost exclusively merger-induced starbursts.
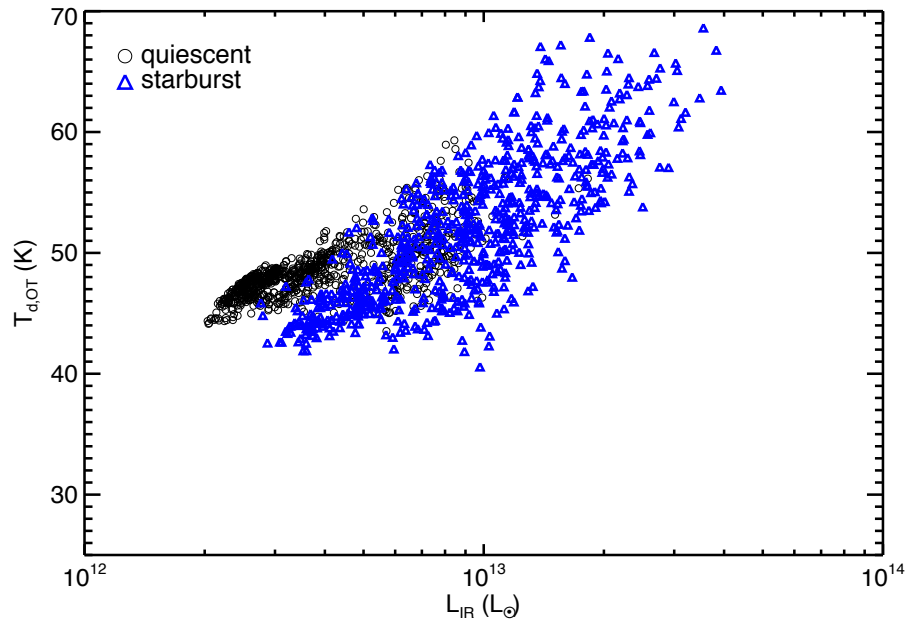
Figure 3.2.—: Same as Figure 3.1, but the PACS 100 and 160 μm photometry has also been used in the fit. The same trends noted before still hold, but adding the shorter-wavelength PACS data causes T_d to be systematically higher and increases the scatter in the $T_d - L_{\mathrm{IR}}$ relation.

point neither form of the single-T modified blackbody provides a good fit. When performing the Levenberg-Marquardt least-squares fit we have assumed $10 \text{ K} \leq T_d \leq 100 \text{ K}$, $1.0 \leq \beta \leq 2.5$, and ten per cent flux uncertainty.

The median T_d values are 30 K (48 K) for the quiescently star-forming galaxies and 35 K (52 K) for the starbursts when the SPIRE+SCUBA+AzTEC (PACS+SPIRE+SCUBA+AzTEC) photometry is used. The key trends to take away from this plot are that effective T_d correlates with luminosity, and the most luminous, hottest sources are almost exclusively starbursts. When the PACS photometry is (not) used, almost all sources with $T_d \gtrsim 55$ (35) K are starbursts. Thus one can use a cut in T_d to cleanly select starbursts from a galaxy population. Note also that inclusion of the PACS photometry results in both systematically increased T_d and larger scatter.

There is increasing evidence that the simple single-T OT modified blackbody form given in Equation (3.5) provides a poor fit to the FIR SEDs of simulated and observed high-redshift ULIRGs on the Wien side of the SED (Chapter 2; Lupu et al. 2010; Conley et al. 2011; A. Sajina, submitted). This is perhaps not surprising since the method is "quaintly anachronistic" (Wu et al. 2009). This is demonstrated in Figure 3.8, which is described in detail below. Instead, more sophisticated forms, such as Equation (3.4) or multi-component models (e.g., Dale & Helou 2002; Clements et al. 2010; Kovács et al. 2010), must be used. Such models can account for non-negligible optical depths in the IR and multiple temperatures of dust,[3] both of which are physically more valid assumptions than those implicit

---

[3]In Equation (3.4) allowing β to vary mimics the effect of a temperature distribution (e.g., Shetty et al. 2009b; Clements et al. 2010).
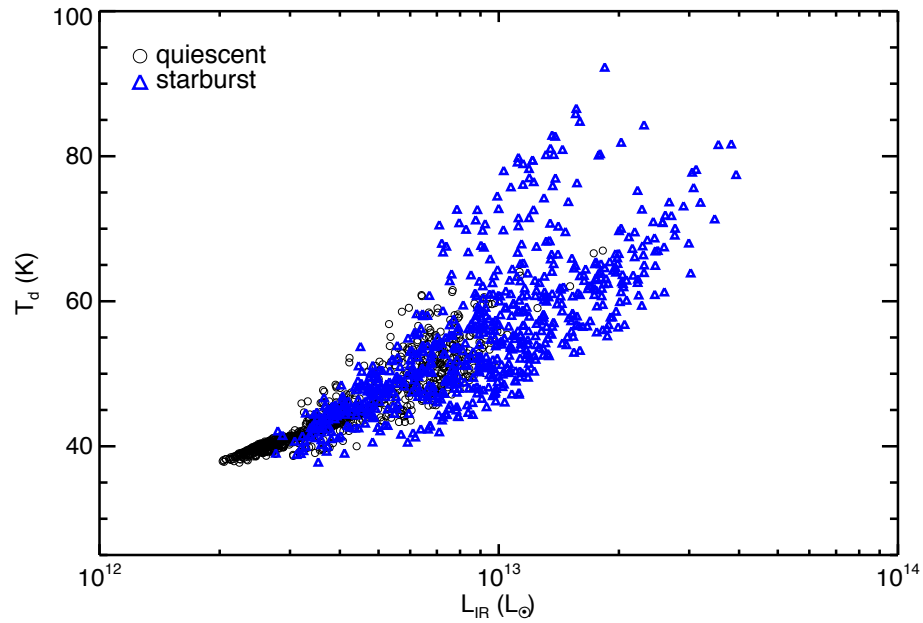
Figure 3.3.—: Same as Figure 3.1, but the effective T_d has been derived by fitting the full form of the modified blackbody (Equation 3.4). The T_d values inferred using this form are systematically higher than when optical thinness is assumed (see text for details), but all qualitative trends seen in Figure 3.1 still hold.
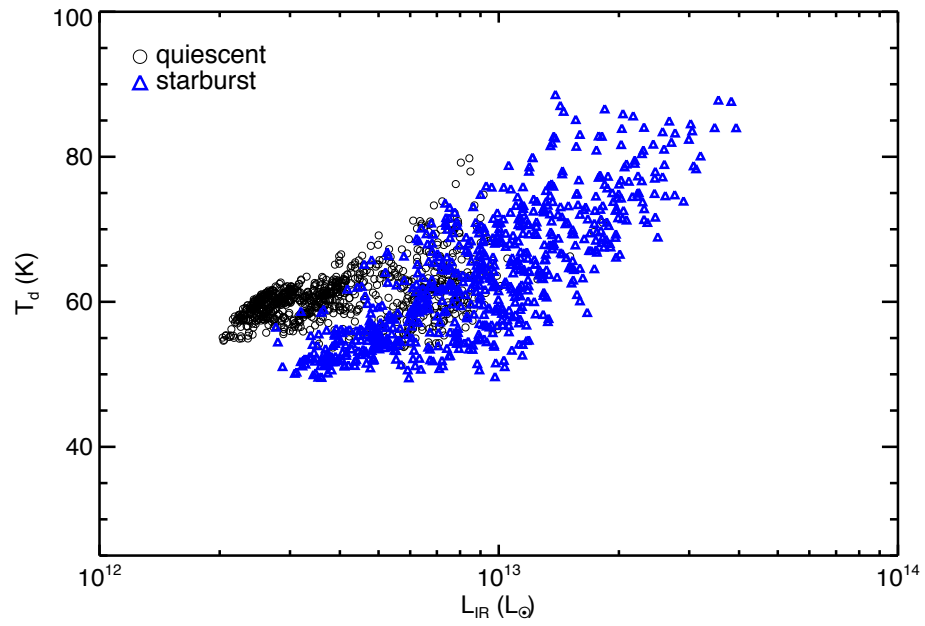
Figure 3.4.—: Same as Figure 3.3, but the PACS 100 and 160 μm photometry has also been used in the fit. Again, addition of the PACS points causes the fitted T_d to be systematically higher.

in the single-T OT blackbody model. Figure 3.3 shows the $T_d - L_{IR}$ plot when we derive the effective T_d by fitting the full form of the modified blackbody, Equation (3.4), to the simulated SPIRE+SCUBA+AzTEC. Figure 3.4 is similar but also includes the PACS 100 and 160 μm points in the SED fits. Again, we have not used the PACS 70 μm point and have assumed 10 K $\leq T_d \leq$ 100 K, 1.0 $\leq \beta \leq$ 2.5, and ten per cent flux uncertainty. We have not constrained ν_0, but in practice it is always greater than $\sim 8 \times 10^{11}$ Hz. The median T_d values are 43 K (60 K) for the quiescently star-forming galaxies and 54 K (63 K) for the starbursts when the SPIRE+SCUBA+AzTEC (PACS+SPIRE+SCUBA+AzTEC) photometry is used. As in Figures 3.1 and 3.2, effective T_d correlates with luminosity, and the most luminous, hottest sources ($T_d \gtrsim$ 70 (60) K when the PACS data are (not) used) are almost exclusively starbursts. Again, inclusion of the PACS photometry results in systematically higher T_d, but the increase in scatter is more modest than when the OT form of the single-T modified blackbody is used.

Comparison of Figures 3.1 - 3.4 above shows that assuming optical thinness results in systematically lower T_d than when Equation (3.4) is used. This occurs because $(1 - e^{-(\nu/\nu_0)^\beta}) < (\nu/\nu_0)^\beta$ for all $\nu > 0$. Thus, for fixed T_d, the assumption of optical thinness will systematically overpredict the flux at frequencies for which $\tau \gtrsim 1$. As a result, for a given SED, T_d derived from Equation (3.5) will be lower than that derived from Equation (3.4). This effect has been demonstrated when fitting SEDs of high-z ULIRGs (e.g., Lupu et al. 2010; Conley et al. 2011; Sajina et al., submitted), and it shows that one should use caution when attempting to interpret T_d physically. We recommend that future observational work use Equation (3.4) when fitting FIR SEDs, as we have found it to be the simplest form that

describes the FIR SEDs of both observed and simulated high-redshift ULIRGs. If a sufficient fit is still not possible then multiple (or a PL distribution of) temperatures can be used, as we will discuss now, but this comes at the expense of at least one additional parameter.

We have also fit a subset (120) of the simulated SEDs assuming a PL temperature distribution with a low-temperature cutoff ($dM_d/dT \propto T^{-\gamma}$ for $T > T_c$, $dM_d/dT = 0$ otherwise) following Kovács et al. (2010). We will summarize our fitting method here but refer the reader to Kovács et al. (2010) for full details of the model. Because of the added parameter γ we have always used the PACS 100 and 160 μm, SPIRE, SCUBA, and AzTEC data. In order to more closely compare to forthcoming *Herschel* observations, we have added errors typical for the GOODS-N field and only used points that would have S/N > 3. We have assumed that single values of β, γ, and R_{eff} can be used for all sources, and we have used a subset of 20 simulated galaxies detected in all bands to fix those parameters in the following manner: We first gridded the $(\beta, \gamma, R_{\text{eff}})$ parameter space. For each point in the grid we fit all 20 sources allowing T_d and M_d to vary. We summed the chi-squared values of the individual fits for each parameter combination and chose the parameter combination with the lowest total chi-squared value. The parameters we determined in this manner are $\beta = 1.6$, $\gamma = 8.7$, and $R_{\text{eff}} = 2$ kpc. The values of β and R_{eff} are in good agreement with those from Kovács et al. (2010), $\beta = 1.5$ and $R_{\text{eff}} = 2$ kpc. Our temperature distribution is steeper than that found by Kovács et al., $\gamma = 6.7$, perhaps because our simulations do not yet include stochastically heated very small grains (VSGs) and thus may underestimate the amount of dust at high temperatures.
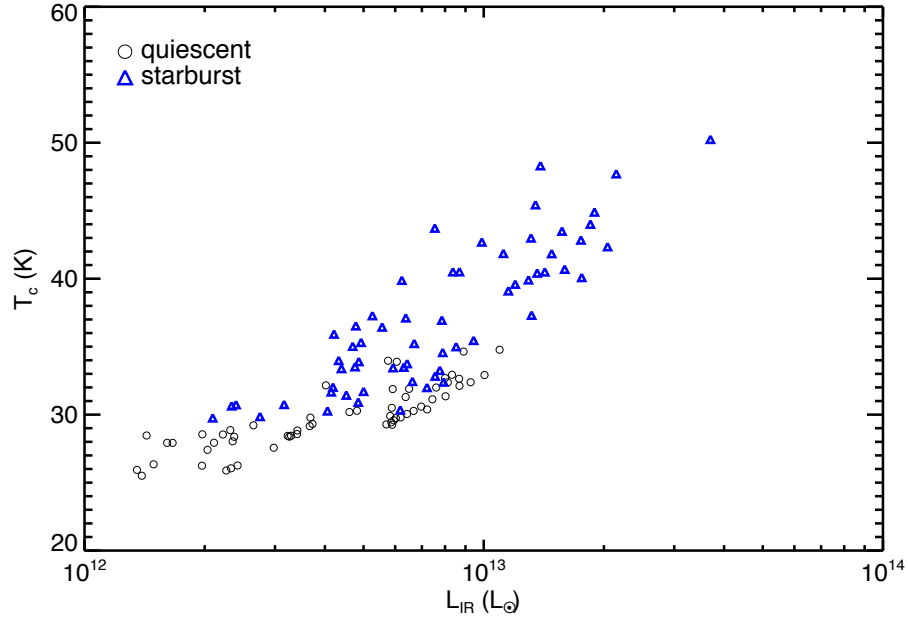
Figure 3.5.—: Same as Figure 3.2, but the effective T_d has been derived by assuming a PL distribution of T_d following Kovács et al. (2010) (the temperature plotted is the low-temperature cutoff of the PL distribution; see text for details). Again, the values of T_d differ, but the trends are insensitive to the manner in which the effective T_d is derived. Here there is a very clear separation in temperature between the two modes: all sources with $T_c \gtrsim 35$ K are starbursts.

Using the above parameter values we have fit the full subset of 120 simulations. The resulting $T_d - L_{\mathrm{IR}}$ plot is shown in Figure 3.5. Note that the temperature plotted here is the low-temperature cutoff, T_c, which is also the temperature of most of the dust because of the steepness of the PL distribution. The median cutoff temperatures are 30 K for the quiescently star-forming galaxies and 36 K for the starbursts. Again, there is a clear correlation between effective T_d and luminosity, and the starbursts are the most luminous and have the highest values of T_c. Here, all galaxies with $T_c \gtrsim 35$ K are starbursts.

Figures 3.1 - 3.5 all show that the $T_d - L_{\mathrm{IR}}$ plot is an excellent way to distinguish between quiescently star-forming galaxies and starbursts. In all five figures there is a clear correlation between T_d and L_{IR}, which agrees with observations of both local (e.g., Kovács et al. 2006; Amblard et al. 2010; Hwang et al. 2010) and high-redshift (e.g., Amblard et al. 2010; Magnelli et al. 2010; Chapman et al. 2010) ULIRGs. Though there is some overlap between the two populations, the most luminous, hottest sources are almost exclusively starbursts. Note that both the $T_d - L_{\mathrm{IR}}$ correlation and the separation between the populations are independent of the fitting method used, though the specific temperature values above which there are no quiescently star-forming galaxies differ (as expected because of the systematic difference in temperatures yielded by the two methods). Thus our simulations make the clear, robust prediction that the most luminous galaxies will have the hottest SEDs and will be almost all late-stage merger-induced starbursts. Put another way, the galaxies in the high-T_d, high-L_{IR} region of the $T_d - L_{\mathrm{IR}}$ plane should typically lie above the SFR-$M_\star$ relation (as shown quantitatively below), or, in recently popular parlance (e.g., Elbaz et al. 2011; Rodighiero et al. 2011; Wuyts et al. 2011),
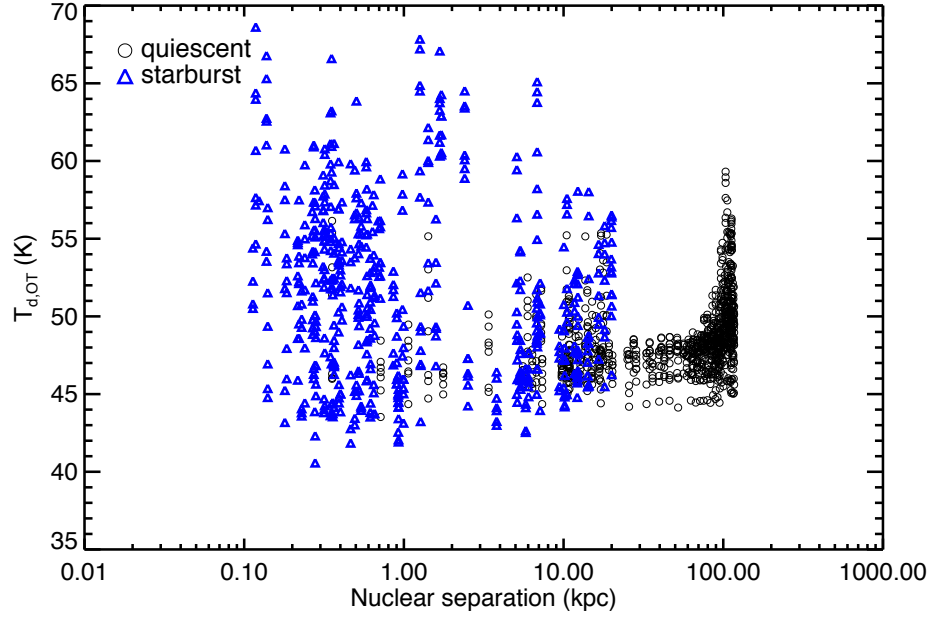
Figure 3.6.—: Effective T_d derived from fitting the single-T OT modified blackbody (Equation 3.5) to the PACS+SPIRE+SCUBA+AzTEC photometry versus nuclear separation in kpc. Though there is a large scatter in effective temperature at a given nuclear separation, the objects with the highest effective T_d ($T_d \gtrsim 55$ K) are almost exclusively late-stage merger-induced starbursts with $d_{\mathrm{BH}} \lesssim 20$ kpc.
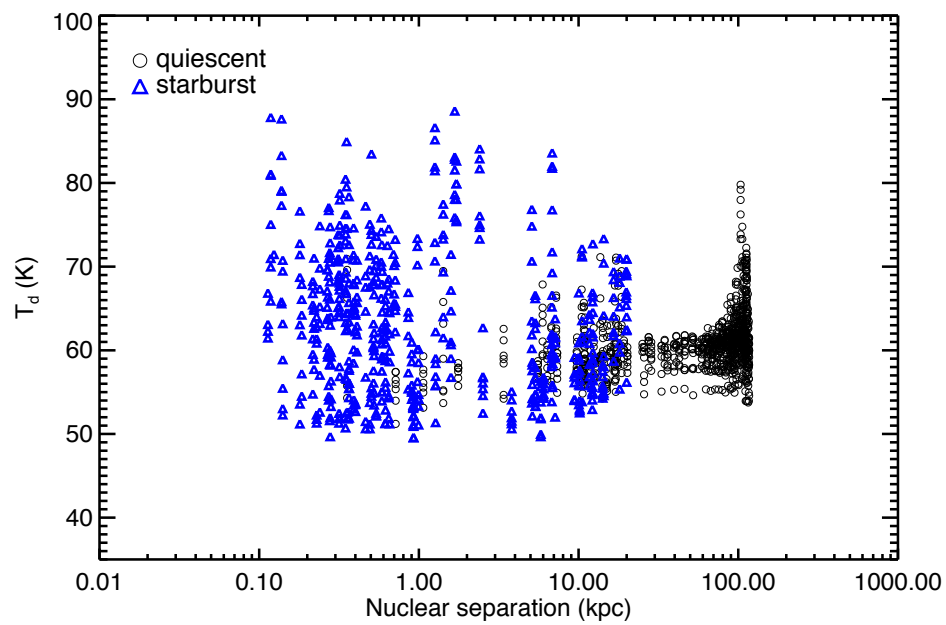
Figure 3.7.—: Same as Figure 3.7, but the full modified blackbody form (Equation 3.4) has been used for the fit.

be outliers from the "main sequence of star formation", as has been observed by Elbaz et al. (2011). Furthermore, as shown in Figures 3.6 and Figure 3.7, the mergers nearest coalescence tend to be those with the hottest effective T_d because the starburst is strongest at final coalescence of the two galaxies.

Comparison of Fitting Forms

In Figure 3.8 we show the rest-frame SED of one of the simulated starbursts viewed from a single viewing angle. The over-plotted data points are the PACS 100 & 170 μm, SCUBA 250, 350, & 500 μm, SCUBA 850 μm, and AzTEC 1.1 mm photometry. The three lines are fits to the photometry using the fitting forms discussed above. Figure 3.9 shows the ratio of the model SED derived from fitting the photometry to the actual SED for each of the fitting methods. It is instructive to consider how well the different forms reproduce the SED beyond the wavelength range spanned by the photometry.[4] As explained above, we expect the OT modified blackbody to under-predict the SED on the Wien side of the SED. Indeed, this model under-predicts the SED shortward of the PACS 100 μm data point. The full form of the modified blackbody fares better, but it also under-predicts the SED for rest-frame wavelength $\lambda_{\mathrm{rest}} \lesssim 20$ μm. The PL temperature distribution model fares best at the shortest wavelengths, but it over-predicts the SED at $\lambda_{\mathrm{rest}} \sim 15 - 25$ μm

---

[4]It is important to keep in mind that the models are "nested" in the sense that the PL T_d distribution model reduces to the single-T modified blackbody as $\gamma \to \infty$, and the single-T modified blackbody reduces to the single-T OT modified blackbody as $\nu_0 \to \infty$.

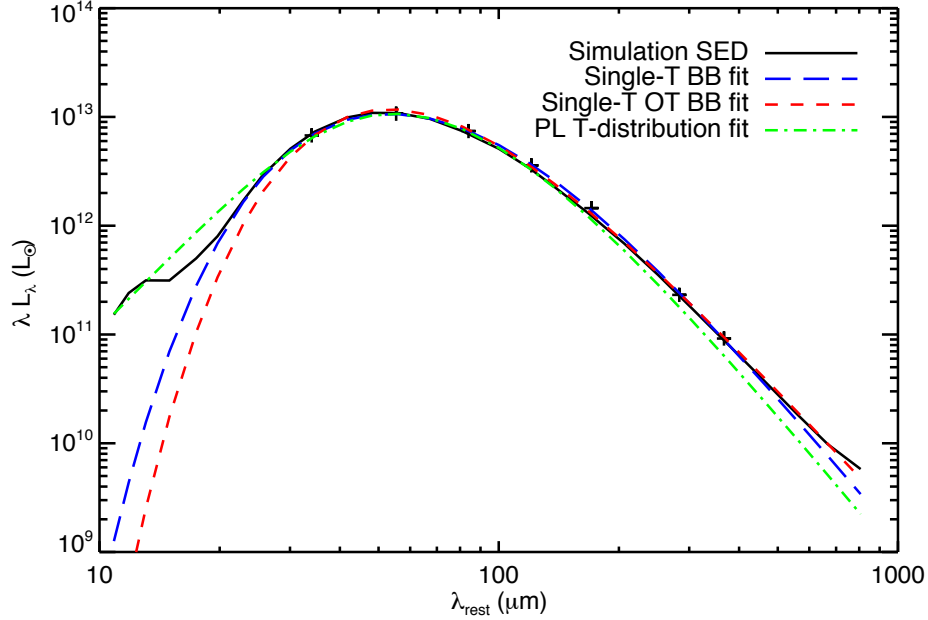Figure 3.8.—: The black line is an example rest-frame FIR SED, $\lambda L_\lambda (L_\odot)$ versus λ_{rest} (μm), of a simulated galaxy. The crosses are the PACS 100 and 170 μm, SCUBA 250, 350, and 500 μm, SCUBA 850 μm and AzTEC 1.1 mm photometry calculated from the simulation SED. The other lines are best fits to the photometric points for different fitting forms: the single-T OT modified blackbody (Equation 3.5, with $T_d = 53$ K, $\beta = 1.1$; red dashed), the full form of the single-T modified blackbody (Equation 3.4, with $T_d = 69$ K, $\beta = 1.5$; blue long-dashed), and the PL T_d distribution model (Kovács et al. 2010; $T_c = 40$ K, $\beta = 1.6$; green dash dot). The derived T_d and β depend strongly on the fitting method, suggesting that these parameters should not be interpreted literally. See text for details.
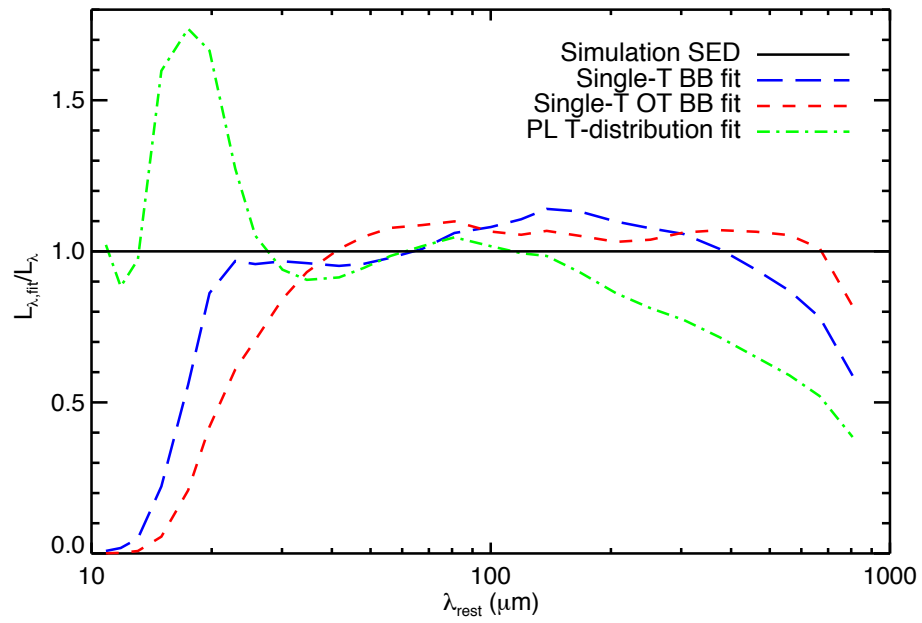
Figure 3.9.—: Ratio of the fitted L_λ to the actual L_λ versus λ_{rest} (μm) for the same SED as in Figure 3.8.

and does not reproduce the detailed shape of the SED.[5] At the longest wavelengths
the OT model is most accurate because the fitted $\beta = 1.1$ for that model is
significantly less than that of both the full modified blackbody ($\beta = 1.5$) and the PL
model ($\beta = 1.6$), resulting in a less steeply declining SED.

All fitting forms are able to fit the photometric points well, though this would
not be the case for the single-T OT modified blackbody if we were to fix $\beta = 1.5$ or
2.0, as is typically done. Despite this, they have varying levels of success describing
the SED beyond the wavelengths spanned by the photometry. Furthermore, the
derived parameters T_d and β, which are often interpreted as a physical T_d and the
intrinsic PL index of the emissivity of the dust grains in the FIR, vary significantly
for the different fitting forms ($T_d = 53$, 69, and 40 K and $\beta = 1.1$, 1.5, and 1.6
for the single-T OT modified blackbody, single-T modified blackbody, and PL
models, respectively). Consequently, it is difficult to interpret the fitted parameters
physically, as the intrinsic properties of the dust do not vary with the method
used to fit the SED. If the fitted T_d have a physical meaning, they may correspond
to different physical temperatures (e.g., the single-T modified blackbody may
recover the luminosity-weighted T_d whereas the PL model may better recover the
mass-weighted temperature). The fitted β values cannot all be equal to the intrinsic
β of the dust, which is ~ 2 for the dust model we use. Instead, since T_d and β are

---

[5]Note, however, that the β, γ, and R_{eff} parameters of the PL temperature dis-
tribution model were not tuned to fit this specific SED but rather determined by
minimizing the total chi squared value for a set of 20 simulated galaxies, as described
above. Only T_d and M_d were allowed to vary when fitting this SED. If all parame-
ters were allowed to vary the fit of the PL temperature distribution model would be
improved, but this is not feasible with the current method because there are almost
as many parameters as data points.

degenerate (e.g., Sajina et al. 2006), the fitted β depends on the T_d distribution in addition to the intrinsic β; non-negligible optical depths in the IR further complicate the picture. Clearly it is necessary to explore how the fitted parameters relate to intrinsic properties of the dust, but we defer further exploration of this complex topic to future work. The only points we wish to make here are that it may be necessary to use forms more complex than the single-T OT modified blackbody to fit IR SEDs and that the parameters derived from the fits should not be interpreted literally. Instead, the models should be thought of as useful ways to encapsulate the data with a few parameters and thus compare galaxy SEDs in a simple manner.

3.3.2   Star Formation Efficiency

Since starbursts form stars much more efficiently than quiescently star-forming galaxies, one should be able to distinguish between them via some observational indicator of star formation efficiency. Daddi et al. (2010) and Genzel et al. (2010) provide evidence that quiescently star-forming galaxies and starbursts follow different KS relations, with the starburst relation having normalization $\sim 10\times$ greater than that for quiescently star-forming disk galaxies. Furthermore, the merger-induced starbursts have global star formation efficiency, SFE $= L_{\rm IR}/M_{\rm H_2}$, $\sim 10\times$ greater than that of the quiescently star-forming disks. In Figure 3.10 we plot SFE versus $L_{\rm IR}$. Figure 3.11 shows SFE versus nuclear separation. Since these simulations do not track molecular gas separately we use the total gas mass to calculate SFE instead.

Figure 3.10 shows a clear correlation between $L_{\rm IR}/M_{\rm gas}$ and $L_{\rm IR}$. At a given $L_{\rm IR}$, the starbursts have SFE up to $5\times$ greater than that of the quiescently star-forming
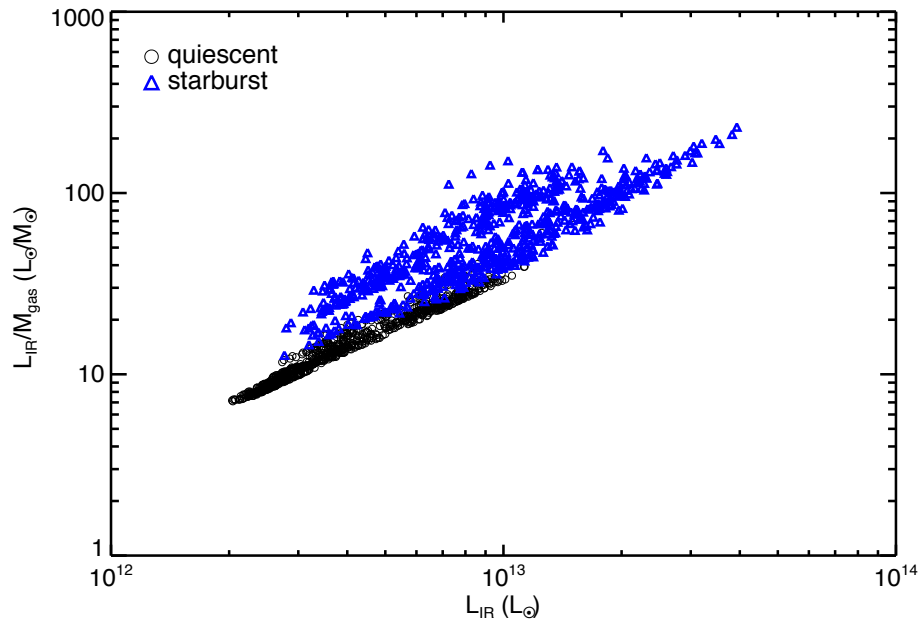
Figure 3.10.—: Global star formation efficiency SFE = L_{IR}/M_{gas} ($L_\odot/M_\odot$) versus L_{IR} ($L_\odot$). SFE increases with L_{IR} and is characteristically higher by a factor of a few for starbursts than for quiescently star-forming disks at fixed L_{IR}.
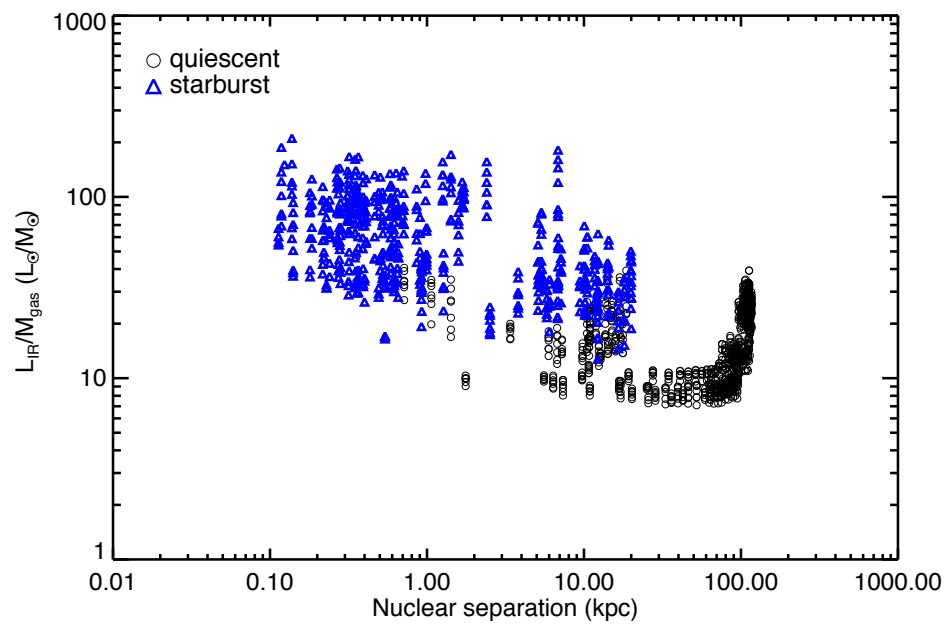
Figure 3.11.—: SFE versus nuclear separation (kpc). The starbursts near coalescence have the highest SFE.

galaxies. Figure 3.11 demonstrates that the SFE increases as the merger advances and is highest for mergers nearest coalescence. The simulations qualitatively reproduce the two trends shown in Figure 1 of Daddi et al. (2010, i.e., the correlation between SFE and L_{IR} and the discrepancy between starbursts and quiescently star-forming galaxies). However, for a given L_{IR} the SFE of the simulated galaxies are $\sim 2 - 3\times$ lower than the observed values. Part of this is because not all of the gas in a galaxy is molecular, so if we used the molecular gas mass rather than the total gas mass the resulting SFEs would be a factor of a few higher. The SFE of the simulated starbursts is only a factor of $\sim 2 - 3\times$ greater than that of the simulated quiescently star-forming galaxies, whereas the observed difference is $\sim 4 - 10\times$. For the starbursts nearest coalescence, however, the difference can be as great as $10\times$ (see Figure 3.11). One possible reason the SFE discrepancy is lower than observed is that, because of the setup of our simulations, galaxies in the pre-burst, quiescently star-forming stage have systematically higher gas fractions than those in the starburst phase. Since the star formation law implemented in the simulations has a non-linear dependence on gas density the SFE will increase with gas fraction.

Inferring the total molecular gas mass from CO observations is notoriously difficult, as the CO-H$_2$ conversion factor $X_{\text{CO}} = N_{\text{H2}}/L'_{\text{CO}}$ depends on the giant molecular cloud surface density and kinetic temperature and velocity dispersion within clouds. As a result, X_{CO} is expected to be a factor of $\sim 2 - 10\times$ lower in starbursts than in disk galaxies (Narayanan et al. 2011b; Shetty et al. 2011a,b). For this reason it would be best for us to predict the CO line luminosity for our simulated galaxies, as has been done by, e.g., Narayanan et al. (2009), and, ideally, to self-consistently track formation and destruction of molecular gas as done by,

e.g., Robertson & Kravtsov (2008). However, doing so requires introduction of another code in addition to the two employed and the corresponding complexities and uncertainties, so we feel this is best left to future work.

Still, despite these uncertainties, the simulations make the robust prediction that those systems with largest SFE at a given L_{IR} will be merger-induced starbursts. From the discussion in Section 3.3.1 we see that the sources with the highest SFE should also tend to have the highest luminosities and effective T_d.

3.3.3 Obscuration

In Figure 3.12 we plot the total IR luminosity divided by the rest-frame far-UV luminosity, $L_{\mathrm{IR}}/L_{\mathrm{FUV}}$—often referred to as the IR excess (IRX)—versus L_{IR}. Figure 3.13 shows IRX versus nuclear separation. The IRX serves as a measure of the amount of obscuration of a galaxy. IRX increases with L_{IR}, as has previously been both observed (e.g., Wang & Heckman 1996; Buat & Burgarella 1998; Buat et al. 1999, 2005, 2007, 2009; Adelberger & Steidel 2000; Hopkins et al. 2001; Bell 2003; Reddy et al. 2010) and demonstrated by simulations (Jonsson et al. 2006). The quiescently star-forming galaxies tend to have lower $L_{\mathrm{IR}}/L_{\mathrm{FUV}}$ (the median value is 145) than the starbursts (median 228), primarily because the starbursts are typically more luminous. At a given L_{IR}, the starbursts and quiescently star-forming disks have very similar $L_{\mathrm{IR}}/L_{\mathrm{FUV}}$. Jonsson et al. (2006) have previously demonstrated this result using similar simulations, and they argue that the correlation arises because both SFR and dust obscuration correlate with density. The right panel shows that obscuration increases with merger stage; physically this occurs because the galaxies
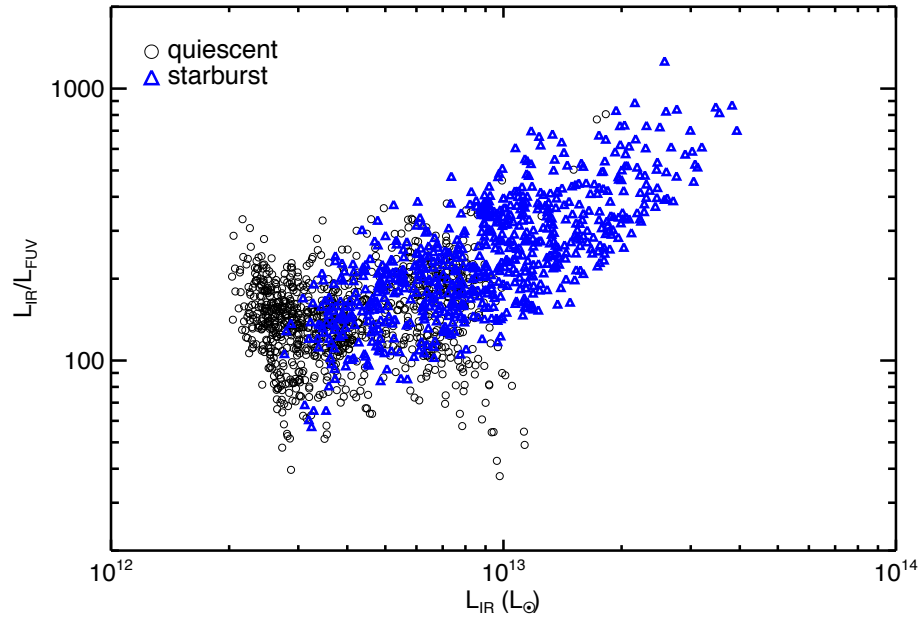
Figure 3.12.—: IR excess ($\mathrm{IRX} \equiv L_{\mathrm{IR}}/L_{\mathrm{FUV}}$) versus L_{IR} ($L_{\odot}$). For the starbursts, IRX is correlated with L_{IR}. The starbursts are typically more obscured (have higher IRX) than the quiescently star-forming galaxies. However, for fixed L_{IR} the starbursts and quiescently star-forming disks have similar IRX values, so the starbursts typically have higher IRX because they are typically more luminous than the quiescently star-forming disks.

Figure 3.13.—: IRX versus nuclear separation (kpc). For the starbursts, IRX is anti-correlated with nuclear separation because as the galaxies coalesce the centrally concentrated, heavily obscured starburst becomes dominant over the more extended star formation.

are more compact at coalescence than during the pre-burst, infalling-disk stage, and, for a fixed dust mass, a smaller size results in a larger optical depth. Furthermore, the 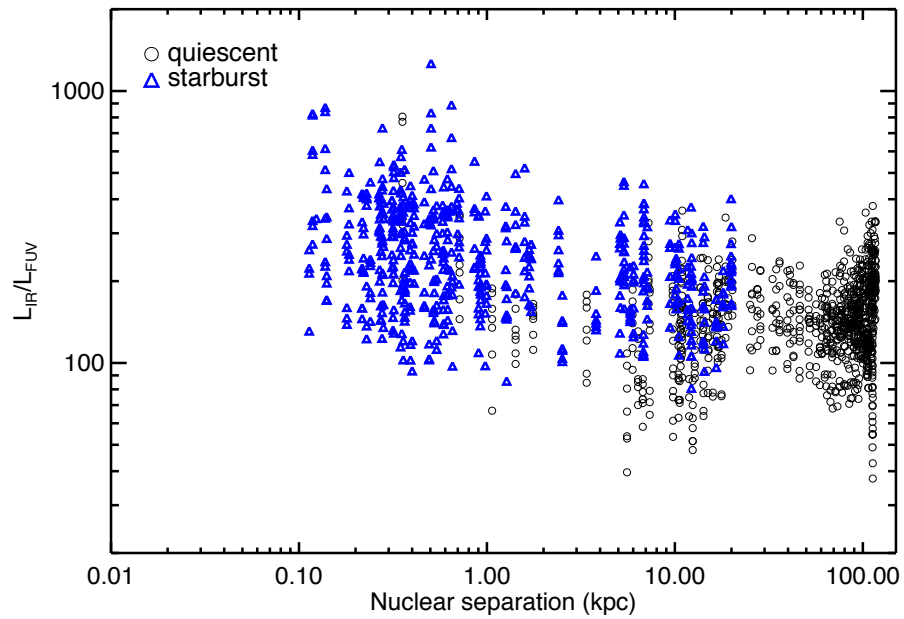stars formed in the starburst, which dominate the luminosity, are centrally concentrated and thus typically more obscured than stars distributed throughout the initial disks.

The assumption we have made about sub-resolution dust obscuration in our simulations may cause the obscuration of the quiescently star-forming galaxies to be biased high. This is because we have ignored the SH03 multiphase ISM structure when calculating the optical depths, effectively assuming that the cold phase of the ISM has a volume filling factor of unity. This assumption is likely reasonable for the central regions of the merger-induced starbursts (e.g., Downes & Solomon 1998), but it may be too extreme for the quiescently star-forming disk galaxies. (Note, however, that Jonsson et al. (2006) used a different sub-resolution ISM treatment and found a qualitatively similar result, suggesting that similarity of the IRX-L_{IR} relations for quiescently star-forming galaxies and starbursts is insensitive to the assumptions made about sub-resolution dust obscuration.)

3.3.4   SFR-$M_\star$ Relation

As discussed in Section 3.1.1, if the tight SFR-$M_\star$ relation observed is set by gas accretion then galaxies that lie above the relation must be undergoing transient events that temporarily boost their SFR above what can be sustained over long time periods. Major mergers are one type of event that causes galaxies to move above the relation. We plot the SFR-$M_\star$ relation for our simulated galaxies in Figure 3.14
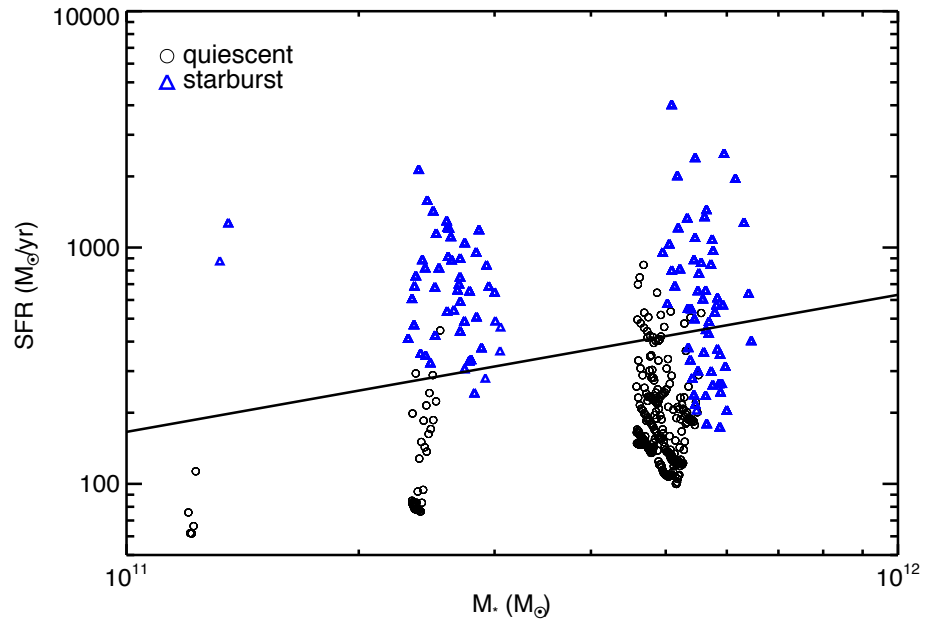
Figure 3.14.—: SFR ($M_\odot$ yr^{-1}) versus $M_\star$ for all snapshots with $f_g < 0.4$. The solid line is the relation for the $z = 2.0 - 2.5$ bin of Karim et al. (2011). Simulated galaxies above the observed relation are almost exclusively starbursts, and the starbursts typically lie above the relation.

along with the observed relation for $z = 2.0 - 2.5$ from Karim et al. (2011). Almost all objects above the observed relation are starbursts, and most of the starbursts are above the relation. For a given $M_\star$ the starbursts can have SFR as much as $\sim 10\times$ greater than the quiescently star-forming galaxies. Furthermore, in our idealized simulations the pre-burst disks have systematically higher f_g because there is no cosmological gas accretion. Since SFR scales super-linearly with gas surface density this will bias the quiescently star-forming galaxies' SFR high relative to the starbursts. Thus the magnitude of the difference between starbursts and quiescently star-forming disks' SFR shown in Figure 3.14 should be taken as a lower limit.

Observationally, whether SMGs lie on the SFR-$M_\star$ relation depends sensitively on the measured L_{IR} used to infer the SFR and the inferred $M_\star$. The latter is especially difficult to infer, as different authors have inferred masses differing by a factor of ~ 6 for the same SMGs (Michałowski et al. 2010a,b, 2011; Hainline et al. 2010). Michałowski et al. (2011) have demonstrated that the Hainline et al. values are systematically lower than those of Michałowski et al. primarily because Hainline et al. use single-component SFHs whereas Michałowski et al. use two components. The latter is more reasonable for the simulated merger-driven starburst SMGs, whose SFHs can be approximated by a instantaneous burst superimposed on a constant SFH, and also more general, so we prefer the Michałowski et al. (2011) values. If the Michałowski et al. (2011) masses are used, SMGs lie much closer to the SFR-$M_\star$ relation than they do if the Hainline et al. (2010) masses are used, though there are still some outliers mixed in. This conclusion is consistent with our claim that the SMG population is a mix of both quiescently star-forming and starburst galaxies.

3.4   Discussion

If one wishes to understand star formation it is crucial to look beyond the local universe, because the SFR density of the universe was greatest at $z \sim 2-3$ (e.g., Hopkins 2004; Hopkins & Beacom 2006; Hopkins et al. 2010a; Karim et al. 2011). Furthermore, the bulk of the star formation at those redshifts was obscured (e.g., Bouwens et al. 2011; Magnelli et al. 2011), so studying IR-luminous galaxies at those redshifts is crucial. Unfortunately, galaxies become fainter and physical resolution poorer as one moves from $z \sim 0$ to higher redshift, so observations of high-redshift galaxies are significantly less detailed than for local galaxies; in particular, in the IR, $z \sim 2-3$ galaxies are often aptly described as "blobs". It is thus tempting to use wisdom gleaned from detailed observations of local galaxies to guide the interpretation of observations high-redshift galaxies. This is perfectly acceptable if the only difference between local galaxies and those at $z \sim 2-3$ is that the latter are further away. However, this is clearly not the case, so one must apply local universe-derived wisdom with caution.

Assuming what is true locally is also true at $z \sim 2-3$ can be problematic. For example, as discussed in Section 3.3.2, locally it seems that the CO-H_2 conversion factor X_{CO} differs for ULIRGs (i.e., merger-induced starbursts) and quiescently star-forming disk galaxies (e.g., Solomon et al. 1997; Downes & Solomon 1998). If one wishes to, e.g., study possible evolution of the KS law with redshift then, lacking other options, it is necessary to assume some CO-H_2 conversion factor for the high-redshift galaxy populations observed. Choosing an appropriate X_{CO} requires determining whether the high-redshift galaxies are analogous to local merger-induced

starbursts or quiescently star-forming disks. For example, since it is commonly thought that SMGs are merger-driven starbursts, Daddi et al. (2010) and Genzel et al. (2010) use the starburst X_{CO} value for SMGs. If, however, SMGs are a mix of quiescently star-forming, early-stage mergers and late-stage, merger-induced starbursts, as we have argued in Sections 2.4.2 and 3.1.2, then a single X_{CO} value is not appropriate for the population. In this case, use of the ULIRG X_{CO} value will artificially accentuate the apparent differences between SMGs and more typical galaxies at high redshift. Still, the different KS law normalizations and SFEs for starbursts and quiescently star-forming galaxies demonstrated by Daddi et al. (2010) and Genzel et al. (2010) persist even when the same X_{CO} value is used for all populations, so the qualitative picture may be robust despite this complication; the quantitative details, however, crucially depend on correctly distinguishing starbursts and quiescently star-forming galaxies.

Choosing which value of X_{CO} to use is only one example of when it is important to distinguish quiescently star-forming and starburst galaxies. In general, anytime we wish to make comparisons between low- and high-redshift galaxies we must be sure we are comparing appropriate populations. For SMGs in particular, a commonly asked question is "Are SMGs analogous to local ULIRGs?" This question implicitly has two parts: 1. Local ULIRGs are late-stage, merger-induced starbursts; is this also true of SMGs? 2. If so, how do starbursts at $z \sim 2 - 3$ compare to those at $z \sim 0$? We have argued that the answer to the first question is no. Thus if one wishes to address the second question the subpopulation of starburst SMGs must be separated from the rest. Otherwise the second question would become "How does a mixed population of quiescently star-forming and starburst galaxies at $z \sim 2 - 3$

compare to starbursts at $z \sim 0$?"; this is not a physically meaningful comparison.

Furthermore, if one wishes to understand which mode of star formation dominates the SFR density of the universe one must be able to separate the modes. Even when one can clearly identify mergers (e.g., by the presence of tidal features) one cannot assume that those galaxies are dominated by merger-induced star formation, as the SFR elevation caused by the mutual tidal torques is significant only near coalescence and, depending on the gas content and bulge fraction of the progenitors, possibly first passage. (See Hopkins et al. 2010a for further discussion of the distinction between star formation in mergers and merger-induced star formation.) The problem is amplified at higher redshifts because mergers cannot be as easily identified as they can locally.

Fortunately, the integrated SED of a galaxy contains much information about the star formation mode powering it, so it is possible to use the diagnostics we have presented here to distinguish between star formation modes. It is our hope that this work will facilitate physically motivated comparisons of high- and low-redshift galaxies and thus further our understanding of star formation and, consequently, galaxy formation.

3.5   Conclusions

We have combined high-resolution 3-D hydrodynamic simulations of $z \sim 2$ major mergers of disk galaxies and 3-D Monte Carlo dust RT calculations to investigate the differences between quiescently star-forming and starburst galaxies. We have

focused on the SMG population as a case study because, as argued in Section 2.4.2 and elaborated in Section 3.1.2, the SMG population is likely a mix of quiescently star-forming galaxies and merger-induced starbursts. Our models make robust observational predictions for how quiescently star-forming galaxies on the "main sequence of star formation" should differ from merger-induced starbursts, which lie above the SFR-$M_\star$ relation. We present multiple observational diagnostics which can distinguish quiescently star-forming and starburst galaxies based on integrated data alone. The testable predictions and observational diagnostics presented in this work include:

1. Effective T_d—derived from fitting either a single-T OT modified blackbody, the full form of the single-T modified blackbody, or a model including a power-law distribution of T_d—correlates with $L_{\rm IR}$, and the galaxies in the high-$L_{\rm IR}$, high-T_d region of the $T_d - L_{\rm IR}$ plot are almost exclusively merger-induced starbursts.

2. Star formation efficiency, $L_{\rm IR}/M_{\rm gas}$, correlates with $L_{\rm IR}$, and the sources with highest SFE at a given luminosity are starbursts.

3. Obscuration, as parameterized by IRX $\equiv L_{\rm IR}/L_{\rm FUV}$, correlates with $L_{\rm IR}$. The most luminous starbursts have IRX a factor of a few greater than quiescently star-forming galaxies. At fixed $L_{\rm IR}$ the IRX values are similar for quiescently star-forming disks and starbursts, so the reason starbursts have higher typical IRX is primarily because they are typically more luminous than quiescently star-forming galaxies.

4. Effective T_d, star formation efficiency, and obscuration are all inversely

correlated with nuclear separation because the starburst mode becomes more dominant as the galaxies coalesce.

5. Most starbursts lie above the SFR-$M_\star$ relation (aka main sequence of star formation), whereas most quiescently star-forming galaxies lie close to it (by definition).

One can apply these observational diagnostics to test our claim that the SMG population is a mix of quiescently star-forming galaxies and merger-induced starbursts and to constrain the relative contribution of the different types of galaxies. Furthermore, the tests presented here provide physically motivated ways to observationally separate quiescently star-forming galaxies and starbursts, enabling one to more cleanly study the underlying physics than when heterogenous samples (e.g., SMGs) are used. Though we have focused on the SMG population here, most of the diagnostics can be applied to other galaxy populations.

Finally, we have explored how well various IR SED fitting forms describe our simulations' SEDs. For a given SED, the fitted T_d and β can vary significantly depending on what form is used, so these parameters should not be interpreted literally. In future work we will more thoroughly investigate how well the different FIR SED fitting methods describe our simulated galaxy SEDs, determine how the inferred dust properties relate to the actual physical properties, and develop an improved method for fitting the FIR SEDs of large samples of galaxies.

Chapter 4

Submillimeter-Selected Galaxy Number Counts Do Not Provide Evidence for a Top-Heavy Initial Mass Function

All problems in extragalactic astrophysics can be solved by a suitable choice of the IMF. – Romeel Davé

Resorting to altering the initial mass function is a sign of moral weakness... the last refuge of scoundrels. – Mike Edmunds

Abstract

Explaining the observed submillimeter-selected (SMG) galaxy counts has been a difficult task for galaxy formation models. As a result, some authors have suggested that a top-heavy—or even flat—initial mass function (IMF) may be required. We re-analyze this claim using a novel approach: We combine a simple, semi-empirical model for galaxy abundances and merger rates with high-resolution, 3-D hydrodynamical simulations and 3-D dust radiative transfer in order to predict SMG counts. Since the stellar mass functions, gas and dust masses, and sizes of our galaxies are constrained to match observations we are able to focus on uncertainties related to the dynamical evolution of galaxy mergers and the dust radiative transfer. We use a Kroupa IMF, as we wish to test whether the observed counts can be matched without resorting to a top-heavy IMF. The counts predicted by our model are in reasonable agreement with the observed SMG counts, suggesting that the observed SMG counts do not provide evidence for IMF variation. We discuss possible reasons why our model differs from previous work.

4.1   Introduction

Submillimeter-selected galaxies (SMGs; Smail et al. 1997; Barger et al. 1998; Hughes et al. 1998; Eales et al. 1999; see Blain et al. 2002 for a review) are amongst some of the most luminous, rapidly star-forming galaxies known, with luminosities in excess of $10^{12} L_\odot$ and star formation rates (SFR) of order $\sim 10^2 - 10^4 \ M_\odot \ \mathrm{yr}^{-1}$ (e.g., Kovács et al. 2006; Coppin et al. 2008; Michałowski et al. 2010a, 2011). They have stellar

masses of $\sim 10^{11} M_\odot$, though recent estimates (Hainline et al. 2010; Michałowski et al. 2010a, 2011) differ by a factor of ~ 6, and typical gas fractions of $\sim 40\%$ (Tacconi et al. 2006, 2008).

Locally, ultra-luminous infrared galaxies (ULIRGs) seem to be exclusively late-stage major mergers (e.g., Lonsdale et al. 2006), as the strong tidal torques exerted by the galaxies upon one another when they are near coalescence cause significant gas inflows and, consequently, bursts of star formation (e.g., Hernquist 1989; Barnes & Hernquist 1991, 1996; Mihos & Hernquist 1996). Thus it is natural to suppose that SMGs, the most luminous, highly star-forming galaxies at high redshift, are also late-stage major mergers undergoing starbursts. There is significant observational support for this picture (e.g., Ivison et al. 2002, 2007, 2010; Chapman et al. 2003; Neri et al. 2003; Smail et al. 2004; Swinbank et al. 2004; Greve et al. 2005; Tacconi et al. 2006, 2008; Bouché et al. 2007; Biggs & Ivison 2008; Capak et al. 2008; Younger et al. 2008, 2010; Iono et al. 2009; Engel et al. 2010). However, there may not be enough major mergers of galaxies of the required masses to account for the observed SMG abundances (e.g., Davé et al. 2010). Consequently, explaining the abundance of SMGs has proven to be a challenge for galaxy formation models.

Various authors have attempted to explain the observed abundance of SMGs using phenomenological models (e.g., Pearson & Rowan-Robinson 1996; Blain et al. 1999b; Devriendt & Guiderdoni 2000; Lagache et al. 2003; Negrello et al. 2007), semi-analytic models (SAMs; e.g., Guiderdoni et al. 1998; Blain et al. 1999a; Granato et al. 2000; Kaviani et al. 2003; Granato et al. 2004; Baugh et al. 2005; Fontanot et al. 2007; Fontanot & Monaco 2010; Lacey et al. 2008, 2010; Swinbank et al. 2008; Lo Faro et al. 2009; González et al. 2011), and hydrodynamical cosmological

simulations (Fardal et al. 2001; Davé et al. 2010). Granato et al. (2000, hereafter G00) presented one of the first SAMs to self-consistently calculate dust absorption and emission by coupling the GALFORM SAM of Cole et al. (2000) with the GRASIL spectrophotometric code (Silva et al. 1998). This was a significant advance over previous work, which effectively treated the dust temperature as a free parameter. Self-consistently computing dust temperatures made matching the submm counts significantly more difficult; the submm counts predicted by the G00 model were a factor of $\sim 20\times$ less than those observed (Baugh et al. 2005). Granato et al. (2004) presented an alternate model, based on spheroid formation via monolithic collapse, which predicts submm counts in good agreement with those observed and reproduces the evolution of the K-band luminosity function. However, this model does not treat halo or galaxy mergers.

Of particular interest is the work of Baugh et al. (2005, hereafter B05), which we will discuss in detail here. B05 set out to modify the G00 model so that it would reproduce the properties of both $z \sim 2$ SMGs and Lyman-break galaxies (LBGs) while also matching the observed $z = 0$ optical and IR luminosity functions. B05 made various modifications to the G00 model. The modifications include: 1. Modifying the star-formation timescale in disks so that gas is consumed less rapidly at high redshift and thus the mergers at those redshifts are more gas-rich. 2. Allowing minor mergers to trigger starbursts if the gas fraction of the more-massive galaxy exceeds 75%. 3. Adopting a flat initial mass function (IMF) in starbursts.[1]

---

[1]Specifically, the IMF they use is $dn/d\log M = $ constant for the mass range $0.15 < M < 125 M_\odot$. The Kroupa (2001) IMF has $dn/d\log M \propto m^{-1.3}$ for $m > 1 M_\odot$, so the difference between the B05 IMF and that observed locally is considerable.

4. Changing the dust emissivity in starbursts at wavelengths > 100 μm from $\epsilon_\nu \propto \nu^2$ to $\epsilon_\nu \propto \nu^{3/2}$.

Adopting a flat IMF in starbursts was the key change that enabled B05 to match the observed submm counts. For a given SFR, a more top-heavy IMF yields more luminosity emitted and dust produced per unit SFR. As a result, a starburst of a given SFR forming stars with a flat IMF is significantly brighter ($\sim 4\times$ at 1500 Å) and has a colder spectral energy distribution (SED) than a starburst with the same SFR but a Kennicutt IMF. The significant increase in dust mass is essential for increasing the submm flux; if luminosity were increased and dust mass were held constant, the SED would become much hotter and the resulting increase in submm flux would be significantly mitigated. The interested reader should see Section 1 of B05 and Chapter 2 for further discussion.

The submm counts of the G00 model were dominated by quiescently star-forming galaxies. The B05 modifications increased the S_{850} per unit SFR for starbursts by $\sim 5\times$ (G.-L. Granato, private communication), causing starbursts to account for a factor of 10^3 more sources at $S_{850} = 3$ mJy than in G00. As a result, in the B05 model ongoing starbursts dominate the counts for $0.1 \lesssim S_{850} \lesssim 30$ mJy. Interestingly, these starbursts are triggered predominantly by minor mergers (B05; González et al. 2011).

Swinbank et al. (2008) present a detailed comparison of the properties of SMGs in the B05 model with those of observed SMGs. The redshift distribution, far-IR SEDs, velocity dispersions, and halo masses (see also Almeida et al. 2011) are in good agreement. However, there is some tension between the models and observations.

Most notably, the rest-frame K-band fluxes of the B05 SMGs are $\sim 10\times$ lower than observed; the most plausible explanation is that the masses of the SMGs in the B05 SAM are too low (Swinbank et al. 2008). This disagreement is one reason it is worthwhile to explore alternative SMG models.

An even more compelling reason to model the SMG population in an alternative manner is to test whether a top-heavy IMF is required to explain the observed SMG counts. Matching the submm counts is the main reason B05 needed to adopt a flat IMF in starbursts. Using the same model, Lacey et al. (2008) show that the flat IMF is necessary to reproduce the evolution of the mid-IR luminosity function. Others (e.g., Guiderdoni et al. 1998; Blain et al. 1999a; Davé et al. 2010) have also suggested that the IMF may be top-heavy in SMGs. However, the use of a flat IMF in starbursts remains controversial: though there are some theoretical reasons to believe the IMF is more top-heavy in starbursts, there is to date no clear evidence for strong, systematic IMF variation in *any* environment (Bastian et al. 2010 and references therein). Furthermore, in local massive ellipticals, the probable descendants of SMGs, the IMF may actually be *bottom-heavy* (van Dokkum & Conroy 2010, 2011). Finally, the large parameter space of SAMs can yield multiple, qualitatively distinct solutions that satisfy all observational constraints (Bower et al. 2010; Lu et al. 2011b,a), so it is possible that a top-heavy IMF in starbursts is not *required* to match the observed submm counts even though it enables B05 to match the submm counts. Thus it is useful to explore other methods to predict the submm counts and to determine whether a match can be achieved without using a top-heavy IMF.

In previous work we have shown that major mergers can reproduce the observed

SMG 850 μm fluxes and typical SED (Narayanan et al. 2010a); CO spatial extents, linewidths, and excitation ladders (Narayanan et al. 2009); stellar masses (Narayanan et al. 2010a; Hayward et al. 2011; Michałowski et al. 2011); and the intersection of the SMG and dust-obscured galaxy (DOG; Dey et al. 2008) populations (Narayanan et al. 2010b) observed for SMGs. In Chapter 2 we explored how the (sub)mm flux depends on galaxy properties, showing that (sub)mm flux increases significantly sub-linearly with SFR. Furthermore, starbursts are significantly less efficient at boosting (sub)mm flux than quiescent star formation. One implication of this work is that the SMG population is heterogeneous: major mergers contribute both as coalescence-induced starbursts and during the pre-coalescence, infall stage, when the merging disks are blended into one (sub)mm source because of the large ($\sim$ 15", or $\sim$ 130 kpc at $z \sim 2$) beams of the single-dish (sub)mm telescopes used to perform large SMG surveys. We refer to the latter as 'galaxy-pair SMGs'. Similarly, compact groups may be blended into one source and can thus also contribute to the population. The most massive, highly star-forming isolated disks may also contribute. Finally, it has been observationally demonstrated that there is a contribution from physically unrelated galaxies blended into one source (Wang et al. 2011). It is becoming increasingly clear that the SMG population is likely a mix of various classes of sources; if one subpopulation does not dominate the population, physically interpreting observations of SMGs will be significantly more complicated than previously assumed.

In this work we present a novel method to predict the (sub)mm counts from mergers and quiescently star-forming disk galaxies. We utilize a combination of 3-D hydrodynamical simulations, on which we perform radiative transfer in

post-processing to calculate the UV-mm SEDs, and a semi-empirical model (SEM) of galaxy formation to predict the number counts and redshift distribution of SMGs in our model. We wish to address two main questions: 1. Can the observed (sub)mm counts be reproduced by our model without using of a top-heavy IMF? 2. What are the relative contributions of merger-induced starbursts, galaxy-pair SMGs, and quiescently star-forming disks to the predicted (sub)mm counts?

The remainder of this chapter is organized as follows: In Section 4.2 we present the details of the simulations we use to determine the time evolution of galaxy mergers and to translate physical properties of model galaxies into observed-frame (sub)mm flux densities. In Section 4.3 we discuss how we combine the simulations with a semi-empirical model to predict the (sub)mm counts for merger-induced starburst SMGs (Section 4.3.1) and isolated disk and galaxy-pair SMGs (Section 4.3.2). In Section 4.4 we present the predicted counts and redshift distribution of our model SMGs and the relative contribution of each subpopulation. We discuss implications for the IMF and compare to previous work in Section 4.5 and conclude in Section 4.6.

4.2 Simulation Methodology

Predicting SMG counts requires three main ingredients: 1. Since SFR and dust mass are the most important properties for predicting the (sub)mm flux of a galaxy (Chapter 2), one must model the time evolution of those properties for individual disks and mergers. 2. The physical properties of the model galaxies must be used to determine the observed-frame (sub)mm flux density of those galaxies. 3. One must

put the model galaxies in a cosmological context; this requires knowing the stellar mass function (SMF) and merger rates. Ideally, one could combine a cosmological hydrodynamical simulation with dust radiative transfer to self-consistently predict the (sub)mm counts. However, this is currently infeasible because the resolution required for the radiative transfer calculations cannot be achieved for a cosmological simulation large enough to contain a significant number of SMGs (see, e.g., Davé et al. 2010).

Instead, we predict (sub)mm counts using a combination of an observationally-derived, simple analytical model (which we refer to as a 'semi-empirical models', or SEM) and idealized high-resolution simulations of galaxy mergers. The method we use for each of the three model ingredients depends on the subpopulation being modeled. The physical properties of the isolated disk galaxies and early-stage mergers (in the latter the mutual tidal torques are not yet strong enough to induce a significant starburst) are determined using the SEM. For the late-stage mergers hydrodynamical simulations are used. Dust radiative transfer is used to translate the physical properties into observed (sub)mm flux density: for the isolated disks and early-stage mergers the scaling relations from Chapter 2 are used whereas

Table 4.1.   Summary of methods

Ingredient	Isolated disks	Early-stage mergers	Merger-induced starbursts
Physical properties	analytic	analytic	simulations
Submm flux density	Ch. 2 relations	Ch. 2 relations	simulations
Cosmological context	observed SMF	merger rates from SEM	merger rates from SEM
		+ duty cycle from sims	+ duty cycle from sims

for the late-stage mergers the (sub)mm light curves are taken directly from the simulations. Finally, the isolated galaxies are put in a cosmological context using an observed SMF. For the mergers, merger rates from the SEM and duty cycles from the simulations are used. The methods are summarized in Table 4.1, and each component of the modeling is discussed in detail below.

We emphasize that we do not attempt to model the SMG population in an ab initio manner as SAMs do. Instead, we construct our model so that the disk abundances, galaxy merger rates, gas fractions, and metallicities are consistent with observations. This will enable us to test whether, given a demographically accurate galaxy population, we are able to reproduce the SMG counts. If we are not, then our simulations or radiative transfer calculations must be incorrect in some way.[2]

We will first describe the combination of hydrodynamical simulations and dust radiative transfer we used to model the evolution of merging galaxies and to calculate (sub)mm flux density. The methodology of the hydrodynamical simulations and radiative transfer is identical to that of presented in the previous chapters and similar to that of Narayanan et al. (2010a,b, but see Section 2.2.2 for importance differences), so here we will only summarize the details of the simulations and provide more details about the novel aspects of this work.

---

[2]Alternatively, some aspect of the observations may be incorrect, but claiming the observations must be wrong because they do not agree with one's models is generally considered a weak argument (perhaps the second-to-last refuge of a scoundrel), so we will not advance it here.

4.2.1 Hydrodynamical Simulations

We have performed a suite of simulations of isolated and merging disk galaxies with GADGET-2 (Springel et al. 2001; Springel 2005), a TreeSPH (Hernquist & Katz 1989) code that computes gravitational interactions via a hierarchical tree method (Barnes & Hut 1986) and gas dynamics via smoothed-particle hydrodynamics (SPH; Lucy 1977; Gingold & Monaghan 1977; Springel 2010). It explicitly conserves both energy and entropy (Springel & Hernquist 2002). Beyond the core gravitational and gas physics, the version of GADGET-2 we use includes radiative heating and cooling (Katz et al. 1996). Star formation is implemented using a volume-density-dependent Kennicutt-Schmidt (KS) law (Schmidt 1959; Kennicutt 1998a), $\rho_{\mathrm{SFR}} \propto \rho_{\mathrm{gas}}^{N}$, with a low-density cutoff. We use $N = 1.5$, which reproduces the global K-S law and is consistent with observations of high-redshift disk galaxies (Krumholz & Thompson 2007; Narayanan et al. 2008a, 2011a).

Furthermore, our simulations include a two-phase sub-resolution model for the interstellar medium (ISM; Springel & Hernquist 2003, hereafter SH03) in which cold, dense clouds are in pressure equilibrium with a diffuse, hot medium. The division of mass, energy, and entropy between the two phases is affected by star formation, radiative heating and cooling, and supernova feedback, which heats the diffuse phase and evaporates the cold clouds (Cox et al. 2006b). The simulations also include a simple model for feedback from active galactic nuclei (AGN) in which black hole (BH) sink particles, initialized with mass $10^{5}h^{-1}M_{\odot}$, undergo Eddington-limited Bondi-Hoyle accretion (Hoyle & Lyttleton 1939; Bondi & Hoyle 1944; Bondi 1952). They deposit 5% of their luminosity ($L = 0.1\dot{m}c^{2}$, where $\dot{m}$ is the mass accretion

rate and c is the speed of light) to the surrounding ISM. This choice is made so that the normalization of the $M_{BH} - \sigma$ relation is recovered (Matteo et al. 2005). We refer the reader to Springel et al. (2005) for a comprehensive description of the AGN feedback model.

Each disk galaxy is composed of a dark matter halo with a Hernquist (1990) profile and an exponential gas and stellar disk with gas initially accounting for 80 per cent of the total disk mass. The mass of the baryonic component is 4% of the total. The galaxies are scaled to $z = 3$ following the method described in Robertson et al. (2006a,b); we refer the reader to those works for full details. Dark matter particles have gravitational softening lengths of $200h^{-1}$ pc whereas gas and star particles have $100h^{-1}$. We use 6×10^4 dark matter, 4×10^4 stellar, 4×10^4 gas, and 1 BH particle per disk galaxy. The detailed properties of the progenitor galaxies are given in Table 4.2. Note that we have chosen galaxy masses such that the mergers, based upon our simulations, will contribute to the bright SMG population (meaning at some time during the simulation they have observed 850 μm flux density $S_{850} > 3$ mJy). More massive galaxies will also contribute but are increasingly more rare, so

Table 4.2.   Progenitor disk galaxy properties

Name	M_{halo} (km s^{-1})	$M_{\star,\mathrm{init}}$ ($h^{-1}M_\odot$)	$M_{\mathrm{gas,init}}$ ($h^{-1}M_\odot$)	$f_{\mathrm{gas,init}}$ ($h^{-1}M_\odot$)
b6	6.2×10^{12}	5.3×10^{10}	2.2×10^{11}	0.8
b5.5	3.2×10^{12}	2.7×10^{10}	1.1×10^{11}	0.8
b5	1.6×10^{12}	1.4×10^{10}	5.6×10^{10}	0.8
b4	5.7×10^{11}	4.9×10^{9}	2.0×10^{10}	0.8

our simulations should be representative of all but the brightest, rarest SMGs.

We simulated each disk galaxy in isolation for $1.5h^{-1}$ Gyr and used these isolated disk simulations as part of the suite to derive the scaling relations presented in Chapter 2. Our suite also includes a number of simulations of major and minor galaxy mergers. For the merger simulations, two of the progenitor disk galaxies are placed on parabolic orbits with initial separation $R_{\mathrm{initial}} = 5R_{\mathrm{virial}}/8$ and pericentric distance equal to twice the disk scale length, $R_{\mathrm{peri}} = 2R_d$ (Robertson et al. 2006a,b). The evolution of the system is followed for $1.5h^{-1}$ Gyr, which is sufficient time for the galaxies to coalescence and for significant star formation and AGN activity to cease. The details of the merger simulations are given in Table 4.3. For each combination of progenitor disks in Table 4.3 we have run simulations using orbits i-p of Cox et al. (2006a), giving a total of 48 merger simulations to be used to determine the (sub)mm duty cycles.

4.2.2   Radiative Transfer

In post-processing we use the 3-D Monte Carlo radiative transfer code SUNRISE to calculate the UV-mm SEDs of the simulated galaxies. We have previously simulated galaxies with colors/SEDs consistent with local SINGS (Kennicutt et al. 2003; Dale et al. 2007) galaxies (Jonsson et al. 2010); local ULIRGs (Younger et al. 2009a); massive, quiescent, compact $z \sim 2$ galaxies (Wuyts et al. 2009, 2010); 24 μm-selected galaxies (Narayanan et al. 2010b); K+A/post-starburst galaxies (Snyder et al. 2011); and XUV disks (Bush et al. 2010), among other populations, so we are confident that SUNRISE can be used to model the high-z SMG population. We will briefly review

the details of SUNRISE here, but we refer the reader to Jonsson et al. (2006), Jonsson et al. (2010), and Jonsson & Primack (2010) for full details of the SUNRISE code.

SUNRISE uses the output of the GADGET-2 simulations to specify the details of radiative transfer problem to be solved, specifically the input radiation field and dust geometry. The star and BH particles from the GADGET-2 simulations are used as sources of emission. Star particles are assigned STARBURST99 (Leitherer et al. 1999) SEDs according to their ages and metallicities. Star particles present at the start of the GADGET-2 simulation are assigned ages assuming that their stellar mass was formed at a constant rate equal to the star formation rate of the initial snapshot and gas and stellar metallicities $Z = 0.015$. We have chosen this value so that the starbursts lie roughly on the observed mass-metallicity relation; however, the results are fairly robust to this choice because a factor of $2\times$ change in dust mass changes the (sub)mm flux by only ~ 50 per cent since (sub)mm flux scales approximately as $M_d^{0.6}$ (Equation 2.1). Black hole particles are assigned luminosity-dependent templates derived from observations of un-reddened quasars (Hopkins et al. 2007), where the luminosity is determined using the accretion rate from the GADGET-2 simulations as described above.

The dust distribution is determined by projecting the total gas-phase metal density in the GADGET-2 simulations onto a 3-D adaptive mesh refinement grid, assuming a dust-to-metal ratio of 0.4 (Dwek 1998; James et al. 2002). We have used a maximum refinement level of 10, which results in a minimum cell size of $55h^{-1}$ pc. This refinement is sufficient to ensure the SEDs are converged to within a few per cent. Note that we assume the ISM is smooth on scales below the GADGET-2 resolution and do not make use of the Groves et al. (2008) sub-resolution

photodissociation region model. The details of, motivation for, and implications of this choice are discussed in Sections 2.2.2 and 2.4.6. We assume the dust has properties given by the Milky Way R=3.1 dust model of Weingartner & Draine (2001) as updated by Draine & Li (2007).

Once the star and BH particles are assigned SEDs and the dust density field specified, SUNRISE performs the radiative transfer using a Monte Carlo approach by emitting photon packets which are scattered and absorbed by dust as they propagate through the ISM. The energy absorbed by dust is re-radiated in the IR. Dust temperatures, which depend on both grain size and the local radiation field, are calculated assuming the dust is in thermal equilibrium. The ISM of our simulated galaxies can often be optically thick at IR wavelengths, so SUNRISE calculates the effects of dust self-absorption using an iterative method. This is crucial for ensuring accurate dust temperatures.

The SUNRISE calculation yields spatially-resolved SEDs (analogous to integral field unit spectrograph data) of the simulated galaxies viewed from different viewing angles. Here we have used 7 cameras distributed isotropically in solid angle. We use the SCUBA-2 and AzTEC filter response curves to calculate the (sub)mm flux densities from the integrated SED of the system.

Table 4.3.   Merger parameters

Name	μ	R_{peri} $(h^{-1}$ kpc$)$	R_{init} $(h^{-1}$ kpc$)$
b6b6	1	6.7	70
b6b5.5	0.52	6.7	70
b6b5	0.26	6.7	70
b6b4	0.09	6.7	70
b5.5b5.5	1	5.3	57
b5b5	1	4.0	44

4.3 Predicting (Sub)mm Number Counts

In order to calculate the total SMG number counts predicted by our model we must account for all subpopulations, including the infall-stage, galaxy-pair SMGs discussed in Chapters 2 and 3, late-stage, merger-induced starbursts, and isolated disks. To calculate the counts for the two subpopulations associated with mergers we must combine the duty cycles (time the merger has (sub)mm flux greater than some flux cut) of the mergers with merger rates, as the number density is calculated by multiplying the duty cycle by the merger rate. For the isolated disks we require the number density of a disk galaxy as a function of its properties and the (sub)mm flux associated with that galaxy. We will describe our methods for predicting the counts of each subpopulation now.

4.3.1 Late-Stage, Merger-Induced Starbursts

In order to predict number counts of the population of late-stage, merger-induced starburst SMGs, we combine merger rates—which depend on mass, mass ratio, gas fraction, and redshift—from the SEM with (sub)mm light curves from our simulations. For the SMG subpopulation attributable to mergers, the number density of sources with flux density greater than S_λ at redshift z is

$$
\begin{aligned}
n(> S_\lambda, z) \quad &\equiv \quad \frac{dN(> S_\lambda, z)}{dV} \\
&= \quad \int \frac{dN}{dV\, dt\, d\log M_{\mathrm{bar}} d\mu df_g}(M_{\mathrm{bar}}, \mu, f_g, z) \\
&\quad \times \quad \tau(S_\lambda, M_{\mathrm{bar}}, \mu, f_g, z) d\log M_{\mathrm{bar}} d\mu df_g,
\end{aligned}
\tag{4.1}
$$

where $dN/dV\,dt\,d\log M_{\mathrm{bar}}d\mu df_g(M_{\mathrm{bar}},\mu,f_g,z)$ is the number of mergers per comoving volume element per unit time per dex stellar mass per unit mass ratio per unit gas fraction, in general a function of progenitor stellar mass $M_\star$, merger mass ratio μ, gas fraction at merger f_g, and redshift z, and $\tau(S_\lambda,M_{\mathrm{bar}},\mu,f_g,z)$ is the amount of time (duty cycle) for which a merger with most-massive-progenitor baryonic mass M_{bar}, mass ratio μ, and gas fraction f_g at redshift z has flux density $> S_\lambda$.

Duty Cycles

We calculate the duty cycles $\tau(S_{850})$ and $\tau(S_{1.1})$ for various S_{850} and $S_{1.1}$ values for the late-stage, merger-induced starburst phase of our merger simulations. We neglect the dependence of duty cycle on gas fraction because sampling the range of initial gas fractions in addition to masses, mass ratios, and orbits is computationally prohibitive. Instead, as described above, we initialize the mergers with gas fraction $f_g = 0.8$ so that sufficient gas remains at merger coalescence, and we discard all snapshots with gas fraction > 40 per cent so that our simulated galaxies have gas fractions consistent with those observed (Tacconi et al. 2006, 2008). Since we expect mergers to also contribute to the SMG population during the infall stage we treat this separately below. We have also neglected any redshift dependence because for $1 \lesssim z \lesssim 10$ the negative K-correction makes the (sub)mm flux for fixed luminosity almost independent of redshift (e.g., Blain et al. 2002). For each S_λ we average the duty cycles for each set of models with identical (M_{bar},μ) and then fit the resulting $\tau(M_{\mathrm{bar}},\mu)$ surface with a second-degree polynomial in M_{bar} and μ in order to estimate the duty cycle for (M_{bar},μ) values not explicitly sampled by our simulations.

Merger Rates

The other ingredient needed to predict the counts for merger-induced starbursts is the merger rates. We use rates from the semi-empirical model described in detail in Hopkins et al. (2010a,c,b), which we will briefly summarize here. The model starts with a halo mass function that has been calibrated using high-resolution N-body simulations. Galaxies are assigned to halos using an observed SMF and the halo occupation formalism (Conroy & Wechsler 2009). We use a fiducial SMF that is a combination of multiple observed IMFs, with each covering a subset of the total redshift range. For $z < 2$ we use the SMF of star-forming galaxies from Ilbert et al. (2010). For $2.0 \leq z \leq 3.75$ we use the SMF of Marchesini et al. (2009, hereafter M09) because their survey is among the widest and deepest available and because they have performed the most systematic analysis of the random and systematic uncertainties affecting the SMF determination. For $z > 3.75$ we extrapolate the Fontana et al. (2006, hereafter F06) SMF because the extrapolation agrees reasonably well with the $4 < z < 7$ constraints from González et al. (2011). Our composite SMF at integer redshifts in the range $z = 0 - 6$ is plotted in Figure 4.1. The galaxies are assigned gas fractions as a function of stellar mass using observed correlations (see Hopkins et al. 2010b for a list of observations used). Finally, we use halo-halo merger rates from high-resolution N-body simulations and translate to galaxy-galaxy merger rates assuming the galaxies merge on a dynamical friction timescale.
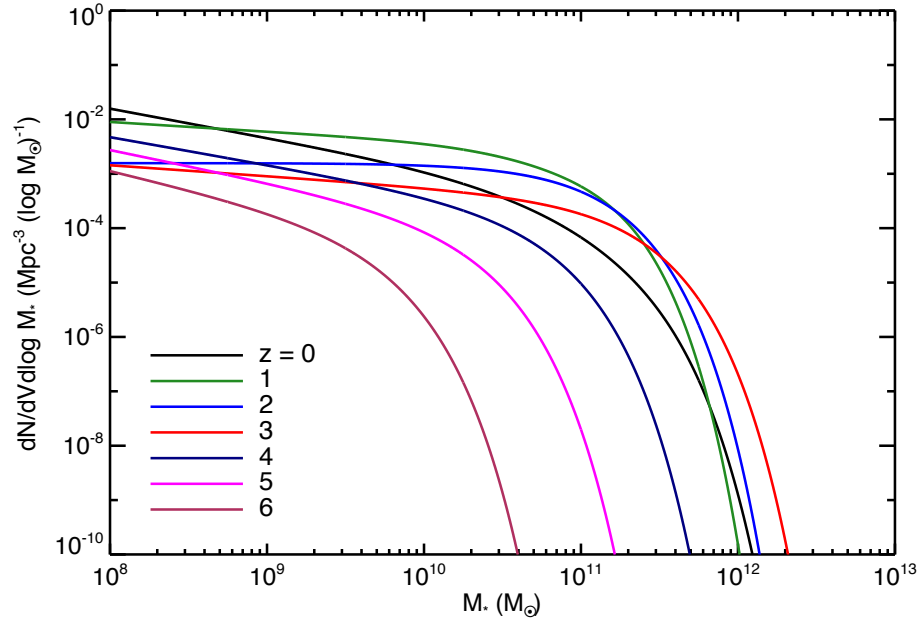
Figure 4.1.—: Number density of disk galaxies, $dN/dV\, d\log M_\star$ $(\mathrm{Mpc}^{-3}$ $(\log M_\odot)^{-1})$, versus $M_\star(M_\odot)$ for integer redshifts in the range $z = 0 - 6$ for our fiducial SMF. For $z < 2$ we use the SMF for star-forming galaxies of Ilbert et al. (2010). For $2 \leq z \leq 3.75$ we use the SMF of M09, and for $z > 3.75$ we extrapolate the SMF of F06.

Predicted Counts

Using the above assumptions, Equation (4.1) becomes

$$
\begin{aligned}
n(> S_\lambda, z) &= \int \frac{dN}{dV \, dt \, d\log M_\star \, d\mu}(M_\star, \mu, f_g > f_{\text{g,crit}}, z) \\
&\times \quad \tau(S_\lambda, M_\star, \mu, z) d\log M_\star d\mu.
\end{aligned}
\tag{4.2}
$$

To get the observable cumulative counts, number per square degree, we must multiply by $dV/d\Omega dz$, the comoving volume element in solid angle $d\Omega$ and redshift interval dz, and integrate over redshift,

$$
\frac{dN(> S_\lambda)}{d\Omega} = \int \frac{dN(> S_\lambda, z)}{dV} \frac{dV}{d\Omega dz}(z) dz,
\tag{4.3}
$$

where

$$
\frac{dV}{d\Omega dz}(z) = \frac{c}{H_0} \frac{(1+z)^2 D_A^2(z)}{E(z)}.
\tag{4.4}
$$

Here $D_A(z)$ is the angular diameter distance at redshift z and $E(z) = \sqrt{\Omega_m(1+z)^3 + \Omega_k^2(1+z)^2 + \Omega_\Lambda}$ (Hogg 1999).

4.3.2   Isolated Disks and Early-Stage Mergers

We treat the isolated disks and early-stage mergers, which are dominated by quiescent SF, in a semi-empirical manner, assigning galaxy properties based off observations. In order to calculate the observed (sub)mm flux densities using the scaling relations of Chapter 2, we must determine the SFR and dust mass of a galaxy as a function of stellar mass and redshift. We then use SMF and merger rates to calculate the (sub)mm counts for these populations.

Assigning Galaxy Properties

Following Hopkins et al. (2010a,b), we assign gas fractions and sizes as a function of stellar mass using observationally derived relations. We present the relevant relations below, but we refer the reader to Hopkins et al. (2010a,b,c) for full details, including the list of observations used to derive the relations and justifications for the forms used.

The gas fraction, $f_{\mathrm{gas}} = M_{\mathrm{gas}}/(M_{\mathrm{gas}} + M_\star)$, of a galaxy of stellar mass $M_\star$ and redshift z, as determined from observations listed in Hopkins et al. (2010a), is given by Equation (1) of Hopkins et al. (2010a),

$$
\begin{aligned}
f_{\mathrm{gas}}(M_\star | z = 0) \quad &\equiv \quad f_0 \approx \frac{1}{1 + (M_\star/10^{9.15} M_\odot)^{0.4}}, \\
f_{\mathrm{gas}}(M_\star, z) \quad &= \quad f_0 \left[1 - \tau(z) \left(1 - f_0^{3/2} \right) \right]^{-2/3},
\end{aligned}
\tag{4.5}
$$

where $\tau(z)$ is the fractional look-back time to redshift z. Note that, at a given mass, galaxy gas fractions increase with redshift. At fixed redshift they decrease with stellar mass. Using $f_{\mathrm{gas}}(M_\star, z)$ we can calculate the gas mass as a function of $M_\star$ and z,

$$
M_{\mathrm{gas}}(M_\star, z) = \frac{f_{\mathrm{gas}}(M_\star, z)}{1 - f_{\mathrm{gas}}(M_\star, z)} M_\star.
\tag{4.6}
$$

Similarly, we parameterize the disk size as a function of mass and redshift using observations listed in Hopkins et al. (2010a). The relation (Equation 2 of Hopkins et al. 2010a) is

$$
\begin{aligned}
R_e(M_\star | z = 0) \quad &\equiv \quad R_0 = 5.28 \text{ kpc} \left(\frac{M_\star}{10^{10} M_\odot} \right)^{0.25}, \tag{4.7} \\
R_e(M_\star, z) \quad &= \quad R_0 (1 + z)^{-0.6}. \tag{4.8}
\end{aligned}
$$
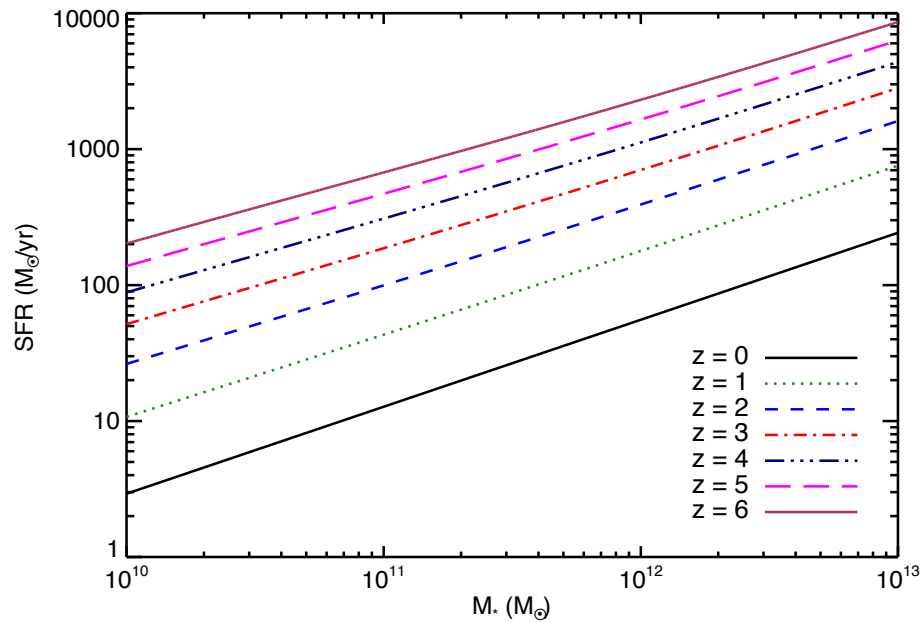
Figure 4.2.—: Star formation rate $(M_\odot \text{ yr}^{-1})$ versus stellar mass $(M_\odot)$ for model disk galaxies at integer redshifts in the range $z = 0 - 6$. The normalization of the relation increases with redshift both because gas fractions are higher and galaxies more compact.

We assume the quiescent disks obey the KS relation (Schmidt 1959; Kennicutt 1998a),

$$\dot{\Sigma}_\star = 1.3 \times 10^{-4} M_\odot \ \mathrm{yr}^{-1} \mathrm{kpc}^{-2} \left(\frac{\Sigma_{\mathrm{gas}}}{M_\odot \mathrm{pc}^{-2}} \right)^{n_K}, \tag{4.9}$$

where $\dot{\Sigma}_\star$ and Σ_{gas} are the SFR and gas surface densities respectively and $n_K = 1.4$ (Kennicutt 1998a), at all redshifts, as is supported by observations (e.g., Daddi et al. 2010; Genzel et al. 2010; Narayanan et al. 2011a). We have normalized the relation assuming a Kroupa (2001) IMF. Assuming $\Sigma_{\mathrm{gas}} \approx M_{\mathrm{gas}}/(\pi R_e^2)$ and $\dot{\Sigma}_\star \approx \dot{M}_\star/(\pi R_e^2)$, where $\dot{M}_\star$ is the SFR, we find

$$\dot{M}_\star(M_\star, z) = 1.3 \left(\frac{10^4}{\pi} \right)^{n_K - 1} \left(\frac{M_{\mathrm{gas}}(M_\star, z)}{10^{10} M_\odot} \right)^{n_K} \times \left(\frac{R_e(M_\star, z)}{\mathrm{kpc}} \right)^{-2(n_K - 1)} M_\odot \ \mathrm{yr}^{-1},$$

$$\tag{4.10}$$

which can be recast in terms of $M_\star$ rather than M_{gas} using Equations (4.5) and (4.6). Figure 4.2 shows the SFR-$M_\star$ relation for given by Equation (4.10) for integer redshifts in the range $z = 0 - 6$.

In addition to the SFR we need the dust mass to calculate the (sub)mm flux densities. In order to determine the dust mass we must know the gas-phase metallicity. Observations have shown that metallicity increases with stellar mass; this relationship has been constrained for redshifts $z \sim 0 - 3.5$ (Tremonti et al. 2004; Savaglio et al. 2005; Erb et al. 2006; Kewley & Ellison 2008; Maiolino et al. 2008). Maiolino et al. (2008) have parameterized the evolution of the mass-metallicity relation (MMR) with redshift using the form

$$12 + \log(\mathrm{O/H}) = -0.0864 [\log M_\star - \log M_0(z)]^2 + K_0(z). \tag{4.11}$$

They determine the values of $\log M_0$ and K_0 at redshifts $z = 0.07, 0.7, 2.2,$ and 3.5 using the observations of Kewley & Ellison (2008), Savaglio et al. (2005), Erb

et al. (2006), and their own work, respectively. To crudely capture the evolution of the MMR with redshift we have fit the values of $\log M_0$ and K_0 given in Table 5 of Maiolino et al. (2008) as power laws in $(1+z)$, finding $\log M_0(z) \approx 11.07(1+z)^{0.094}$ and $K_0(z) \approx 9.09(1+z)^{-0.017}$.

Using $12 + \log(\mathrm{O/H})_\odot = 8.69$ (Asplund et al. 2009), we have

$$
\begin{aligned}
\log(\mathrm{O/H}) - \log(\mathrm{O/H})_\odot \;=\;& -8.69 \\
& - 0.0864 \left[\log M_\star - 11.07(1+z)^{0.94}\right]^2 \\
& + 9.09(1+z)^{-0.017}.
\end{aligned}
\tag{4.12}
$$

The solar metal fraction is $Z_\odot = 0.0142$ (Asplund et al. 2009), so

$$
Z(M_\star, z) = 0.0142 \left(10^{\log(\mathrm{O/H})-\log(\mathrm{O/H})_\odot}\right).
\tag{4.13}
$$

We assume the dust mass is proportional to the gas-phase metal mass, $M_d = M_{\mathrm{gas}} Z f_{\mathrm{dtm}}$. Thus

$$
M_d(M_\star, z) = M_\star \left(\frac{f_{\mathrm{gas}}(M_\star, z)}{1 - f_{\mathrm{gas}}(M_\star, z)}\right) \times Z(M_\star, z) f_{\mathrm{dtm}},
\tag{4.14}
$$

where we use dust-to-metal ratio $f_{\mathrm{dtm}} = 0.4$ (Dwek 1998; James et al. 2002).

Combining Equations (4.10) and (4.14) with Equation (2.1),

$$
\begin{aligned}
S_{850} \;=\;& 0.65 \text{ mJy} \left(\frac{\dot{M}_\star}{100 \, M_\odot \, \mathrm{yr}^{-1}}\right)^{0.42} \left(\frac{M_d}{10^8 M_\odot}\right)^{0.58} \\
S_{1.1} \;=\;& 0.30 \text{ mJy} \left(\frac{\dot{M}_\star}{100 \, M_\odot \, \mathrm{yr}^{-1}}\right)^{0.36} \left(\frac{M_d}{10^8 M_\odot}\right)^{0.61},
\end{aligned}
\tag{4.15}
$$

we get $S_{850}(M_\star, z)$ and $S_{1.1}(M_\star, z)$,

$$
\begin{aligned}
S_{850} &= 0.65 \text{ mJy} \left[0.013 \left(\frac{10^4}{\pi} \right)^{0.4} \left(\frac{M_{\text{gas}}}{10^{10} M_\odot} \right)^{1.4} \left(\frac{R_e}{\text{kpc}} \right)^{-0.8} \right]^{0.42} \\
&\times \left[\left(\frac{M_\star}{10^8 M_\odot} \right) \left(\frac{f_{\text{gas}}}{1 - f_{\text{gas}}} \right) Z(M_\star, z) f_{\text{dtm}} \right]^{0.58}, \quad\quad (4.16)
\end{aligned}
$$

$$
\begin{aligned}
S_{1.1} &= 0.30 \text{ mJy} \left[0.013 \left(\frac{10^4}{\pi} \right)^{0.4} \left(\frac{M_{\text{gas}}}{10^{10} M_\odot} \right)^{1.4} \left(\frac{R_e}{\text{kpc}} \right)^{-0.8} \right]^{0.36} \\
&\times \left[\left(\frac{M_\star}{10^8 M_\odot} \right) \left(\frac{f_{\text{gas}}}{1 - f_{\text{gas}}} \right) Z(M_\star, z) f_{\text{dtm}} \right]^{0.61}. \quad\quad (4.17)
\end{aligned}
$$

Figures 4.3 and 4.4 show the $S_{850} - M_\star$ and $S_{1.1} - M_\star$ relations given by Equations (4.16) and (4.17), respectively, for isolated disks at integer redshifts in the range $z = 0 - 6$. As redshift increases, galaxies become gas-rich and compact; both effects cause the SFR for a given $M_\star$ to increase (see Figure 4.2). The higher gas fraction also causes the gas-phase metal mass to increase, though the shift in the MMR downward somewhat mitigates this effect. Both the increased SFR and M_d cause a higher (sub)mm flux for a given $M_\star$. Note that in order to get an SMG ($S_{850} \gtrsim 3 - 5$ mJy or $S_{1.1} \gtrsim 1 - 2$ mJy) at $z \sim 2 - 3$ we require $M_\star \gtrsim 10^{11} M_\odot$, which is confirmation that the predictions of our RT calculations are consistent with observed SMGs (see also Michałowski et al. 2011).

Isolated Disk Counts

For a given S'_λ and z, we invert the $S_\lambda(M_\star, z)$ functions (Equations 4.16 and 4.17) to get the minimum $M_\star$ required for a galaxy at redshift z to have $S_\lambda > S'_\lambda$, $M_\star(S'_\lambda|z)$. To get the number density $n(> S'_\lambda, z)$ we then simply use the SMF to calculate

$$
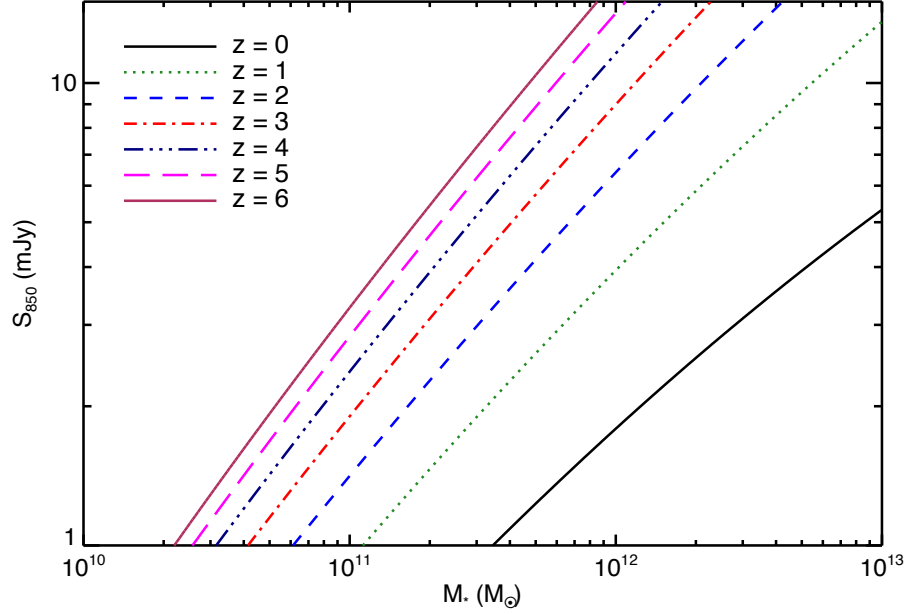n(> S'_\lambda, z) = n \left[> M_\star(S'_\lambda|z), z \right], \quad\quad (4.18)
$$

Figure 4.3.—: Observed-frame 850-μm flux density (S_{850}; mJy) versus stellar mass ($M_\star$; $M_\odot$) for isolated disks at integer redshifts in the range $z = 0 - 6$ (see Equation 4.16). The (sub)mm flux of a disk of fixed $M_\star$ increases with redshift for two reasons: 1. As shown in Figure 4.2, the normalization of the SFR-$M_\star$ relation increases with redshift. 2. For fixed $M_\star$, gas fraction increases with redshift. This causes the gas-phase metal mass to increase, although this is partially offset by the MMR shifting downward. Both the increased SFR and increased dust mass cause (sub)mm flux to increase.
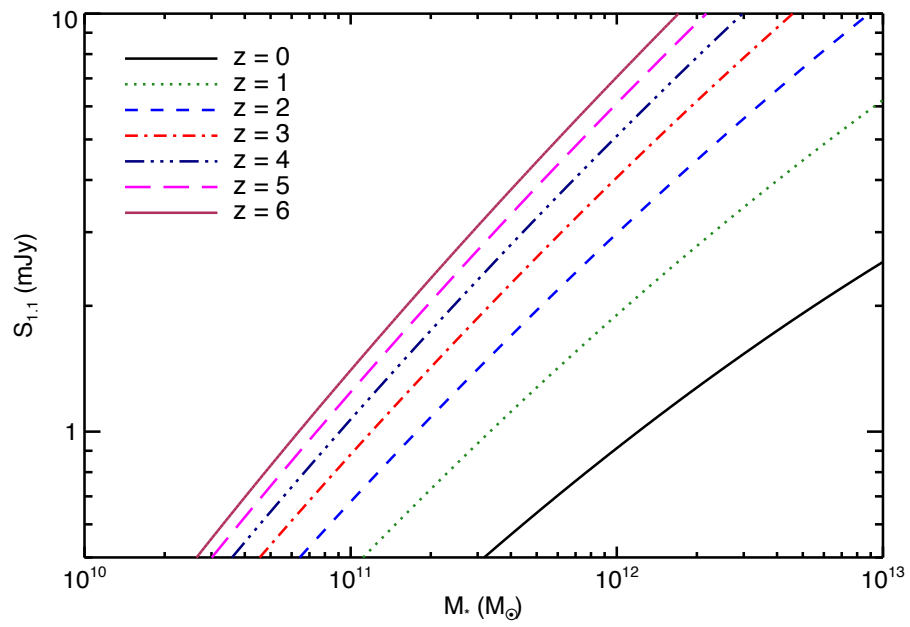
Figure 4.4.—: Same as Figure 4.3, but for observed-frame 1.1-mm flux density (Equation 4.17).

and we use Equation (4.3) to calculate the predicted counts.

Infall-Stage, Galaxy-Pair SMGs

During the infall stage of a merger the disks are dominated by quiescent star formation that would occur even if they were not merging. Only for nuclear separation $\lesssim 10$ kpc do the disks have SFR significantly elevated by the mutual tidal interactions. So, during the infall stage we assume the disks are in a steady state (i.e., they have constant SFR and dust mass); even without a source of additional gas this is a reasonable approximation for the infall stage to within a factor of $\lesssim 2$ (see Figure 2.2). For a merger of two progenitors with stellar masses $M_{\star,1}$ and $M_{\star,2}$ the total flux density is $S_\lambda = S_\lambda(M_{\star,1}) + S_\lambda(M_{\star,2})$. The typical beam sizes of single-dish (sub)mm telescopes are 15", or ~ 130 kpc at $z \sim 2$; when the projected separation is less than this distance the sources would begin to be smeared into a single source. We assume the galaxies should be treated as a single source if the physical separation is < 100 kpc. From our simulations, which use cosmologically-motivated orbits, we find that this timescale is of order ~ 500 Myr. Though the timescale depends slightly on the most-massive-progenitor mass, we neglect this dependence because it is subdominant to various other uncertainties. Therefore the duty cycle for a given S'_{850} and merger described by more-massive progenitor mass $M_{\star,1}$ and stellar mass ratio $\mu = M_{\star,2}/M_{\star,1}$ at redshift z is 0.5 Gyr if $S_{850}(M_{\star,1}) + S_{850}(M_{\star,1}\mu) > S'_{850}$ and 0 otherwise. With the duty cycle in hand, we can use Equations (4.2) and (4.3) to calculate the predicted number density and counts.

4.4 Results

Here we present the key results of this work, the SMG number densities, cumulative number counts, and redshift distribution predicted by our model. We will only present the AzTEC (Wilson et al. 2008) 1.1-mm counts here because, to date, the best constrained blank-field counts (i.e., those from the deepest and widest surveys) have been determined using that instrument (Austermann et al. 2010; Aretxaga et al. 2011). For completeness and in anticipation of SCUBA-2 (Holland et al. 2006), we will present the 850-μm counts and redshift distribution in the published version of this work. However, the 850-μm and 1.1-mm fluxes are rather simply related, as $S_{850}/S_{1.1}$ varies little (see Equation 2.1, for example). Different authors find different values for the ratio, but it is likely in the range $\sim 2 - 4$ (Austermann et al. 2009; Scott et al. 2010). Our simulations suggest the ratio is slightly greater than 2. This ratio can be used as an approximate way to translate the $S_{1.1}$ values presented here into S_{850}.

Before we present the results for the total population, however, we will explore the importance of the SMF used by comparing the number densities and redshift distributions of isolated disk SMGs predicted by our model when we use three different SMFs.

4.4.1 The Importance of the Stellar Mass Function

The SMF used to calculate disk abundances is of vital importance to the predicted counts. As explained above, we do not attempt to predict the SMF but rather utilize
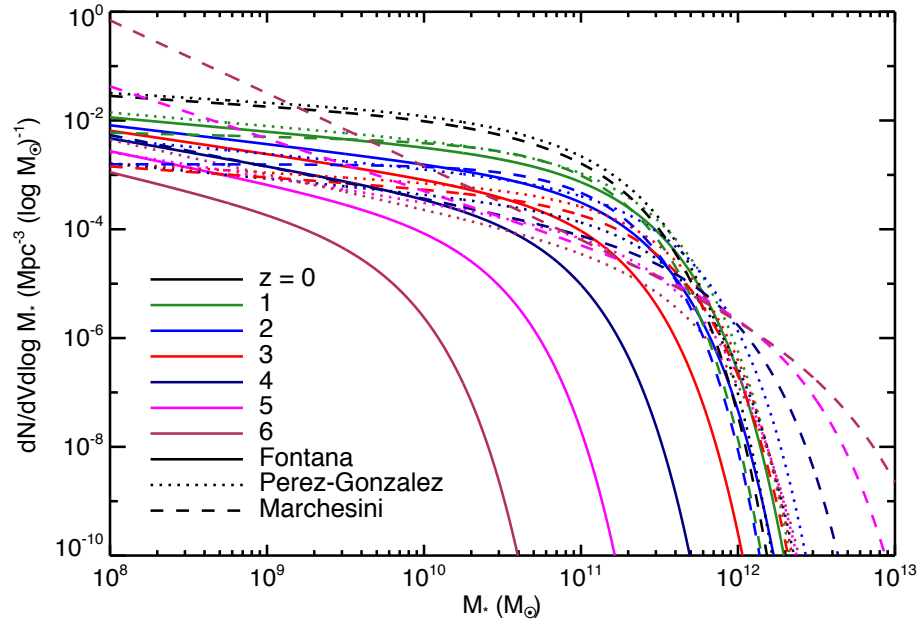
Figure 4.5.—: Number density of disk galaxies $(\mathrm{Mpc}^{-3}\ (\log M_\odot)^{-1})$ versus $M_\star\ (M_\odot)$ for the three SMFs used in this work at integer redshifts in the range $z = 0 - 6$. The solid lines correspond to F06, dotted to P08, and dashed to M09.

one drawn from observations. For this work we have compared the predictions when we use three different SMFs, those of F06, Pérez-González et al. (2008, hereafter P08), and M09, because these are representative of the range of observed SMFs presented in the literature. These SMFs are compared in Figure 4.5. The SMFs are similar up to $z \sim 2$. For $z \gtrsim 3$, however, the F06 SMF values are significantly lower than the others at the high-mass end; since $M_\star \gtrsim 10^{11} M_\odot$ is required in order to have a bright SMG the high-mass end is of greatest importance.

Unfortunately, the aforementioned observations constrain the SMF only for $z \lesssim 4$ and $\log M_\star \lesssim 10^{11.6} M_\odot$, so we must extrapolate beyond these limits. The extrapolated F06 SMF behaves as one expects, but extrapolation of the P08 and M09 SMFs results in surprising behavior. For P08, the abundance of the most massive galaxies evolves very little out to even $z = 6$. For example, according to the extrapolation, $M_\star = 10^{11.5} M_\odot$ star-forming galaxies were almost as abundant at $z \sim 6$ as at $z \sim 2$. The extrapolation of the M09 SMF is even more extreme: the abundance of $M_\star \gtrsim 10^{11.5} M_\odot$ *increases* beyond $z \sim 2 - 3$.

The significant differences among the three extrapolated SMFs results in drastically different predictions for the (sub)mm counts. In order to explore these differences in a simple way we focus on the predicted number density and redshift distribution of isolated disk SMGs, as these are more simply related to the adopted SMF than the other subpopulations. Figures 4.6, 4.8, and 4.10 show the predicted number density of isolated disk SMGs when the F06, P08, and M09 SMFs, respectively, are used. Figures 4.7, 4.9, and 4.11 show the corresponding redshift distributions for different S_{11} cuts.
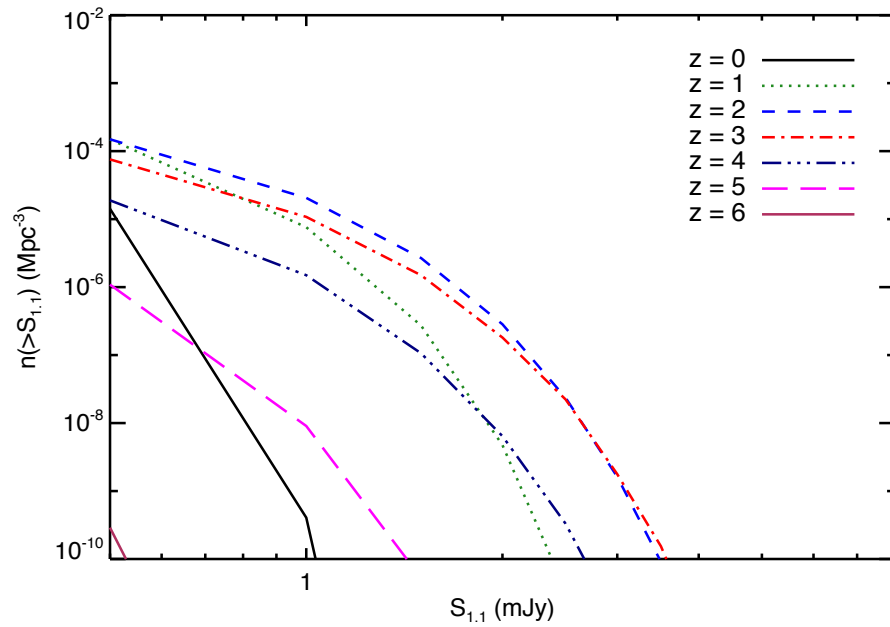
Figure 4.6.—: Predicted number density of isolated disk SMGs (Mpc^{-3}) versus $S_{1.1}$ (mJy) for integer redshifts in the range $z = 0 - 6$ when the extrapolated F06 SMF is used. The number density rises from $z = 0$ to $z \sim 2 - 3$ and then decreases beyond that range.
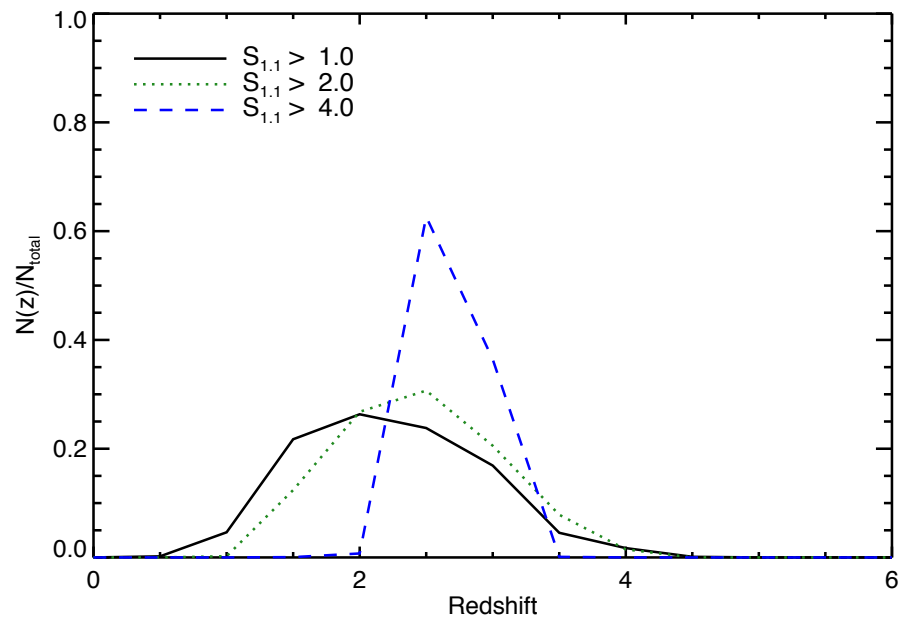
Figure 4.7.—: Predicted redshift distribution of isolated disk SMGs for different $S_{1.1}$ cuts (in mJy) when the extrapolated F06 SMF is used.
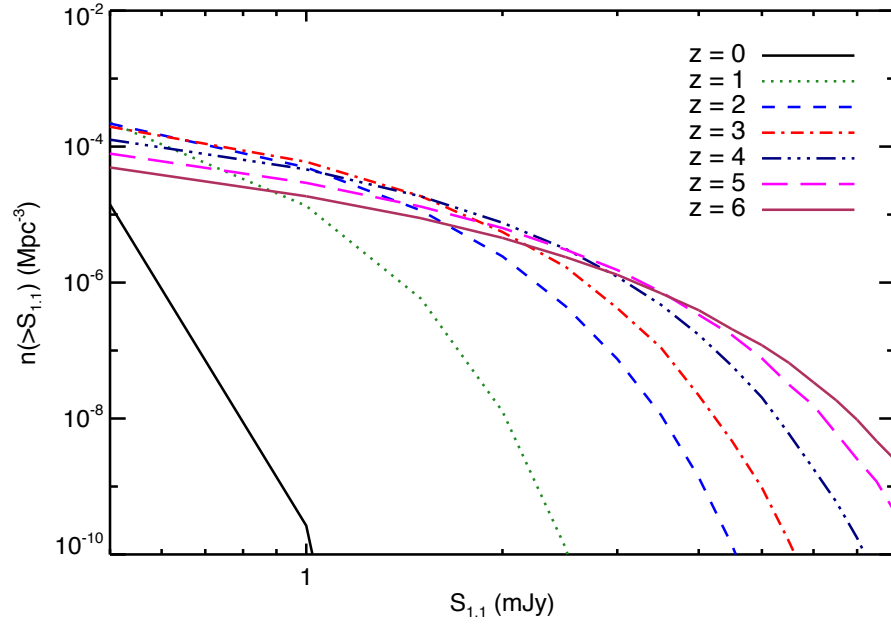
Figure 4.8.—: Predicted number density of isolated disk SMGs (Mpc^{-3}) versus $S_{1.1}$ (mJy) for integer redshifts in the range $z = 0 - 6$ when the extrapolated P08 SMF is used. The evolution of number density with redshift is drastically different than when the F06 SMF is used: At the faint end there is very little evolution in the range $1 < z < 6$, whereas at the bright end the counts *increase monotonically* with redshift.
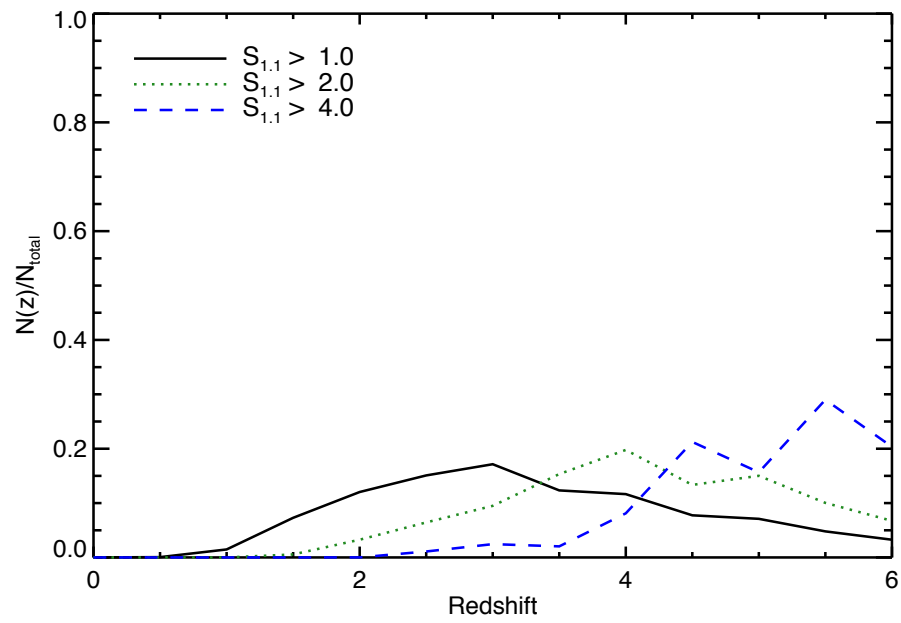
Figure 4.9.—: Predicted redshift distribution of isolated disk SMGs for different $S_{1.1}$ cuts when the extrapolated P08 SMF is used.
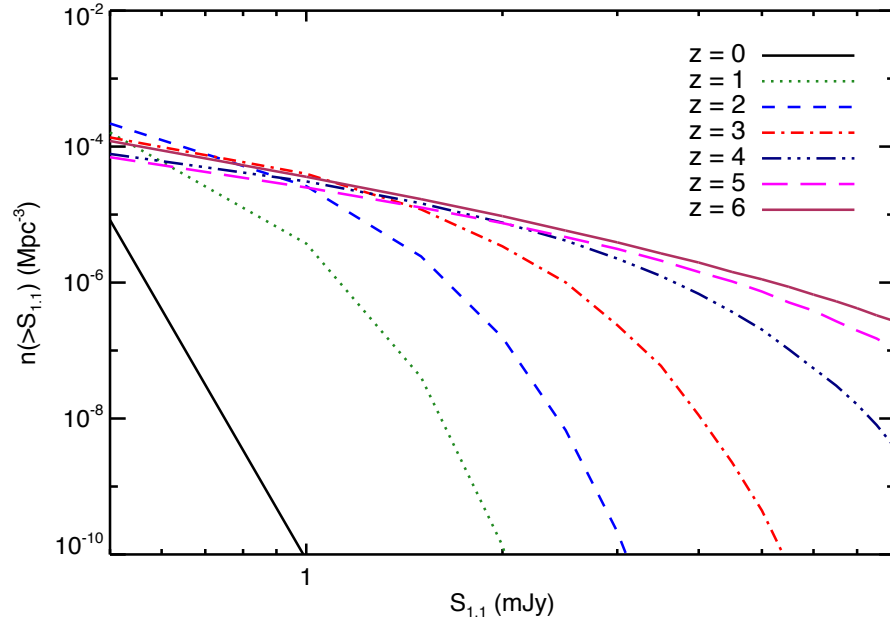
Figure 4.10.—: Predicted number density of isolated disk SMGs (Mpc^{-3}) versus $S_{1.1}$ (mJy) at integer redshifts in the range $z = 0 - 6$ when the extrapolated M09 SMF is used. The evolution of number density with redshift is again drastically different than when the F06 SMF is used: For $S_{1.1} \gtrsim 1$ mJy, the counts *increase monotonically* with redshift, and the increase with z is more drastic than when the P08 SMF is used.
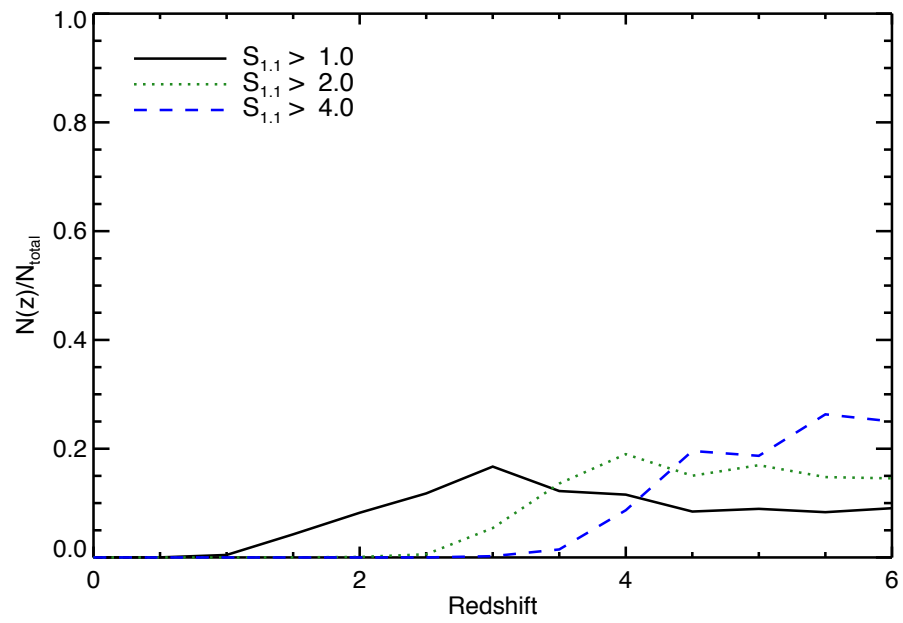
Figure 4.11.—: Predicted redshift distribution of isolated disk SMGs for different $S_{1.1}$ cuts when the extrapolated M09 SMF is used.

When the F06 SMF is used the isolated disk SMGs are most abundant at $z \sim 2-3$, dropping off significantly at lower and higher redshifts. The behavior when the P08 or M09 SMFs are used is drastically different: For the P08 SMF, the redshift distribution is broader and peaks at higher redshift. The result when M09 is used is similar, but the distribution is even more biased to $z > 4$.

The observed redshift distribution of 1.1-mm sources peaks at $z \sim 2.6$, and there are less than a few per cent of SMGs at $z \lesssim 1.5$ and $z \gtrsim 4$ (Yun et al. 2011). The redshift distribution predicted when the F06 SMF is used (Figure 4.7) is thus broadly consistent with that of observed SMGs. We should not make too much of this comparison since we have not yet included the other SMG subpopulations, but the agreement is encouraging nevertheless. On the other hand, the redshift distributions predicted when the P08 (Figure 4.9) and M09 (Figure 4.11) SMFs are used are in severe disagreement with the observed distribution, as both predict that the typical bright SMG is at $z \gtrsim 4$. This disagreement, along with the counterintuitive behavior of the extrapolated SMFs described above, suggests that we should not use the extrapolations of the P08 or M09 SMFs.

As explained above, we have opted to use a fiducial SMF that is a combination of multiple observed IMFs (Ilbert et al. 2010 SMF of star-forming galaxies for $z < 2$, M09 for $2 \leq z \leq 3.75$, and the extrapolation of F06 for $z > 3.75$). The above comparisons show that, if we must extrapolate beyond $z \sim 4$, then the extrapolation of the F06 SMF is preferred. Encouragingly, this extrapolation agrees reasonably well with the $4 < z < 7$ constraints of González et al. (2011), so perhaps the extrapolation is not as treacherous as one might expect. Regardless, it is clear that the SMF used is a significant uncertainty. Since our model relies on use of an

observed SMF, we cannot eliminate this uncertainty but rather only constrain the effect of this uncertainty on our predictions.

4.4.2 Predicted SMG Number Density and Cumulative Counts

Figure 4.12 shows the cumulative number density of 1.1-mm sources $n(> S_{1.1})$ (Mpc^{-3}) predicted by our model (using the fiducial composite SMF) versus $S_{1.1}$ at integer redshifts in the range $z = 0 - 6$. Figure 4.13 shows the total cumulative 1.1-mm number counts (solid line), which are calculated from the cumulative number density using Equation (4.3). Note, however, that "numbers add up to nothing" (N. Young, private communication). We have decomposed the counts into isolated disks (dotted line), galaxy pairs (i.e., mergers during the infall stage; dashed line), and starbursts induced at merger coalescence (dash-dotted line); the relative contribution of each subpopulation is discussed in Section 4.4.3. The data points in Figure 4.13 are observed counts from various surveys: Aretxaga et al. (2011, survey area 0.72 deg^{-2}; circles), Austermann et al. (2009, 0.15 deg^{-2}; asterisks), Austermann et al. (2010, 0.7 deg^{-2}; squares), Hatsukade et al. (2011, 0.25 deg^{-2}; diamonds), and Scott et al. (2010, 0.075 deg^{-2}; triangles). The predicted and observed counts are in good agreement at the lowest fluxes, but the predicted counts are less than those observed at the bright end. The Austermann et al. (2010) and Aretxaga et al. (2011) surveys are the two largest (both covered ~ 0.7 deg^{-2}), so their counts should be least affected by cosmic variance and thus most robust. Thus it is encouraging that the disagreement with the Austermann et al. (2010) counts is $\lesssim 2\times$ for $S_{1.1} \leq 4$ mJy,
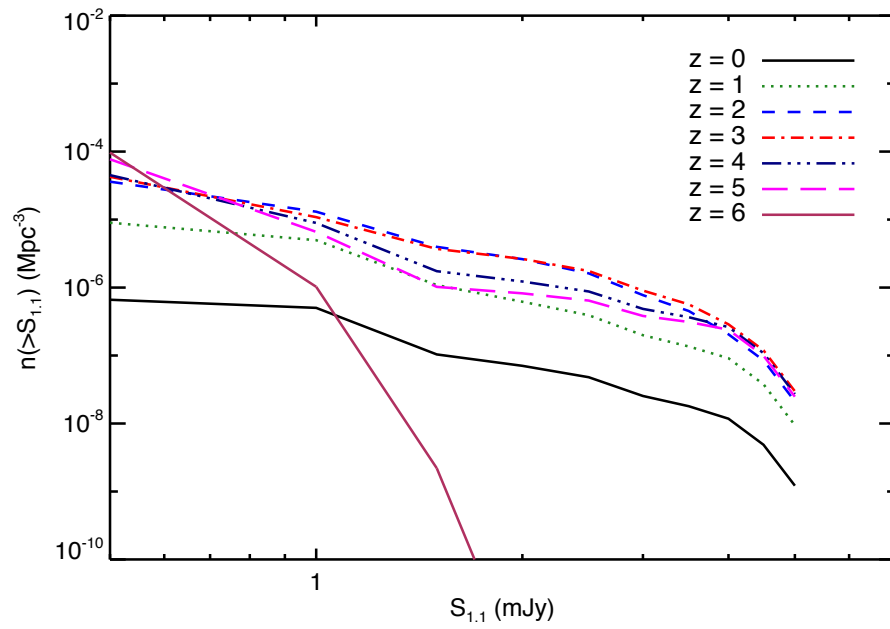
Figure 4.12.—: Predicted cumulative number density $n(> S_{1.1})$ (Mpc^{-3}) versus $S_{1.1}$ (mJy) at integer redshifts in the range $z = 0 - 6$.
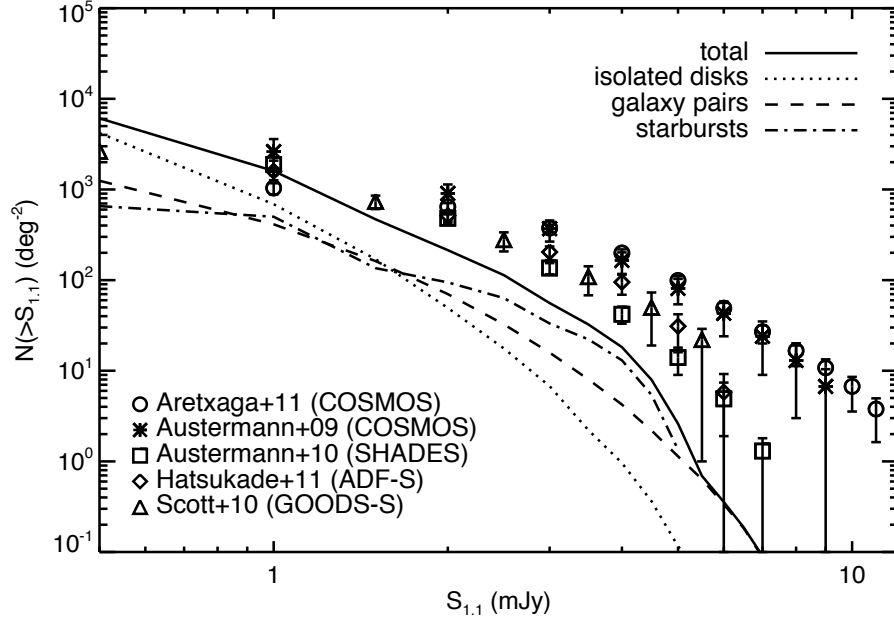
Figure 4.13.—: Predicted cumulative 1.1-mm counts for the SMG population, $N(>$ $S_{1.1})$, in deg^{-2}, versus $S_{1.1}$ (mJy), decomposed into the three SMG subpopulations we model. The dotted line corresponds to isolated disk galaxies, the dashed to galaxy-pair SMGs (i.e., infall-stage, pre-starburst mergers), and the dash-dotted to merger-induced starbursts. The solid line is the total for all SMG subpopulations we model. The points are observed counts from Aretxaga et al. (2011, survey area 0.72 deg^{-2}; circles), Austermann et al. (2009, 0.15 deg^{-2}; asterisks), Austermann et al. (2010, 0.7 deg^{-2}; squares), Hatsukade et al. (2011, 0.25 deg^{-2}; diamonds), and Scott et al. (2010, 0.075 deg^{-2}; triangles). N.B. The steepness of the cutoff in the starburst counts at $S_{1.1} \gtrsim 4$ mJy is artificial; see text for details.

especially since the modeling uncertainties arising from the SMF alone can be of this order. At first glance the disagreement at higher fluxes may seem problematic, and the disagreement between our predicted counts and those observed by Aretxaga et al. (2011) is significant even for the lower flux bins ($\sim 3\times$ for the $S_{1.1} > 2$ mJy bin). However, upon further consideration the disagreement will not seem so alarming, as there are numerous caveats that must be kept in mind when interpreting this plot.

First, the steepness of the cutoff in the starburst counts at $S_{1.1} \gtrsim 4$ mJy is artificial: Since we determine the fluxes of the isolated disks and galaxy pairs in an analytic way we can extrapolate to arbitrarily high masses for those populations. For the starbursts, however, we are limited by the the parameter space spanned by our merger simulations. None of our merger simulations reach $S_{1.1} > 5.5$ mJy, so the duty cycle for *all* starbursts for $S_{1.1} > 5.5$ mJy is zero. However, if we were to simulate a galaxy more massive than our most massive model (b6) it would reach a correspondingly higher flux, so the predicted counts for $S_{1.1} > 5.5$ mJy would no longer be zero. Thus for $S_{1.1} \gtrsim 4 - 5$ mJy the starburst counts should be considered a lower limit.

Still, even if one generously extrapolates the starburst counts beyond $S_{1.1} = 4$ mJy it is clear that our total predicted counts would still fall significantly short of those from Aretxaga et al. (2011). However, this is not reason to reject our model, as Aretxaga et al. (2011) conclude that the excess of sources at $S_{1.1} \gtrsim 5$ mJy relative to the SHADES field observed by Austermann et al. (2010) is that the excess sources are galaxies whose fluxes have been moderately amplified by galaxy-galaxy and galaxy-group lensing. At even higher fluxes the effect of lensing is even more significant (Negrello et al. 2007; Paciga et al. 2009; Lima et al. 2010), and it would

be incredibly difficult to explain the sources with mm flux density $\gg 10$ mJy observed by Vieira et al. (2010) and Negrello et al. (2010) if they are not strongly lensed. We do not include the effects of gravitational lensing in our models, so it is unsurprising that we significantly under-predict the counts of Aretxaga et al. (2011) for $S_{1.1} \gtrsim 4 - 5$ mJy.

Finally, we do not attempt to model some other potential contributors to the SMG population. In particular, we do not include contributions from small groups, clusters, multiple mergers, or physically unrelated sources blended into a single (sub)mm source (see Wang et al. 2011 for evidence of the last).

Thus, given these caveats and the modeling uncertainties, our predicted counts are reasonably consistent with those observed. Recall that our model is conservative in the sense that it uses a Kroupa—rather than top-heavy or flat—IMF and is tied to observations whenever possible. The consistency of the predicted and observed counts suggests that the observed SMG counts *may not* provide evidence for IMF variation; this will be discussed in detail in Section 4.5.1.

4.4.3   Relative Contributions of the Subpopulations

In Chapters 2 and 3 we argued that the SMG population is not exclusively late-stage merger-induced starbursts but rather a heterogeneous collection of starbursts, infall-stage mergers ('galaxy-pair SMGs'), and isolated disks. However, so far we have only presented the physical reasons one should expect such heterogeneity. It is important to quantify the relative importance of each subpopulation, so we do this now.
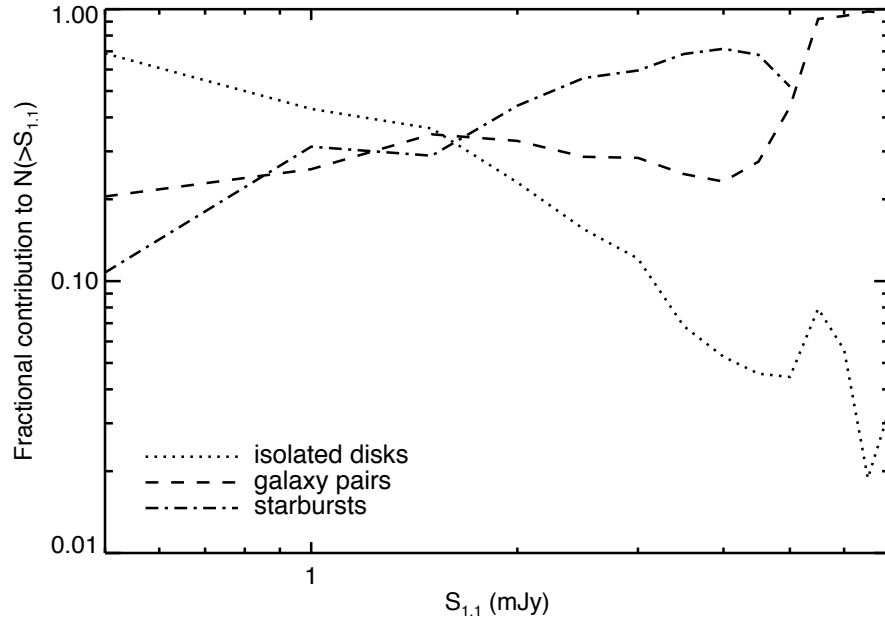
Figure 4.14.—: Fractional contribution of each subpopulation to the total cumulative counts versus $S_{1.1}$. Lines are the same as in Figure 4.13. At the lowest fluxes the isolated disks dominate, whereas at higher fluxes the starbursts dominate. The galaxy pairs contribute $\sim$ 20-40 per cent at $S_{1.1} \lesssim 4$ mJy. As explained above, the decline in the starburst contribution for $S_{1.1} \gtrsim 4$ mJy is artificial, so the relative fractions plotted for $S_{1.1} \gtrsim 4$ mJy should only be taken as upper limits for the galaxy pairs and isolated disks and a lower limit for the starbursts.

The counts shown in Figure 4.13 are divided into subpopulations, but the relative contributions can be read more easily from Figure 4.14, which shows the fractional contribution of each subpopulation to the total cumulative counts. At the lowest fluxes the isolated disks dominate the counts. For $2 \lesssim S_{1.1} \lesssim 5$ mJy the starbursts dominate, though the galaxy pairs always contribute at least ~ 20 per cent. At $S_{1.1} \sim 4 - 5$ mJy the starburst contribution begins to drop off steeply, but, as explained above, this is artificial. Consequently, for $S_{1.1} \gtrsim 4 - 5$ mJy the plotted galaxy pair and isolated disk contributions should be considered upper limits and the starburst contribution a lower limit.

One of the novel aspects of our work is that we include the contribution of the galaxy-pair subpopulation of SMGs. From Figure 4.14 we see that at all fluxes $S_{1.1} \lesssim 5$ mJy the galaxy pairs account for ~ 20-40 per cent of the total predicted counts, so they are a significant subpopulation of our model SMGs. As explained in Chapter 3, the galaxy-pair SMGs are *not* physically analogous to the merger-induced starburst SMGs; thus their potentially significant contribution to the SMG population can complicate physical interpretation of the observed properties of SMGs.

It is interesting to compare the relative contributions of the isolated disk and galaxy-pair subpopulations, as the relative contributions can be understood—at least schematically—in a simple way. For a major merger of two galaxies with $M_\star = M_{\mathrm{iso}}$, the flux of the resulting galaxy-pair SMG is roughly twice that of the individual isolated disks, $2S_{1.1}(M_{\mathrm{iso}})$. Since $S_{1.1}$ depends sublinearly on $M_\star$ (see Figure 4.4), for an isolated disk to have $S_{1.1}$ equal to that of the galaxy pair it must have $M_\star \gtrsim 3M_{\mathrm{iso}}$. Thus the relative contribution of the two subpopulations depends

on whether the number density of $M_\star = 3M_{\mathrm{iso}}$ disks divided by that of $M_\star = M_{\mathrm{iso}}$ disks, $n(3M_{\mathrm{iso}})/n(M_{\mathrm{iso}})$, is greater than the fraction of $M_\star = M_{\mathrm{iso}}$ disks undergoing a major merger, which is the merger rate times the duty cycle ($\sim$500 Myr). If the former is larger then the $M_\star = 3M_{\mathrm{iso}}$ disks will dominate the pairs of $M_\star = M_{\mathrm{iso}}$ disks, whereas if the merger fraction is higher than the relative number density the galaxy pairs will dominate.

The latter scenario is definitely plausible for bright SMGs, which are on the exponential tail of the SMF. For example, at $z \sim 2$, a galaxy with $M_\star = 1 \times 10^{11} M_\odot$ undergoes ~ 0.3 mergers per Gyr. Thus, if we assume a duty cycle of 500 Myr for the galaxy-pair phase, about 15% of such galaxies will be in galaxy pairs. For the M09 SMF, the number density of $M_\star = 3 \times 10^{11} M_\odot$ galaxies is $\sim 8\%$ that of $M_\star = 1 \times 10^{11} M_\odot$ galaxies. Therefore, by the above logic, the pairs of $M_\star = 1 \times 10^{11} M_\odot$ galaxies will contribute more to the submm counts than the isolated $M_\star = 3 \times 10^{11} M_\odot$ disks. This simple picture demonstrates why the galaxy pairs become dominant over the isolated disks for $S_{1.1} \gtrsim 2$ mJy. However, the threshold for dominance depends on both the $S_{1.1} - M_\star$ scaling and the shape of the SMF at the high-mass end. Thus observationally constraining the fraction of the SMG population that is galaxy pairs can provide useful constraints on both the (sub)mm flux-$M_\star$ relation and the shape of the massive end of the SMF.

Unfortunately, the relative contribution of the starburst subpopulation cannot be explained in as simple a manner. The duty cycles for the merger-induced starbursts depend sensitively on progenitor mass and merger mass ratio, so the mapping from merger rate to number density is not as simple as it is for the isolated disks and galaxy pairs. Fortunately, the SMF uncertainty, which we have shown to

be very significant for the overall counts, is relatively unimportant for the relative contribution of starbursts and galaxy pairs. Thus the relative contributions of starbursts and galaxy pairs depends primarily on their relative duty cycles. The duty cycles are uncertain, but, given that in our fiducial model the galaxy pairs contribute $\sim 20 - 40$ per cent of the total counts and the uncertainty in the duty cycles is definitely less than $2 - 3\times$, the prediction that both the starburst and galaxy pair subpopulations are significant (i.e., more than a few per cent of the population) is robust.

Though there have been many observational hints suggesting the importance of the galaxy-pair contribution (see Sections 2.4.2 and 3.1.2), the physical importance of this subpopulation has to date not been fully appreciated, and the fractional contribution of galaxy-pair SMGs to the total counts remains relatively poorly constrained. However, some authors have quoted the fraction of the SMGs in their surveys with multiple counterparts, so it is worth comparing our prediction to those numbers. One of the earliest observational indications of this population came from the 260-arcmin^2 SCUBA 8-mJy survey: of this sample of 850-μm sources, Ivison et al. (2002) found that ~ 25 per cent have multiple radio counterparts. Approximately ten per cent of the GOODS-N 850-μm (Pope et al. 2006), GOODS-N 1.1-mm (Chapin et al. 2009), SHADES 850$-\mu$m (Ivison et al. 2007; Clements et al. 2008), and GOODS-S 1.1-mm (Yun et al. 2011) sources have multiple counterparts. These fractions are somewhat smaller than the $\sim$ 20-40 per cent contribution shown in Figure 4.14, but both the predicted and observed fractions are uncertain. As explained above, the predicted fraction depends sensitively on the shape of the upper-end of the SMF and the relation between (sub)mm flux and $M_\star$. Observations,

on the other hand, may miss the more widely separated counterparts and cases when one of the counterparts is significantly more obscured (though the latter should not be significant for radio counterpart identification).

It is worthwhile to obtain stronger observational constraints on the galaxy-pair contribution to SMGs and to perform detailed follow-up observations of the multiple-counterpart SMGs. For example, high-resolution interferometric observations of molecular gas emission can yield much information. Of the 12 SMGs presented in Engel et al. (2010), 5 have CO emission that is resolved into two components with kinematics consistent with two merging disks. In two of the cases the projected separation of the two components is > 20 kpc; such objects are prime examples of the galaxy-pair subpopulation. (See also Tacconi et al. 2006, 2008; Bothwell et al. 2010; Riechers et al. 2011a,b.) Furthermore, Wang et al. (2011) presented two SMGs where the CO emission is resolved into multiple, *physically distinct* counterparts. Such objects constitute yet another potentially important subpopulation. Thus it is clear that more high-resolution observations of multiple-counterpart SMGs are needed to clarify the nature of the population; ALMA will be especially useful for this.

4.4.4 Predicted Redshift Distribution

In addition to the number counts a successful model for the SMG population must reproduce the redshift distribution. Figure 4.15 shows the redshift distribution of 1.1-mm sources predicted by our model for different 1.1-mm flux cuts. The redshift distributions are relatively broad, peaking in the range $z \sim 2 - 4$ and falling off at
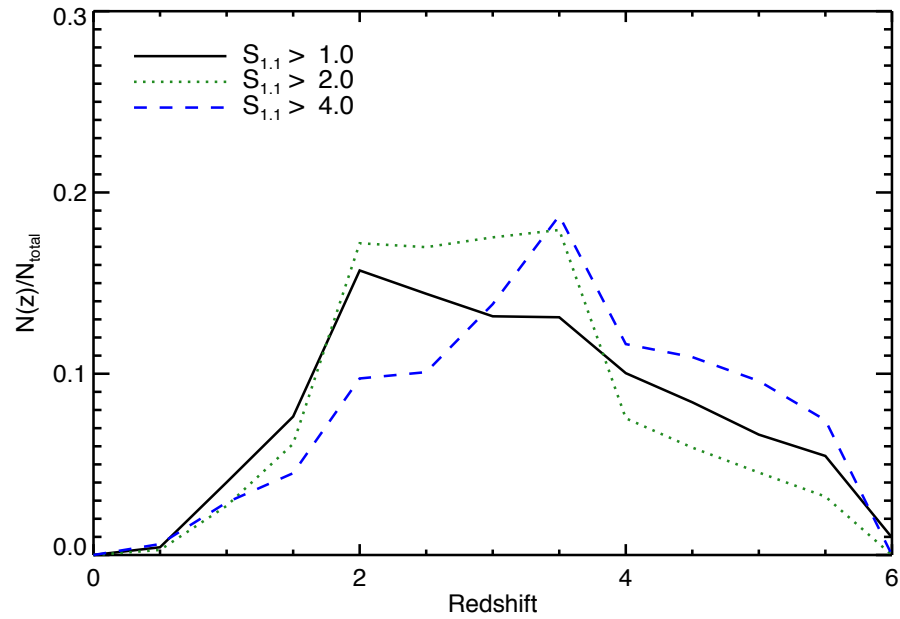
Figure 4.15.—: Predicted redshift distribution of 1.1-mm sources for three different flux cuts: $S_{1.1} > 1$ mJy (black solid line), > 2 mJy (green dotted), and > 4 mJy (blue dashed). The mean redshift for the $S_{1.1} > 1$ mJy sources is 2.9, for the $S_{1.1} > 2$ mJy sources 3.1, and for the $S_{1.1} > 4$ mJy sources 3.4.

lower and higher redshifts. The $S_{1.1} > 1$ mJy sources have mean redshift 2.9, the $S_{1.1} > 2$ mJy sources 3.1, and the $S_{1.1} > 4$ mJy sources 3.4, so there is a tendency for the brighter sources to be at higher redshifts.

The distributions presented here should be compared to the observed distributions. Yun et al. (2011) have recently determined the redshift distribution of 1.1-mm sources in the GOODS-S field (from the catalog of Scott et al. 2010). In Figures 4 and 5 they show the total redshift distribution of sources in both GOODS-S and GOODS-N, where the latter is from Chapin et al. (2009). The distribution can be approximated by a log-normal distribution with mean redshift 2.6 and $\sigma = 0.2$. The observed distribution should be compared to that for our $S_{1.1} > 1$ mJy bin. The typical redshifts for the predicted and observed 1.1-mm sources are similar. However, our model predicts a broader distribution, especially for the high-redshift tail. This discrepancy may suggest that the extrapolation of the F06 SMF we use for $z > 3.75$ over-predicts the number of massive galaxies. However, the observed redshift distributions are still relatively poorly constrained, and the redshift distributions for 850-μm (Chapman et al. 2005; Aretxaga et al. 2007) and 1.1-mm sources may differ significantly (see Yun et al. 2011). It will thus be interesting to compare our predicted redshift distribution of 850-μm sources to those observed and those predicted by other models.

4.5   Discussion

4.5.1   Are Modifications to the IMF Required to Match the Observed SMG Counts?

One of the primary motivations for this work is to reexamine the claim of B05 that SMG number counts provide evidence for a flat IMF. In order to test this claim we have assumed the null hypothesis—that the IMF in SMGs does not differ from what is observed locally—and used a Kroupa IMF. The ability of our model to match the observed counts suggests that the observed SMG counts do not provide evidence for a top-heavy IMF. Given the uncertainties inherent in our model we cannot say conclusively that SMGs do not form stars via a top-heavy IMF, but we argue it is premature to claim that they do.

It may be objected that our fiducial counts are still $2 - 3\times$ less than those observed by Austermann et al. (2010). (The discrepancy is greater when we compare to the counts of Aretxaga et al. (2011), but, as explained above, it is almost certain that this is due to gravitational lensing, which is not included in our model, so this is not a criticism of the model predictions.) However, one must keep in mind the considerable uncertainties and caveats described above, and, perhaps more importantly, recall that the discrepancy between the G00 model and the observed counts was $20\times$ at $S_{850} = 3$ mJy, which is significantly greater than the discrepancy for our model. Furthermore, in the G00 model quiescent galaxies overwhelmingly dominated the counts. B05 found that use of a flat IMF in starbursts caused the counts contributed by starbursts to increase by *three orders of magnitude*. Thus if we

were to use a similar IMF in starbursts our predicted counts would likely overpredict the observed counts by $> 100\times$.[3] The clear conclusion is that, in our model, any significant modification to the IMF is not required or justified.

4.5.2 Differences Between Our Model and B05

Since we find that, contrary to the claims of B05, a top-heavy IMF is not required to match the observed SMG counts, it is worthwhile to examine why our results differ from those of B05. While we defer a detailed comparison of SAMs and our model to future work (Benson et al., in preparation), we will briefly discuss possible reasons for the discrepancy here. There are three general components of our model which can disagree: the cosmological context (abundances and merger rates), the evolution of SFR and dust mass for individual mergers, and the RT calculation.

RT calculation: The RT calculation is fairly easy to compare, so we will start there. In Chapter 2 we showed that the (sub)mm flux density of our simulated galaxies can be well parameterized as a power law in SFR and dust mass (Equation 4.15). If the same relation does not hold in the B05 model then differences in the RT may be one cause of the discrepancy. While we have been unable to compare directly with the B05 model, we have compared with a SAM that uses a similar RT treatment (Benson 2010). We have found that relations similar to Equation (2.1) hold for the SMGs in the SAM, so it appears that the RT is not the cause of the

---

[3]We have not explicitly checked this because modifying the IMF in our models requires re-running both the GADGET and SUNRISE simulations, and we would have to re-run the entire suite to robustly predict the (sub)mm counts. We do not feel the check justifies such a large computational expense.

discrepancy.

Merger evolution: Perhaps the time evolution of the SFR and/or dust mass in the B05 SAM and our model differs. This is more difficult to compare directly than the RT, so we will only suggest possible differences here. B05 parameterize the SFR in bursts as $\dot{M}_\star = M_{\mathrm{gas,c}}/\tau_\star$, where $M_{\mathrm{gas,c}}$ is the cold gas mass and $\tau_\star$ is a SFR timescale given by $\tau_\star = \max[f_{\mathrm{dyn}}\tau_{\mathrm{dyn}}, \tau_{\star\mathrm{burst,min}}]$. Here $f_{\mathrm{dyn}} = 50$, τ_{dyn} is the dynamical time of the newly formed spheroid, and $\tau_{\star\mathrm{burst,min}} = 0.2$ Gyr. The major merger shown in Figure 2.2 has $M_{\mathrm{gas}} \sim 10^{11} M_\odot$ when the galaxies are at coalescence. Let us suppose that all the gas is cold. Then the maximum SFR given by the B05 prescription is $10^{11} M_\odot/0.2$ Gyr $= 500$ $M_\odot$ yr^{-1}, $\sim 9\times$ less than that of the simulation. If the dust mass is kept constant, Equation (4.15) implies that a $9\times$ decrease in SFR results in a $2.4\times$ decrease in (sub)mm flux, which would significantly affect the predicted counts. This is of course only a crude comparison, but it seems plausible that the SFHs of starbursts in the B05 model may disagree with those in our simulations.

Further evidence that the physical modeling of merger-induced starbursts may account for some of the discrepancy comes from the differing importance of starbursts in the two models. In the B05 model starburst dominate both the submm counts by a large margin and contribute significantly to the SFR density of the universe, dominating over quiescently star-forming disks for $z \gtrsim 3$. In our model isolated disks dominate at the lowest (sub)mm fluxes and quiescently star-forming galaxy-pair SMGs provide a significant contribution to the bright counts. Furthermore, in our model merger-induced starbursts account for $\lesssim 5$ per cent of the SFR density of the universe at all redshifts (Hopkins et al. 2010a).

B05 explain that the key way the flat IMF boosts the submm counts in their model is by increasing the dust produced per unit SFR by $\sim 6\times$. This results in a colder SED and thus higher submm flux for fixed luminosity. It is thus important to compare the evolution of galaxies' dust masses in the B05 model to ours. However, the dust mass of a galaxy depends on its detailed SFH, so it is difficult to back out from the B05 SAM in a simple way. It would be possible to compare the two models in a simple way by examining, e.g., the ratios of dust to stellar and dust to gas mass. Unfortunately we have been unable to find the appropriate information about the B05 model in the literature; however, we will do this comparison in Benson et al. (in preparation).

Cosmological context: The third major component that of the models that can disagree is the cosmological context, which includes the SMF and merger rates. In Section 4.4.1 we showed that the predicted number densities and redshift distribution of isolated disk SMGs is very sensitive to the assumed SMF. Thus it is worthwhile to compare the SMF in the SAMs to the observationally derived SMFs we have used. While we have not found a direct comparison of the B05 SMF in the literature, Swinbank et al. (2008) have shown that the B05 model under-predicts the rest-frame K-band fluxes of SMGs, suggesting the masses of their model SMGs are lower than observed. This would be a natural result of under-prediction of the abundance of massive galaxies. Under-prediction of the SMF would also cause an under-prediction of the merger rate of massive galaxies at those redshifts. If, indeed, the B05 model under-predicts the SMF then they need to compensate by making the starburst contribution significantly higher: They do this by enabling very gas-rich minor mergers to cause strong starbursts (in their model minor mergers account for

about three-quarters of the SMG population; González et al. 2011) and modifying the IMF in starbursts so that, for a given SFR, they have much higher submm flux. An under-prediction of the abundance of all massive galaxies and subsequent need to strongly boost the starburst contribution would explain why the relative contributions of starbursts and quiescent galaxies differ so significantly.

Finally, one additional potential reason for the discrepancy is that, to our knowledge, the B05 model does not seem to account for blending of multiple galaxies into one (sub)mm source, which can be significant for both merging disks and physically distinct galaxies (Wang et al. 2011). Our models suggest that galaxy-pair SMGs can account for tens of per cent of the SMG population attributable to isolated disks and mergers. The types of sources Wang et al. (2011) observed could boost this contribution further.

4.6 Conclusions

We have presented a novel approach to predict the number density, counts, and redshift distribution of (sub)mm-selected galaxies. We combined a simple semi-empirical model for galaxy abundances and merger rates with the results of 3-D hydrodynamic simulations and dust radiative transfer in order calculate the contributions to the counts from isolated disks, galaxy pairs (aka infall-stage mergers), and late-stage merger-induced starbursts. Our model is constrained to observations as much as possible; as a result, we are able to isolate the effects of uncertainties related the dynamical evolution of mergers and the dust radiative transfer—which are perhaps uniquely relevant to the SMG population—from more

general issues that affect the high-redshift galaxy population as a whole, such as the SMF. Furthermore, we have used a Kroupa—as opposed to flat or top-heavy—IMF, as we wish to test whether we can match the observed counts without modifying the IMF from what is observed locally.

Our fiducial model predicts cumulative 1.1-mm counts $\sim 2 - 3\times$ less than the observed Austermann et al. (2010) counts, but the model is consistent with the observations given the level of uncertainty in the modeling. Since we have not modified the IMF, our result suggests that we cannot reject the null hypothesis (that the IMF in high-redshift starbursts is no different than the IMF in local galaxies). One of the main conclusions of our work is thus that *SMG number counts do not provide evidence for a top-heavy IMF.*

In Chapters 2 and 3 we have argued that some fraction of the SMG population must be widely separated merging disk galaxies blended into one (sub)mm source. We have termed this subpopulation 'galaxy-pair SMGs'. In these galaxy-pair SMGs the two disk galaxies are not yet strongly interacting, so they are physically analogous to quiescent disk galaxies rather than merger-induced starburst. We have for the first time modeled the contribution of this subpopulation to the total (sub)mm counts. Our model predicts that galaxy-pair SMGs account for $\sim 20 - 40$ per cent of the population. Though the precise fraction is sensitive to the details of the modeling, the prediction that galaxy pairs contribute significantly to the population (i.e., tens of per cent rather than a few per cent or less) is robust. The observational diagnostics presented in Chapter 3 can be used to determine the relative fraction of the SMG population that is quiescent galaxies, thereby testing this prediction of our model.

Except at the lowest fluxes ($S_{1.1} < 2$ mJy), merger-induced starbursts account for the bulk of the population not accounted for by galaxy-pair SMGs. Thus, contrary to the claims of Davé et al. (2010), we find that isolated disks contribute negligibly to the bright SMG population. This, too, is a robust testable prediction of our model.

We have also compared the redshift distribution of our predicted SMGs to that observed. The typical redshifts of the model and observed SMGs are similar, but the model may overpredict the number of SMGs at $z \gtrsim 4$. This may be because the SMF used in our models over-predicts the number of massive galaxies at those redshifts.

Since our conclusion that (sub)mm counts can be matched without IMF modification is in direct contradiction with the conclusion of B05 we have discussed possible reasons for the discrepancy between our results. First, to our knowledge, B05 do not treat blending of (sub)mm sources; thus their model does not include the galaxy-pair subpopulation, which can account for almost half of the (sub)mm counts. Second, there may be significant differences in their SFR prescription for mergers and the results of our simulations. Finally, it is likely that the B05 model under-predicts the abundance of massive galaxies at $z \sim 2 - 4$. If so, then the inability of the B05 model to match the submm counts without IMF modification may be reflective of a more general issue rather than one specific to SMGs. We will present a detailed comparison of the ingredients of our models and multiple SAMs, including that of B05, and an investigation of the origin of the significant difference in predictions in future work.

Chapter 5

Conclusions and Future Directions

Just as hundreds of millions of years ago the Earth was dominated by creatures unlike any known today, ten billion years ago the universe was populated with galaxies more extreme than any that exist in our current epoch. In that distant past, typical galaxies formed stars at rates comparable to those of the most highly star-forming galaxies that exist today, and the most extreme star-formers make even mighty Arp 220 seem like *Anchiornis* compared to *Spinosaurus.* Unlike paleontologists, we are literally able to look back in time thanks to the finite speed of light, but the great distance between us and high-redshift galaxies prevents us from examining those strange specimens in as spectacular detail as we can examine our own Milky Way and other galaxies in the Local Group. Thus in order to understand these strange creatures, we must, like paleontologists, make inferences from relatively limited data.[1]

---

[1] A further parallel between dinosaurs and high-redshift galaxies is that alternate theories claiming that both populations are much younger than generally believed

By definition, astrophysicists[2] utilize physics to interpret and understand astronomical observations. In this dissertation I have attempted to do exactly that. While I have been involved in work studying a diversity of the galaxy species that populate the universe both near and far, my pet galaxy population,—and, coincidentally, the focus of this dissertation—is that of submm-selected galaxies. Since their discovery in the late-1990s, SMGs have garnered much attention for their extreme luminosities ($L_{\rm bol} \gtrsim 10^{12} L_\odot$) and star formation rates (SFR $\sim 10^2 - 10^4 M_\odot \ {\rm yr}^{-1}$) and because their properties and abundance have been difficult to explain for many galaxy formation models. I have used a combination of hydrodynamical simulations, radiative transfer calculations, and simple analytical models to attempt to create SMGs from scratch and to investigate several open questions about this interesting population.

Locally, the most luminous, rapidly star-forming galaxies are late-stage major mergers. SMGs represent some of the most luminous, rapidly star-forming galaxies at $z \sim 1-4$, so it is natural to expect that they, too, are merger-induced starbursts. Indeed, to date this has been the most commonly believed explanation for the population. In early work we confirmed that major mergers of gas-rich galaxies can indeed have properties similar to those of SMGs (Narayanan et al. 2009, 2010a),

have been put forth by vocal minorities. These theories attract some attention from the general public but are largely—and justifiably—ignored by the scientific community, so we will not discuss them further here. After all, "the aimless blade of science slashed the pearly gates" (N. Young, private communication).

[2]This particular sub-species of *Homo sapiens* should not be confused with astrologers, who predict the future through observations of celestial bodies and use of ambiguous language, or astronomers, who name stars. The latter can win the Nobel Prize in Physics, but the former have been unsuccessful to date.

but we have suggested that the idea that *all* SMGs are merger-induced starbursts is incorrect. In each chapter we have suggested some modifications to the canonical wisdom about SMGs.

In Chapter 2 we investigated how the observed-frame (sub)mm flux density depends on galaxy properties in order to better understand the nature of the SMG selection. We found that a galaxy's SFR (or L_{bol}) and dust mass are the key determinants of its observed-frame (sub)mm flux. Our simulations suggest that (sub)mm flux scales with SFR much more weakly in starbursts than in quiescently star-forming disk galaxies. This is primarily because the sharp decline in dust mass during the starburst causes the SED of the galaxy to become hotter, mitigating the increase in (sub)mm flux that would occur if the SED were simply scaled upward with L_{bol}, and also because the "contamination" from stars formed pre-burst prevents L_{bol} from scaling linearly with SFR as it would for a simplistic (and commonly assumed) instantaneous burst star formation history. Consequently, starbursts are significantly less efficient at making SMGs than one might naively expect. An interesting corollary of this work is that early-stage mergers, where the infalling disks are not yet strongly interacting but are close enough to be blended into one submm source, may contribute significantly to the SMG population. We refer to such objects as "galaxy-pair SMGs". While galaxy-pair SMGs are still mergers, they are physically more similar to isolated disk galaxies because they are powered by quiescent rather than starburst star formation.

Observers will not (and should not) believe in the galaxy-pair subpopulation of SMGs simply because the simulations suggest it exists. Thus we have, in Chapter 3, presented various observational diagnostics to distinguish starbursts

and quiescently star-forming galaxies from integrated data alone. We have shown that merger-induced starbursts tend to have hotter SEDs and higher L_{IR}, global star formation efficiency ($L_{\mathrm{IR}}/M_{\mathrm{gas}}$), and IR excess ($L_{\mathrm{IR}}/L_{\mathrm{FUV}}$) than quiescently star-forming galaxies. Furthermore, they tend to lie above the SFR-$M_\star$ relation defined by quiescently star-forming galaxies. These diagnostics can be used to test whether some SMGs are quiescently star-forming galaxy pairs or isolated disks and, if so, to constrain the relative contributions to the population.

In Chapter 4 we turned to one of the most pressing questions about SMGs, whether the observed (sub)mm number counts can be explained by traditional galaxy formation models. Some previous work has suggested that modification of the IMF may be required in order for the models to predict counts consistent with those observed. In order to reexamine this tantalizing claim and approach the question in a novel way, we combined the simulation methodology used in the preceding two chapters with a simple empirically-constrained model for galaxy number densities and merger rates. We have shown that our model predicts (sub)mm counts only slightly less than those observed, and the counts should be considered consistent given the modeling uncertainties. As a result, we have argued that the observed (sub)mm counts do not give cause to reject the null hypothesis that the IMF is universal. Furthermore, we have suggested that galaxy pairs may contribute to the SMG population at the tens of per cent level, whereas isolated disks contribute significantly only for the faintest sources.

While it is almost certainly true that the brightest SMGs are late-stage major mergers undergoing a strong starburst, the picture of SMGs we have painted here is more nuanced than the canonical one. Imminent observations from telescopes such

as *Herschel*, SCUBA-2, and ALMA will easily be able to confirm or deny our claims and thereby enable us to refine and improve our models.

We will continue to utilize simulations such as those presented here for various applications; projects underway include testing the effectiveness of SFR (Hayward et al., in preparation) and AGN (Snyder et al., in preparation) indicators and SED modeling (Smith et al., in preparation) and comparison to observed 24-μm-selected galaxies (Sajina et al., in preparation), local interacting galaxies (Lanz et al., in preparation), and quasars (Hao et al., in preparation). However, our models are clearly far from perfect, so the focus of my postdoctoral research will be developing improved simulations. One of the key ways I will improve the simulations is by using the code AREPO (Springel 2010) rather than GADGET. AREPO combines the advantages while simultaneously avoiding many pitfalls of both the standard grid-based and SPH approaches by using an Eulerian method on an adaptive grid that moves with the fluid. This moving mesh approach is demonstrably better than SPH at resolving shocks, and it does not artificially suppress fluid instabilities in the way that SPH can. Furthermore, unlike traditional Eulerian methods, it is Galilean invariant. Early cosmological simulations with AREPO give significantly different results than identical simulations performed with GADGET-2 (Vogelsberger et al. 2011; Keres et al. 2011; Sijacki et al. 2011), so the first step I will take is to do a comparison of identical idealized merger simulations run with both AREPO and GADGET-2. I will then proceed to run a large suite of high-resolution idealized merger simulations with AREPO and SUNRISE. This simulation suite will provide a wealth of data and will enable numerous interesting projects. Furthermore, by providing a large set of simulated galaxy SEDs coarsely sampling the parameter

space spanned by real galaxies it will be possible for observers to "fit" their observed SEDs simply by doing brute force comparison with our model SEDs; in this way we may make SED modeling virtually obsolete. The work is really just beginning; as regards this dissertation, however, to quote Jim Morrison, "This is the end."

References

Adelberger, K. L., & Steidel, C. C. 2000, ApJ, 544, 218

Alexander, D. M., Bauer, F. E., Chapman, S. C., Smail, I., Blain, A. W., Brandt, W. N., & Ivison, R. J. 2005a, ApJ, 632, 736

Alexander, D. M., Smail, I., Bauer, F. E., Chapman, S. C., Blain, A. W., Brandt, W. N., & Ivison, R. J. 2005b, Nature, 434, 738

Alexander, D. M., et al. 2008, AJ, 135, 1968

Almeida, C., Baugh, C. M., & Lacey, C. G. 2011, MNRAS, 1312

Amblard, A., et al. 2010, A&A, 518, L9

Aretxaga, I., et al. 2007, MNRAS, 379, 1571

—. 2011, MNRAS, 415, 3831

Asplund, M., Grevesse, N., Sauval, A. J., & Scott, P. 2009, ARA&A, 47, 481

Austermann, J. E., et al. 2009, MNRAS, 393, 1573

Austermann, J. E., et al. 2010, MNRAS, 401, 160

Barger, A. J., Cowie, L. L., Sanders, D. B., Fulton, E., Taniguchi, Y., Sato, Y., Kawara, K., & Okuda, H. 1998, Nature, 394, 248

Barnes, J., & Hernquist, L. 1991, ApJ, 370, L65

—. 1996, ApJ, 471, 115

Barnes, J., & Hut, P. 1986, Nature, 324, 446

Bastian, N., Covey, K. R., & Meyer, M. R. 2010, arXiv:1001.2965

Baugh, C. M., Lacey, C. G., Frenk, C. S., Granato, G. L., Silva, L., Bressan, A., Benson, A. J., & Cole, S. 2005, MNRAS, 356, 1191 (B05)

Bekki, K., & Shioya, Y. 2000, ApJ, 542, 201

Bell, E. F. 2003, ApJ, 586, 794

Benson, A. J. 2010, arXiv:1008.1786

Bianchi, S. 2008, A&A, 490, 461

Biggs, A. D., & Ivison, R. J. 2008, MNRAS, 385, 893

Blain, A. W., Jameson, A., Smail, I., Longair, M. S., Kneib, J.-P., & Ivison, R. J. 1999a, MNRAS, 309, 715

Blain, A. W., Smail, I., Ivison, R. J., & Kneib, J.-P. 1999b, MNRAS, 302, 632

Blain, A. W., Smail, I., Ivison, R. J., Kneib, J.-P., & Frayer, D. T. 2002, Phys. Rep., 369, 111

Bondi, H. 1952, MNRAS, 112, 195

Bondi, H., & Hoyle, F. 1944, MNRAS, 104, 273

Bothwell, M. S., et al. 2010, MNRAS, 405, 219

Bouché, N., et al. 2007, ApJ, 671, 303

Bouwens, R. J., et al. 2011, arXiv:1109.0994

Bower, R. G., Vernon, I., Goldstein, M., Benson, A. J., Lacey, C. G., Baugh, C. M., Cole, S., & Frenk, C. S. 2010, MNRAS, 407, 2017

Brodwin, M., et al. 2008, ApJ, 687, L65

Buat, V., & Burgarella, D. 1998, A&A, 334, 772

Buat, V., Donas, J., Milliard, B., & Xu, C. 1999, A&A, 352, 371

Buat, V., Marcillac, D., Burgarella, D., Le Floc'h, E., Takeuchi, T. T., Iglesias-Paràmo, J., & Xu, C. K. 2007, A&A, 469, 19

Buat, V., Takeuchi, T. T., Burgarella, D., Giovannoli, E., & Murata, K. L. 2009, A&A, 507, 693

Buat, V., et al. 2005, ApJ, 619, L51

Bush, S. J., Cox, T. J., Hayward, C. C., Thilker, D., Hernquist, L., & Besla, G. 2010, ApJ, 713, 780

Bussmann, R. S., et al. 2009a, ApJ, 693, 750

—. 2009b, ApJ, 705, 184

Calzetti, D. 1997, AJ, 113, 162

Calzetti, D., Armus, L., Bohlin, R. C., Kinney, A. L., Koornneef, J., & Storchi-Bergmann, T. 2000, ApJ, 533, 682

Calzetti, D., Kinney, A. L., & Storchi-Bergmann, T. 1994, ApJ, 429, 582

Capak, P., et al. 2008, ApJ, 681, L53

Carilli, C. L., et al. 2010, ApJ, 714, 1407

Casey, C. M., Chapman, S. C., Smail, I., Alaghband-Zadeh, S., Bothwell, M. S., & Swinbank, A. M. 2011, MNRAS, 411, 2739

Casey, C. M., et al. 2009, MNRAS, 399, 121

Chakrabarti, S., Cox, T. J., Hernquist, L., Hopkins, P. F., Robertson, B., & Matteo, T. D. 2007, ApJ, 658, 840

Chakrabarti, S., Fenner, Y., Cox, T. J., Hernquist, L., & Whitney, B. A. 2008, ApJ, 688, 972

Chakrabarti, S., & McKee, C. F. 2005, ApJ, 631, 792

—. 2008, ApJ, 683, 693

Chakrabarti, S., & Whitney, B. A. 2009, ApJ, 690, 1432

Chapin, E. L., et al. 2009, MNRAS, 398, 1793

Chapman, S. C., Blain, A. W., Smail, I., & Ivison, R. J. 2005, ApJ, 622, 772

Chapman, S. C., Smail, I., Blain, A. W., & Ivison, R. J. 2004, ApJ, 614, 671

Chapman, S. C., Windhorst, R., Odewahn, S., Yan, H., & Conselice, C. 2003, ApJ, 599, 92

Chapman, S. C., et al. 2000, MNRAS, 319, 318

Chapman, S. C., et al. 2010, MNRAS, 409, L13

Chary, R., & Elbaz, D. 2001, ApJ, 556, 562

Clements, D. L., Dunne, L., & Eales, S. 2010, MNRAS, 403, 274

Clements, D. L., et al. 2008, MNRAS, 387, 247

Cole, S., Lacey, C. G., Baugh, C. M., & Frenk, C. S. 2000, MNRAS, 319, 168

Conley, A., et al. 2011, ApJ, 732, L35

Conroy, C., & Wechsler, R. H. 2009, ApJ, 696, 620

Coppin, K., et al. 2008, MNRAS, 384, 1597

Cox, T. J., Dutta, S. N., Matteo, T. D., Hernquist, L., Hopkins, P. F., Robertson, B., & Springel, V. 2006a, ApJ, 650, 791

Cox, T. J., Jonsson, P., Primack, J. R., & Somerville, R. S. 2006b, MNRAS, 373, 1013

Cox, T. J., Jonsson, P., Somerville, R. S., Primack, J. R., & Dekel, A. 2008, MNRAS, 384, 386

da Cunha, E., Charmandaris, V., Díaz-Santos, T., Armus, L., Marshall, J. A., & Elbaz, D. 2010, A&A, 523, A78

Daddi, E., Dannerbauer, H., Krips, M., Walter, F., Dickinson, M., Elbaz, D., & Morrison, G. E. 2009a, ApJ, 695, L176

Daddi, E., et al. 2005, ApJ, 631, L13

—. 2007, ApJ, 670, 156

—. 2009b, ApJ, 694, 1517

—. 2010, ApJ, 713, 686

Dale, D. A., & Helou, G. 2002, ApJ, 576, 159

Dale, D. A., Helou, G., Contursi, A., Silbermann, N. A., & Kolhatkar, S. 2001, ApJ, 549, 215

Dale, D. A., et al. 2007, ApJ, 655, 863

Dannerbauer, H., Daddi, E., Riechers, D. A., Walter, F., Carilli, C. L., Dickinson, M., Elbaz, D., & Morrison, G. E. 2009, ApJ, 698, L178

Dannerbauer, H., Lehnert, M. D., Lutz, D., Tacconi, L., Bertoldi, F., Carilli, C., Genzel, R., & Menten, K. 2002, ApJ, 573, 473

Dannerbauer, H., et al. 2010, ApJ, 720, L144

Davé, R., Finlator, K., Oppenheimer, B. D., Fardal, M., Katz, N., Kereš, D., & Weinberg, D. H. 2010, MNRAS, 404, 1355

Dekel, A., et al. 2009, Nature, 457, 451

Devriendt, J. E. G., & Guiderdoni, B. 2000, A&A, 363, 851

Dey, A., et al. 2008, ApJ, 677, 943

Downes, D., & Solomon, P. M. 1998, ApJ, 507, 615

Draine, B. T., & Li, A. 2007, ApJ, 657, 810

Dunne, L., & Eales, S. A. 2001, MNRAS, 327, 697

Dunne, L., Eales, S. A., & Edmunds, M. G. 2003, MNRAS, 341, 589

Dwek, E. 1998, ApJ, 501, 643

Eales, S., Lilly, S., Gear, W., Dunne, L., Bond, J. R., Hammer, F., Fèvre, O. L., & Crampton, D. 1999, ApJ, 515, 518

Edmunds, M. G., & Eales, S. A. 1998, MNRAS, 299, L29

Elbaz, D., et al. 2011, A&A, 533, A119

Elmegreen, B. G. 1997, in Revista Mexicana de Astronomia y Astrofisica Conference Series, ed. J. Franco, R. Terlevich, & A. Serrano, Vol. 6, 165

Engel, H., et al. 2010, ApJ, 724, 233

Erb, D. K., Steidel, C. C., Shapley, A. E., Pettini, M., Reddy, N. A., & Adelberger, K. L. 2006, ApJ, 646, 107

Fardal, M. A., Katz, N., Weinberg, D. H., Davé, R., & Hernquist, L. 2001, astro-ph/0107290

Faucher-Giguere, C.-A., Keres, D., & Ma, C.-P. 2011, arXiv:1103.0001

Fontana, A., et al. 2006, A&A, 459, 745 (F06)

Fontanot, F., & Monaco, P. 2010, MNRAS, 405, 705

Fontanot, F., Monaco, P., Silva, L., & Grazian, A. 2007, MNRAS, 382, 903

Genzel, R., et al. 2010, MNRAS, 407, 2091

Gingold, R. A., & Monaghan, J. J. 1977, MNRAS, 181, 375

González, J. E., Lacey, C. G., Baugh, C. M., & Frenk, C. S. 2011, MNRAS, 413, 749

Gordon, K. D., Calzetti, D., & Witt, A. N. 1997, ApJ, 487, 625

Granato, G. L., De Zotti, G., Silva, L., Bressan, A., & Danese, L. 2004, ApJ, 600, 580

Granato, G. L., Lacey, C. G., Silva, L., Bressan, A., Baugh, C. M., Cole, S., & Frenk, C. S. 2000, ApJ, 542, 710

Greve, T. R., Pope, A., Scott, D., Ivison, R. J., Borys, C., Conselice, C. J., & Bertoldi, F. 2008, MNRAS, 389, 1489

Greve, T. R., et al. 2005, MNRAS, 359, 1165

Griffin, M. J., et al. 2010, A&A, 518, L3

Groves, B., Dopita, M. A., Sutherland, R. S., Kewley, L. J., Fischera, J., Leitherer, C., Brandl, B., & van Breugel, W. 2008, ApJS, 176, 438

Guiderdoni, B., Hivon, E., Bouchet, F. R., & Maffei, B. 1998, MNRAS, 295, 877

Hainline, L. J., Blain, A. W., Smail, I., Alexander, D. M., Armus, L., Chapman, S. C., & Ivison, R. J. 2010, arXiv:1006.0238

Hatsukade, B., et al. 2011, MNRAS, 411, 102

Hayward, C. C., Kereš, D., Jonsson, P., Narayanan, D., Cox, T. J., & Hernquist, L. 2011, arXiv:2011.0002

Hayward, C. C., Narayanan, D., Jonsson, P., Cox, T. J., Kereš, D., Hopkins, P. F., & Hernquist, L. 2011, in ASP Conf. Ser. 440, Have Observations Revealed a Variable Upper End of the Initial Mass Function?, ed. M. Treyer, T. Wyder, J. Neill, M. Seibert, & J. Lee (San Francisco, CA: ASP), 369

Hernquist, L. 1989, Nature, 340, 687

—. 1990, ApJ, 356, 359

Hernquist, L., & Katz, N. 1989, ApJS, 70, 419

Hildebrand, R. H. 1983, QJRAS, 24, 267

Hobson, M. P., & Padman, R. 1993, MNRAS, 264, 161

Hogg, D. W. 1999, astro-ph/9905116

Holland, W., et al. 2006, in Society of Photo-Optical Instrumentation Engineers (SPIE) Conference Series, Vol. 6275

Holland, W. S., et al. 1999, MNRAS, 303, 659

Holmberg, E. 1941, ApJ, 94, 385

Hopkins, A. M. 2004, ApJ, 615, 209

Hopkins, A. M., & Beacom, J. F. 2006, ApJ, 651, 142

Hopkins, A. M., Connolly, A. J., Haarsma, D. B., & Cram, L. E. 2001, AJ, 122, 288

Hopkins, P. F. 2008, PhD thesis

Hopkins, P. F., Cox, T. J., Dutta, S. N., Hernquist, L., Kormendy, J., & Lauer, T. R. 2009a, ApJS, 181, 135

Hopkins, P. F., Cox, T. J., Kereš, D., & Hernquist, L. 2008a, ApJS, 175, 390

Hopkins, P. F., Cox, T. J., Younger, J. D., & Hernquist, L. 2009b, ApJ, 691, 1168

Hopkins, P. F., & Hernquist, L. 2010, MNRAS, 402, 985

Hopkins, P. F., Hernquist, L., Cox, T. J., Di Matteo, T., Robertson, B., & Springel, V. 2006a, ApJS, 163, 1

Hopkins, P. F., Hernquist, L., Cox, T. J., Dutta, S. N., & Rothberg, B. 2008b, ApJ, 679, 156

Hopkins, P. F., Hernquist, L., Cox, T. J., & Kereš, D. 2008c, ApJS, 175, 356

Hopkins, P. F., Hernquist, L., Cox, T. J., Robertson, B., & Springel, V. 2006b, ApJS, 163, 50

Hopkins, P. F., Lauer, T. R., Cox, T. J., Hernquist, L., & Kormendy, J. 2009c, ApJS, 181, 486

Hopkins, P. F., Quataert, E., & Murray, N. 2011, MNRAS, 417, 950

Hopkins, P. F., Richards, G. T., & Hernquist, L. 2007, ApJ, 654, 731

Hopkins, P. F., Somerville, R. S., Hernquist, L., Cox, T. J., Robertson, B., & Li, Y. 2006c, ApJ, 652, 864

Hopkins, P. F., Younger, J. D., Hayward, C. C., Narayanan, D., & Hernquist, L. 2010a, MNRAS, 402, 1693

Hopkins, P. F., et al. 2009d, MNRAS, 397, 802

—. 2010b, ApJ, 715, 202

—. 2010c, ApJ, 724, 915

Hoyle, F., & Lyttleton, R. A. 1939, Proc. Cam. Philos. Soc., 35, 405

Hughes, D. H., et al. 1998, Nature, 394, 241

Hwang, H. S., et al. 2010, MNRAS, 409, 75

Ilbert, O., et al. 2010, ApJ, 709, 644

Iono, D., et al. 2009, ApJ, 695, 1537

Ivison, R. J., Smail, I., Papadopoulos, P. P., Wold, I., Richard, J., Swinbank, A. M., Kneib, J., & Owen, F. N. 2010, MNRAS, 404, 198

Ivison, R. J., et al. 2002, MNRAS, 337, 1

—. 2007, MNRAS, 380, 199

James, A., Dunne, L., Eales, S., & Edmunds, M. G. 2002, MNRAS, 335, 753

Jonsson, P. 2006, MNRAS, 372, 2

Jonsson, P., Cox, T. J., Primack, J. R., & Somerville, R. S. 2006, ApJ, 637, 255

Jonsson, P., Groves, B. A., & Cox, T. J. 2010, MNRAS, 403, 17

Jonsson, P., & Primack, J. R. 2010, New Astron., 15, 509

Juvela, M. 2005, A&A, 440, 531

Karim, A., et al. 2011, ApJ, 730, 61

Katz, N., Weinberg, D. H., & Hernquist, L. 1996, ApJS, 105, 19

Kaviani, A., Haehnelt, M. G., & Kauffmann, G. 2003, MNRAS, 340, 739

Kennicutt, R. C. 1998a, ApJ, 498, 541

—. 1998b, ARA&A, 36, 189

Kennicutt, Jr., R. C., et al. 2003, PASP, 115, 928

Kereš, D., Katz, N., Fardal, M., Davé, R., & Weinberg, D. H. 2009, MNRAS, 395, 160

Kereš, D., Katz, N., Weinberg, D. H., & Davé, R. 2005, MNRAS, 363, 2

Keres, D., Vogelsberger, M., Sijacki, D., Springel, V., & Hernquist, L. 2011, arXiv:1109.4638

Kewley, L. J., & Ellison, S. L. 2008, ApJ, 681, 1183

Knudsen, K. K., Kneib, J.-P., Richard, J., Petitpas, G., & Egami, E. 2010, ApJ, 709, 210

Kormendy, J., Fisher, D. B., Cornell, M. E., & Bender, R. 2009, ApJS, 182, 216

Kovács, A., Chapman, S. C., Dowell, C. D., Blain, A. W., Ivison, R. J., Smail, I., & Phillips, T. G. 2006, ApJ, 650, 592

Kovács, A., et al. 2010, ApJ, 717, 29

Kroupa, P. 2001, MNRAS, 322, 231

Krumholz, M. R., & McKee, C. F. 2005, ApJ, 630, 250

Krumholz, M. R., & Thompson, T. A. 2007, ApJ, 669, 289

Lacey, C. G., Baugh, C. M., Frenk, C. S., Benson, A. J., Orsi, A., Silva, L., Granato, G. L., & Bressan, A. 2010, MNRAS, 405, 2

Lacey, C. G., Baugh, C. M., Frenk, C. S., Silva, L., Granato, G. L., & Bressan, A. 2008, MNRAS, 385, 1155

Lagache, G., Dole, H., & Puget, J.-L. 2003, MNRAS, 338, 555

Leitherer, C., et al. 1999, ApJS, 123, 3

Leroy, A. K., Walter, F., Brinks, E., Bigiel, F., de Blok, W. J. G., Madore, B., & Thornley, M. D. 2008, AJ, 136, 2782

Li, Y., et al. 2008, ApJ, 678, 41

Lima, M., Jain, B., Devlin, M., & Aguirre, J. 2010, ApJ, 717, L31

Lisenfeld, U., Isaak, K. G., & Hills, R. 2000, MNRAS, 312, 433

Lo Faro, B., Monaco, P., Vanzella, E., Fontanot, F., Silva, L., & Cristiani, S. 2009, MNRAS, 399, 827

Lonsdale, C. J., Farrah, D., & Smith, H. E. 2006, Ultraluminous Infrared Galaxies (Springer Verlag), 285

Lu, Y., Mo, H. J., Katz, N., & Weinberg, M. D. 2011a, arXiv:1109.6658

Lu, Y., Mo, H. J., Weinberg, M. D., & Katz, N. 2011b, MNRAS, 416, 1949

Lucy, L. B. 1977, AJ, 82, 1013

Lupu, R. E., et al. 2010, arXiv:1009.5983

Magdis, G. E., et al. 2010, MNRAS, 409, 22

Magnelli, B., Elbaz, D., Chary, R. R., Dickinson, M., Le Borgne, D., Frayer, D. T., & Willmer, C. N. A. 2011, A&A, 528, A35

Magnelli, B., et al. 2010, A&A, 518, L28

Maiolino, R., et al. 2008, A&A, 488, 463

Marchesini, D., van Dokkum, P. G., Förster Schreiber, N. M., Franx, M., Labbé, I., & Wuyts, S. 2009, ApJ, 701, 1765 (M09)

Matteo, T. D., Springel, V., & Hernquist, L. 2005, Nature, 433, 604

Menéndez-Delmestre, K., et al. 2007, ApJ, 655, L65

—. 2009, ApJ, 699, 667

Michałowski, M. J., Dunlop, J. S., Cirasuolo, M., Hjorth, J., Hayward, C. C., & Watson, D. 2011, arXiv:1108.6058

Michałowski, M. J., Hjorth, J., & Watson, D. 2010a, A&A, 514, A67

Michałowski, M. J., Watson, D., & Hjorth, J. 2010b, ApJ, 712, 942

Mihos, J. C., & Hernquist, L. 1994, ApJ, 437, L47

—. 1996, ApJ, 464, 641

Narayanan, D., Cox, T. J., Hayward, C. C., & Hernquist, L. 2011a, MNRAS, 412, 287

Narayanan, D., Cox, T. J., Hayward, C. C., Younger, J. D., & Hernquist, L. 2009, MNRAS, 400, 1919

Narayanan, D., Cox, T. J., Shirley, Y., Davé, R., Hernquist, L., & Walker, C. K. 2008a, ApJ, 684, 996

Narayanan, D., Hayward, C. C., Cox, T. J., Hernquist, L., Jonsson, P., Younger, J. D., & Groves, B. 2010a, MNRAS, 401, 1613

Narayanan, D., Krumholz, M., Ostriker, E. C., & Hernquist, L. 2011b, 1104, 4118, arXiv:1104.4118

Narayanan, D., et al. 2008b, ApJS, 174, 13

—. 2010b, MNRAS, 407, 1701

Negrello, M., Perrotta, F., González-Nuevo, J., Silva, L., de Zotti, G., Granato, G. L., Baccigalupi, C., & Danese, L. 2007, MNRAS, 377, 1557

Negrello, M., et al. 2010, Science, 330, 800

Neri, R., et al. 2003, ApJ, 597, L113

Noeske, K. G., et al. 2007a, ApJ, 660, L47

—. 2007b, ApJ, 660, L43

Paciga, G., Scott, D., & Chapin, E. L. 2009, MNRAS, 395, 1153

Papadopoulos, P. P., van der Werf, P., Isaak, K., & Xilouris, E. M. 2010, ApJ, 715, 775

Peacock, J. A., et al. 2000, MNRAS, 318, 535

Pearson, C., & Rowan-Robinson, M. 1996, MNRAS, 283, 174

Pérez-González, P. G., et al. 2008, ApJ, 675, 234 (P08)

Poglitsch, A., et al. 2010, A&A, 518, L2

Pope, A., et al. 2006, MNRAS, 370, 1185

—. 2008, ApJ, 675, 1171

Rangwala, N., et al. 2011, arXiv:1106.5054

Reddy, N. A., Erb, D. K., Pettini, M., Steidel, C. C., & Shapley, A. E. 2010, ApJ, 712, 1070

Rex, M., et al. 2010, A&A, 518, L13

Ricciardelli, E., Trujillo, I., Buitrago, F., & Conselice, C. J. 2010, MNRAS, 406, 230

Riechers, D. A., Hodge, J., Walter, F., Carilli, C. L., & Bertoldi, F. 2011a, ApJ, 739, L31

Riechers, D. A., et al. 2011b, ApJ, 733, L11

Robertson, B., Bullock, J. S., Cox, T. J., Di Matteo, T., Hernquist, L., Springel, V., & Yoshida, N. 2006a, ApJ, 645, 986

Robertson, B., Hernquist, L., Cox, T. J., Matteo, T. D., Hopkins, P. F., Martini, P., & Springel, V. 2006b, ApJ, 641, 90

Robertson, B. E., & Bullock, J. S. 2008, ApJ, 685, L27

Robertson, B. E., & Kravtsov, A. V. 2008, ApJ, 680, 1083

Rodighiero, G., et al. 2011, ApJ, 739, L40

Rothberg, B., & Fischer, J. 2010, ApJ, 712, 318

Rothberg, B., & Joseph, R. D. 2004, AJ, 128, 2098

Sajina, A., Scott, D., Dennefeld, M., Dole, H., Lacy, M., & Lagache, G. 2006, MNRAS, 369, 939

Sakamoto, K., Scoville, N. Z., Yun, M. S., Crosas, M., Genzel, R., & Tacconi, L. J. 1999, ApJ, 514, 68

Sakamoto, K., et al. 2008, ApJ, 684, 957

Sanders, D. B., & Mirabel, I. F. 1996, ARA&A, 34, 749

Savaglio, S., et al. 2005, ApJ, 635, 260

Schinnerer, E., et al. 2008, ApJ, 689, L5

Schmidt, M. 1959, ApJ, 129, 243

Scott, K. S., et al. 2010, MNRAS, 405, 2260

Scott, S. E., et al. 2002, MNRAS, 331, 817

Scoville, N. Z., Sargent, A. I., Sanders, D. B., & Soifer, B. T. 1991, ApJ, 366, L5

Shakura, N. I., & Sunyaev, R. A. 1973, A&A, 24, 337

Shetty, R., Glover, S. C., Dullemond, C. P., & Klessen, R. S. 2011a, MNRAS, 412, 1686

—. 2011b, MNRAS, 412, 1686

Shetty, R., Kauffmann, J., Schnee, S., & Goodman, A. A. 2009a, ApJ, 696, 676

Shetty, R., Kauffmann, J., Schnee, S., Goodman, A. A., & Ercolano, B. 2009b, ApJ, 696, 2234

Sijacki, D., Vogelsberger, M., Keres, D., Springel, V., & Hernquist, L. 2011, arXiv:1109.3468

Silk, J. 1997, ApJ, 481, 703

Silva, L., Granato, G. L., Bressan, A., & Danese, L. 1998, ApJ, 509, 103

Smail, I., Chapman, S. C., Blain, A. W., & Ivison, R. J. 2004, ApJ, 616, 71

Smail, I., Ivison, R. J., & Blain, A. W. 1997, ApJ, 490, L5

Snyder, G. F., Cox, T. J., Hayward, C. C., Hernquist, L., & Jonsson, P. 2011, arXiv:1102.3689

Solomon, P. M., Downes, D., Radford, S. J. E., & Barrett, J. W. 1997, ApJ, 478, 144

Somerville, R. S., Hopkins, P. F., Cox, T. J., Robertson, B. E., & Hernquist, L. 2008, MNRAS, 391, 481

Springel, V. 2005, MNRAS, 364, 1105

Springel, V. 2010, MNRAS, 401, 791

Springel, V. 2010, ARA&A, 48, 391

Springel, V., & Hernquist, L. 2002, MNRAS, 333, 649

—. 2003, MNRAS, 339, 289 (SH03)

Springel, V., Matteo, T. D., & Hernquist, L. 2005, MNRAS, 361, 776

Springel, V., Yoshida, N., & White, S. D. M. 2001, NewA, 6, 79

Swinbank, A. M., Smail, I., Chapman, S. C., Blain, A. W., Ivison, R. J., & Keel, W. C. 2004, ApJ, 617, 64

Swinbank, A. M., et al. 2008, MNRAS, 391, 420

Tacconi, L. J., et al. 2006, ApJ, 640, 228

—. 2008, ApJ, 680, 246

—. 2010, Nature, 463, 781

Targett, T. A., Dunlop, J. S., McLure, R. J., Best, P. N., Cirasuolo, M., & Almaini, O. 2011, MNRAS, 412, 295

Toomre, A. 1974, The formation and dynamics of galaxies: Proceedings of the Symposium, 58, 347

Toomre, A., & Toomre, J. 1972, ApJ, 178, 623

Tremonti, C. A., et al. 2004, ApJ, 613, 898

Valiante, E., et al. 2007, ApJ, 660, 1060

van Dokkum, P. G., & Conroy, C. 2010, Nature, 468, 940

—. 2011, ApJ, 735, L13

van Kampen, E., et al. 2005, MNRAS, 359, 469

Városi, F., & Dwek, E. 1999, ApJ, 523, 265

Veilleux, S., Kim, D.-C., & Sanders, D. B. 2002, ApJS, 143, 315

Vieira, J. D., et al. 2010, ApJ, 719, 763

Vogelsberger, M., Sijacki, D., Keres, D., Springel, V., & Hernquist, L. 2011, arXiv:1109.1281

Wang, B., & Heckman, T. M. 1996, ApJ, 457, 645

Wang, W.-H., Cowie, L. L., Barger, A. J., & Williams, J. P. 2011, ApJ, 726, L18

Webb, T. M., et al. 2003, ApJ, 582, 6

Weingartner, J. C., & Draine, B. T. 2001, ApJ, 548, 296

Wilson, G. W., et al. 2008, MNRAS, 386, 807

Witt, A. N., & Gordon, K. D. 1996, ApJ, 463, 681

Witt, A. N., Thronson, H. A., & Capuano, J. M. 1992, ApJ, 393, 611

Wright, E. L. 2006, PASP, 118, 1711

Wu, J., Vanden Bout, P. A., Evans, II, N. J., & Dunham, M. M. 2009, ApJ, 707, 988

Wuyts, S., Cox, T. J., Hayward, C. C., Franx, M., Hernquist, L., Hopkins, P. F., Jonsson, P., & van Dokkum, P. G. 2010, ApJ, 722, 1666

Wuyts, S., et al. 2009, ApJ, 700, 799

Wuyts, S., et al. 2011, ApJ, 738, 106

Younger, J. D., Hayward, C. C., Narayanan, D., Cox, T. J., Hernquist, L., & Jonsson, P. 2009a, MNRAS, 396, L66

Younger, J. D., et al. 2007, ApJ, 671, 1531

—. 2008, ApJ, 688, 59

—. 2009b, MNRAS, 394, 1685

—. 2009c, ApJ, 704, 803

—. 2010, MNRAS, 407, 1268

Yun, M. S., et al. 2011, arXiv:1109.6286